Investigations on segmented polymer networks and protein conjugates based on end-group functionalized poly(2-oxazoline)s

Zur Erlangung des akademischen Grades eines

Dr. rer. nat.

von der Fakultät Bio- und Chemieingenieurwesen

der Technischen Universität Dortmund

genehmigte Dissertation

vorgelegt von

M. Sc. Sascha A. Wilhelm

aus

Siegen

Tag der mündlichen Prüfung: 28.05.2025

1. Gutachter: Prof. Dr. Jörg C. Tiller

2. Gutachter: Prof. Dr. Ralf Weberskirch

Dortmund 2025

Danksagung

Ich möchte Herrn Prof. Jörg C. Tiller herzlich dafür danken, mir die Bearbeitung dieses interessanten Forschungsthemas im Rahmen meiner Promotion ermöglicht zu haben und für die hilfreichen Diskussionen und Anregungen während dieser Zeit. Weiterhin danke ich Herrn Prof. Ralf Weberskirch für die freundliche Bereitschaft, das Koreferat zu übernehmen.
Zusätzlich danke ich Herrn Dr. Frank Katzenberg für seine engagierte Unterstützung und Hilfsbereitschaft sowohl in fachlichen Themen als auch darüber hinaus. Herrn Volker Brandt danke ich für die Präparation und Messung einer Vielzahl von AFM-Proben. Herrn Thorsten Moll möchte ich für die Unterstützung bei technischen Aufgaben im Labor und die Durchführung der GPC-Messungen danken. Weiterhin danke ich Frau Alexandra Riedel für ihre stete Hilfsbereitschaft bei organisatorischen Herausforderungen. Herrn Prof. Wolf Hiller und seinem Team der NMR-Abteilung möchte ich für die schnelle Durchführung der zahlreichen NMR-Messungen danken und Herrn Blöß, Frau Langner und dem Team der Werkstatt für Glasapparatebau der TU Dortmund danke ich herzlich für die Unterstützung bei der Probenvorbereitung für die SAXS-Messungen.
Zusätzlich möchte ich mich besonders bei meinen (ehemaligen) Kollegen Dr. Marko Milovanovic, Paola Andrea Benitez-Duif, Dr. Montasser Hijazi, Dr. Dominik Segiet, Dr. Christian Krumm, Dr. Alina Romanovska, Lena Benski, Dr. Martin Schmidt, Jonas Tophoven, Robert Jerusalem und Michail Maricanov für die hervorragende Arbeitsatmosphäre, Unterstützung und unzählige mehr oder weniger fachliche Diskussionen und Unterhaltungen danken. Außerdem bedanke ich mich bei Dr. Luis Bering für das Korrekturlesen dieser Arbeit.
Weiterhin danke ich allen Studierenden, deren Abschlussarbeiten und Praktika ich betreuen durfte und die mich auf diese Weise mit meiner Forschung und im Laboralltag unterstützt haben: Besten Dank an Thomas Halmanseder, Kübra Celik, Lisa Konieczny, Gizem Karatas, Laura Neukirch, Niklas Sensler und Seher Altuntas.
Besonderer Dank gilt meiner Familie, welche immer für mich da war und mir mit ihrer Unterstützung mein Studium und darüber hinaus vieles ermöglicht hat. Zu guter Letzt danke ich von ganzem Herzen meiner Frau Nicole für ihre Geduld, ihre Fürsorge und ihr Verständnis in den vergangenen Jahren.

The results presented in this work have been prepared in the period from April 2018 to September 2022 at the Chair of Biomaterials and Polymer Sciences at the Faculty of Bio- and Chemical Engineering at the TU Dortmund University under the supervision of Prof. Dr. Jörg C. Tiller.

Publications

M. Schmidt, T. Raidt, S. Ring, S. Gielke, C. Gramse, S. Wilhelm, F. Katzenberg, C. Krumm, J. C. Tiller; Investigations on „near perfect“ poly(2-oxazoline) based amphiphilic polymer conetworks with a crystallizable block, *European Polymer Journal* **2017**, 88, 562.

M. Leurs, B. Dorn, S. Wilhelm, M. Manisegaran, J. C. Tiller; Multicore Artificial Metalloenzymes Derived from Acylated Proteins as Catalysts for the Enantioselective Dihydroxylation and Epoxidation of Styrene Derivatives, *Chemistry* **2018**, 24 (42), 10859.

S. A. Wilhelm, M. Maricanov, V. Brandt, F. Katzenberg, J. C. Tiller; Amphiphilic polymer conetworks with ideal and non-ideal swelling behavior demonstrated by small angle X-ray scattering, *Polymer* **2022**, 1 (242), 124582.

Poster Presentations

S. A. Wilhelm, M. Leurs, S. Konieczny, B. Dorn, M. Manisegaran, J. C. Tiller; Chemically Modified Proteins as Highly Selective Artificial Metalloenzymes, ACS Spring Meeting, Orlando, Florida, USA, **April 2019**.

Abstract

The specific design of defined macromolecular components enables the formation of diverse nanostructured materials with tailored properties. In this work, different poly(2-oxazoline)s (POx) with functional terminal double bonds were synthesized and characterized both for the design of segmented polymer networks (SPNs) and for the conjugation of proteins.

In the first section, two novel families of amphiphilic polymer copolymer networks (APCNs) were prepared by copolymerizing hydrophobic poly(2-(1-ethylpentyl)-2-oxazoline) functionalized on both sides with one of the hydrophilic monomers 2-hydroxyethyl acrylate (HEA) or *N*,*N*-dimethylacrylamide (DMA) while varying the composition. The network syntheses were carried out *via* the macromeric cross-linker approach using a defined, telechelic polymer with a high degree of functionalization to achieve ordered structures in the networks through a component that is as highly defined as possible. All synthesized APCNs were swollen in the solvents water, toluene, or *n*-heptane and the intrinsic nanophases of the materials were investigated by small angle X-ray scattering (SAXS) both in the dry and in the swollen state. The HEA-based APCNs in particular showed ideal nanostructural swelling properties, since swelling in the phase-selective solvents water or *n*-heptane leads to swelling of the respective addressed polymer phase, whereby it was shown that the nanostructural order is retained.

Furthermore, SPNs based on the hydrophilic polymer components polyethylene glycol (PEG) with either poly(2-methyl-2-oxazoline) or poly(2-ethyl-2-oxazoline) were prepared in the following section by cross-linking the bifunctional acrylate end-groups. The obtained SPNs were characterized by SAXS in the dry and swollen state with respect to their nanostructure. Depending on their composition, a SPN system was identified with no initial nanostructure, but in which a clear phase separation could be induced by the influence of elevated temperature or selective solvent.

Furthermore, in a comparative study, polymer-protein conjugates *via* Michael addition reactions between terminally acrylate-functionalized PEG or POx with varying chain lengths and the proteinogenic amino groups of lysozyme as a model protein were investigated. The respective conjugation efficiency was analyzed by SDS-PAGE and the reactivities of the respective polymeric acrylate end-groups were further characterized by ^{1}H-NMR spectroscopy.

Zusammenfassung

Das spezifische Design von definierten makromolekularen Komponenten ermöglicht den Aufbau vielfältiger nanostrukturierter Materialien mit maßgeschneiderten Eigenschaften. In dieser Arbeit wurden unterschiedliche Poly(2-oxazolin)e (POx) mit funktionellen endständigen Doppelbindungen sowohl für das Design von segmentierten Polymernetzwerken (SPNs) als auch für die Konjugation von Proteinen synthetisiert und charakterisiert.

Im ersten Abschnitt wurden durch Copolymerisationen von hydrophobem, beidseitig Acrylat-funktionalisiertem Poly(2-(1-ethylpentyl)-2-oxazolin) mit jeweils einem der hydrophilen Monomere 2-Hydroxyethylacrylat (HEA) oder *N*,*N*-Dimethylacrylamid (DMA) unter Variation der Zusammensetzung zwei neuartige Familien amphiphiler Polymer-Conetzwerke (APCNs) hergestellt. Die Netzwerksynthesen erfolgten über den makromeren Vernetzer-Ansatz unter Einsatz eines definierten, telechelen Polymers mit einem hohen Funktionalisierungsgrad, um durch eine möglichst hochdefinierte Komponente geordnete Strukturen in den Netzwerken zu erreichen. Alle synthetisierten APCNs wurden jeweils in den Lösemitteln Wasser, Toluol oder *n*-Heptan gequollen und die intrinsischen Nanophasen der Materialien wurden mittels Kleinwinkel-Röntgenstreuung (SAXS) sowohl im trockenen Zustand, als auch im gequollenen Zustand untersucht. Speziell die HEA-basierten APCNs zeigten dabei ideale nanostrukturelle Quelleigenschaften, da es bei Quellung in den phasenselektiven Lösemitteln Wasser oder *n*-Heptan zu einer Quellung der jeweiligen adressierten Polymerphase kommt, wobei gezeigt werden konnte, dass die nanostrukturelle Ordnung dabei erhalten bleibt.

Weiterhin wurden im Folgenden Abschnitt SPNs auf Basis der hydrophilen Polymerkomponenten Polyethylenglycol (PEG) mit entweder Poly(2-methyl-2-oxazolin) oder Poly(2-ethyl-2-oxazolin) durch die Vernetzung der bifunktionellen Acrylat-Endgruppen hergestellt. Die erhaltenen SPNs wurden mit Hilfe von SAXS im trockenen und gequollenen Zustand hinsichtlich ihrer Nanostruktur charakterisiert. In Abhängigkeit ihrer Zusammensetzung konnte dabei ein SPN-System identifiziert werden, welches zunächst keine Nanostruktur aufweist, bei dem jedoch durch den Einfluss von erhöhter Temperatur oder selektivem Lösemittel gezielt eine deutliche Phasenseparation induziert werden konnte.

Darüber hinaus wurden in einer vergleichenden Studie Polymer-Protein-Konjugate *via* Michael-Additionsreaktionen zwischen endständig Acrylat-funktionalisiertem PEG oder POx mit variierenden Kettenlängen und den proteinogenen Aminogruppen von Lysozym als Modellprotein untersucht. Die jeweilige Konjugationseffizienz wurde mittels SDS-PAGE analysiert und die Reaktivitäten der jeweiligen polymeren Acrylat-Endgruppen wurden ferner mittels ^{1}H-NMR Spektroskopie charakterisiert.

Declaration on the reproduction of previously published content

Parts of this work were previously published by the author of the thesis as listed:
Chapter 3: Results partially published in reference [A].
Chapter 5: In parts based on results from reference [B].

[A] S. A. Wilhelm, M. Maricanov, V. Brandt, F. Katzenberg, J. C. Tiller; Amphiphilic polymer conetworks with ideal and non-ideal swelling behavior demonstrated by small angle X-ray scattering, *Polymer* **2022**, 1 (242), 124582.

[B] L. Neukirch, Synthese Acrylat-terminierter Poly(2-alkyl-2-oxazolin)e und Acrylat-funktionalisierter Monomethoxypoly(ethylenglykol)e für die Kopplung an Lysozym, Practical Course Protocol, *Chair of Biomaterials and Polymer Science*, *TU Dortmund University*, **2020**.

Table of Contents

1 Introduction

The continuous advancement of synthesis methods, along with the combination of diverse materials with both complementary and contrasting properties, is constantly opening up new opportunities to design and adapt the functionality and attributes of modern materials and substances in a more targeted manner, making it possible to realize increasingly specialized solutions for a wide range of requirements. In particular, new methods are progressively developed at the nanoscale level, enabling completely new morphologies and design options for the resulting macrostructures. This way, highly complex, but also controlled switchable or “smart” materials can be produced, paving the way to innovative applications or technologies.

The synthesis of tailor-made polymers creates the possibility of extending targeted molecular design to a macromolecular level in a variety of ways. Today's world would be inconceivable without synthetic polymers with their wide-ranging properties and resulting applications; these range from highly developed materials for textiles, construction and technology to medical applications such as drug delivery or tissue engineering as well as special applications such as filter membranes, sensors or catalysts.[1] Especially well-defined functional nanomaterials require polymeric compounds with narrowly distributed molar masses in combination with selectively distributed functional groups along these polymer chains.
This broad field of application is based on the extensive possibilities to define structure and modification of polymer compounds, particularly when using controlled synthesis conditions. The design of the main and side chains mainly determines the characteristics of a polymer, whereby properties such as polarity, glass transition temperature, mechanical properties or the formation of crystalline structures can be significantly influenced.[2-3] In addition, modifications can also be realized *via* the end-groups of the polymer chains. The end-group can also have a major influence on polymer properties such as the formation of superstructures, adhesion or solubility.[4] Since the reactivity of functional end-groups in polymer-analogous reactions often differs greatly from the reactivity of low-molecular weight compounds, the adjustment of reaction parameters is often necessary to achieve high conversions.
This work is dedicated to further investigate the potential of well-defined polymers for the application in functional nanomaterials. For this, various poly(2-oxazoline)s were synthesized bearing functional double bonds in their respective end-groups. Based on these functional polymeric compounds, numerous segmented polymer networks (SPNs) with varying compositions as well as polymer-protein conjugates were synthesized and the obtained nanomaterials were characterized in comprehensive studies.

1.1 Poly(2-oxazoline)s

Since the construction of well-defined functional nanomaterials depends on the utilization of controllable constituents, this aim made the usage of a highly definable and versatile polymer system unavoidable. Polymer systems based on 2-oxazolines, as used in this work, have been proven to allow for the design of polymers with a narrow molecular weight distribution in combination with an excellent possibility to introduce functional groups by means of initiator or termination agents, as well as control over the polarity of the chains *via* monomer selection. This polymer family is prepared through living cationic ring-opening polymerization (CROP) starting from 2-R-2-oxazolines with a variety of different properties and functionalities, resulting in a wide range of applications. Poly(2-oxazoline)s (POx) are increasingly being used in biomedicine in particular due to their good biocompatibility and non-toxic behavior.[5] Polymers composed specifically of the hydrophilic monomers 2-methyl-2-oxazoline (MOx) and 2-ethyl-2-oxazoline (EtOx) exhibit so-called stealth behavior.[6] This characteristic, due to their low interaction with human serum proteins, makes them particularly well suited for applications in medicine and cosmetics, for example for various drug delivery systems or conjugation with proteins or drugs.[7-12] Further applications of POx include self-assembling structures[13-15], thermoresponsive polymers[16-17], hydrogels and other networks[18-22].

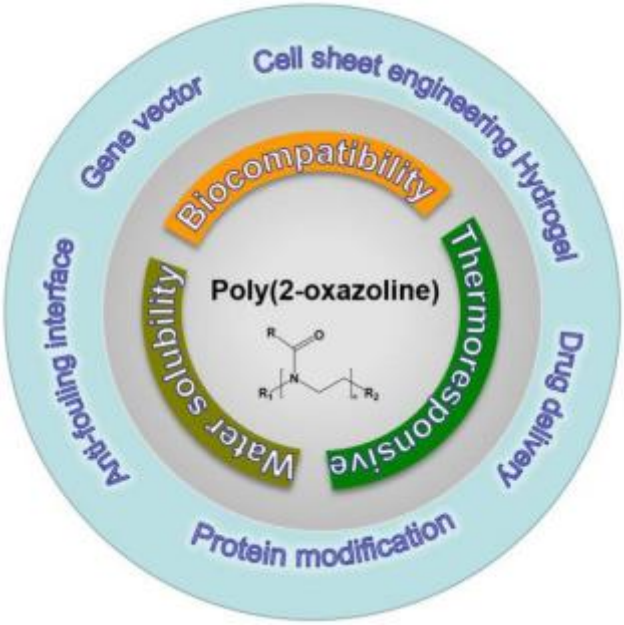

Figure 1.1 Schematic overview of several interesting properties and important biomedical applications of poly(2-oxazoline)s by YANG *et al.*[23]

This variety of tailor-made properties is mainly made possible by the type of polymerization reaction. Living polymerizations were already described by SZWARC in 1956, which also include the cationic ring-opening polymerization used for the polymerization of 2-oxazolines.[24] A key characteristic of living polymerizations is the reactive chain end present during the entire

course of the reaction and the absence of termination and transfer reactions under appropriate reaction conditions.[25] The CROP of 2-oxazolines has been of great scientific interest to polymer scientists around the globe since it was independently described by four research groups in the middle of the 1960s due to the high versatility it offers.[26-29] The general mechanism of the CROP, which was investigated by SAEGUSA and KOBAYASHI, is shown in **Figure 1.2** and can be divided in three steps: initiation, chain propagation and termination.[30-31]

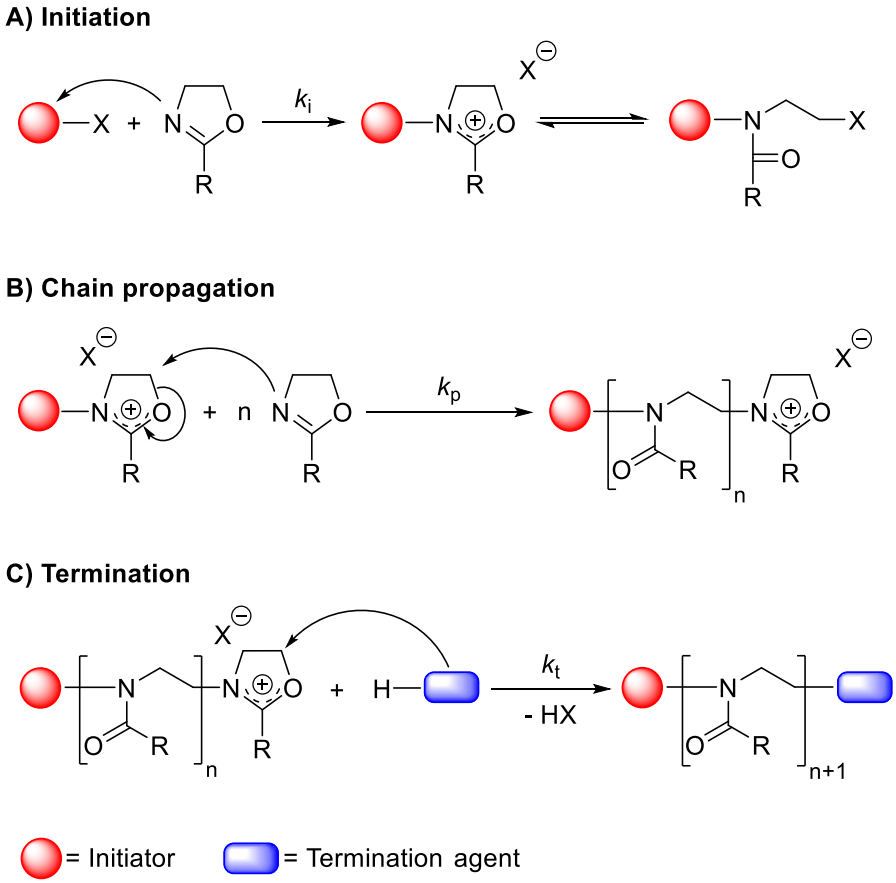

Figure 1.2 General mechanism of the CROP of 2-oxazolines.

The CROP is started by the initiation step through a nucleophilic attack of the heterocyclic nitrogen atom on the electrophilic center of the initiator, leading to the release of the leaving-group anion. This step determines the reaction speed and under ideal conditions k_i is significantly greater than k_p, which allows control of the desired degree of polymerization in combination with narrow molecular weight distributions through nearly simultaneous chain initiations and synchronous chain growth. Suitable initiators include strong Brønsted acids, Lewis acids, sulfonic acid esters or benzyl halides.[30,32] The initiation results in a thermodynamic equilibrium between a chain-opened species with a neutral charge and a cationic, cyclic species as the living chain-end. This equilibrium is determined by the used solvent, the side-

chain residue R and the nucleophilicity of the counter-ion. The utilization of polar aprotic solvents such as acetonitrile in combination with low nucleophilic counter-ions favors the cationic intermediate. By repeated nucleophilic attacks of further 2-oxazoline monomers on the C5 carbon atom of the active oxazolinium cation, the chain propagation proceeds until complete consumption of monomers or termination of the polymerization process.[33] The latter takes place by the addition of a nucleophile, terminating the polymerization reaction onto the 5-position of the cationic oxazolinium ring in a final nucleophilic attack. Suitable termination agents include strong nucleophiles, such as methanolic potassium hydroxide, carboxylates and amines.[25] The driving force for the CROP of 2-oxazolines relies on two aspects: firstly, the ring tension of the five-membered oxazoline ring is eliminated, and secondly, the imino ether group of the monomer is converted to a more stable amide group.[34] Under the right polymerization conditions, well-defined POx with narrow molar mass distributions, *i.e.* dispersities (*Đ*), even with high molar masses can be obtained. Importantly, even minor traces of nucleophilic impurities need to be removed from all used components (initiator, monomers and solvent) by rigorous purification methods prior to the polymerization reaction.

Since microwave technique has been established for the laboratory scale synthesis of POx, unfavorable long reaction times of previously 10 to 20 h during the polymerization process could be overcome, reducing the risk of unwanted side reactions.[35] The enormously accelerated reaction times paved the way for more complex POx designs and reaction components concerning functionalization possibilities[32,36] or combination of different monomers for the assembly of blockcopolymers, such as diblockcopolymers[37], ABA-triblockcopolymers[38], or ABC terblockcopolymers[39].

1.1.1 End-group Functionalization of Poly(2-oxazoline)s

In addition to the possibility to introduce functional groups to poly(2-oxazoline)s using monomers with specific side chain residues, the insertion of terminal functional groups through initiating or terminating agents poses further essential functionalization options. These functional end-groups enable the utilization of polymeric compounds as building blocks in superstructures like various nanomaterials or for coupling reactions among other things. The use of functional initiators offers the opportunity for one-sided modifications with a degree of functionalization d_f of ideally 100%, since every POx chain is started by one functional initiating agent. Although the high functionalization ratio seems very promising to obtain highly functionalized macromolecules, initiators for the CROP of 2-oxazolines need to be carefully selected. Initiators with slow initiation rates have a major impact on the control of the molecular weight and dispersity of the resulting polymer chains.[32,40-43] Furthermore, the nature and persistence of the formed counter-ion of the initiator affects the polymerization kinetics and even the type of polymerization mechanism of the CROP.[32,44-47] Additionally, the functional group of the initiating agent must neither interfere with the active chain ends during the CROP mechanism, nor should it promote chain transfer reactions. Prior protecting of the functional group, carried by the initiator, can therefore become mandatory under these conditions.[48]

Besides the discussed requirements, a wide range of functional initiators were proven as suitable reaction components for the CROP of 2-oxazolines as summarized in **Figure 1.3**. Especially corresponding functional triflates or tosylates emerged as appropriate choices, since they form lowly nucleophilic, stable counter-ions during the polymerization process.[49-50] Among these compatible functional groups are aliphatic double[51-52] or triple bonds[41,53-54], which are of great interest for subsequent “click” reactions, such as thiol-ene coupling and copper-catalyzed azide-alkyne (Huisgen) cycloaddition.[55] Further modifications with amines[56], carboxylic acids[57-58], hydrophobic alkyl chains[59-63], perfluoroalkyl chains[64], allyl[51,65], vinyl[52,66], styryl[67], anthracene[68-69], acetal, oxirane[70], cyclocarbonate[42], silane[71], methacrylate[72-73], and ester[74] groups at the *α*-position of the poly(2-oxazoline) are feasible by utilizing specific functional initiating agents.[32,75]

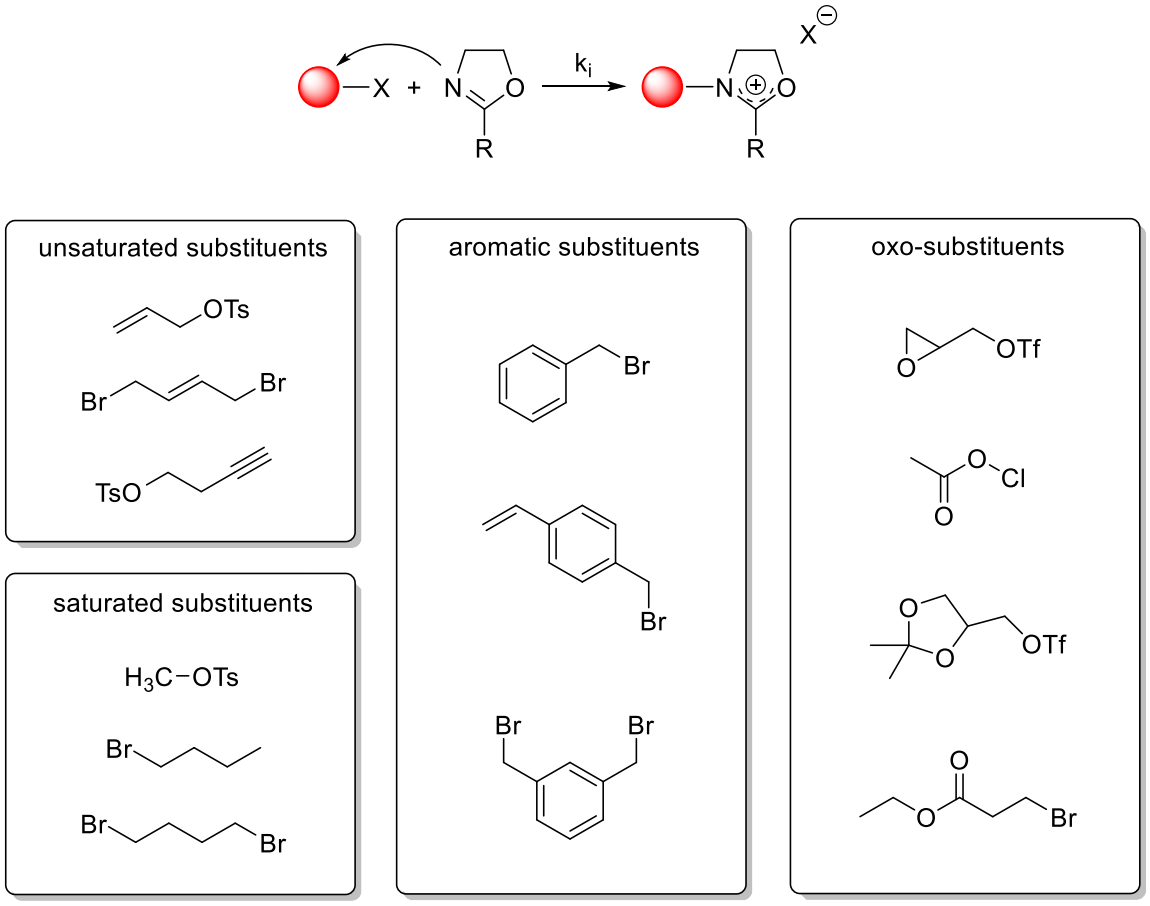

Figure 1.3 Examples of reported functional initiators for the CROP of 2-alkyl-2-oxazolines.[32]

Another approach to introduce terminal functional groups to poly(2-oxazoline)s is the utilization of functional terminating agents. This method represents the most common way to insert functional groups to the *ω*-end of the polymer chain, which allows the usage of otherwise incompatible functionalities for the CROP process compared to functional monomers or initiators. For this, the living ends of the polymer chains are treated with strong nucleophiles after chain propagation, thus terminating the polymerization process. In the case of initiation using a bi- or multifunctional initiating agent, the end-group functionality can get introduced to the polymer two or more times.[52] This approach enables the synthesis of macromonomers, cross-linking agents, or telechelic antimicrobially active compounds.[73,76]

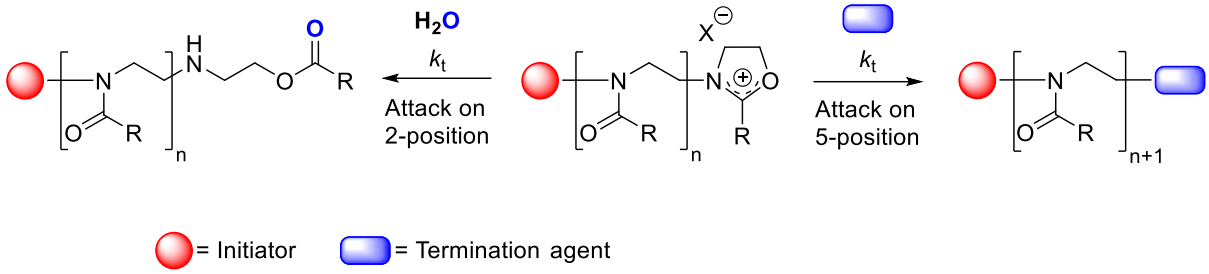

Figure 1.4 Comparison of the two mechanisms for the termination reaction of the CROP of 2-oxazolines; (left) Kinetically controlled termination on the 2-position *via* the attack of a water molecule versus (right) the thermodynamically driven termination reaction on the 5-position *via* a suitable terminating agent.[75]

Termination reactions can take place in a thermodynamically or kinetically controlled form. The different termination mechanisms are depicted in **Figure 1.4**. NUYKEN *et al.* investigated the kinetics of the termination reaction of the CROP of 2-oxazolines in 1996.[77] They found that the termination rate constant (k_t) is influenced by the present counterion introduced by the initiator and the equilibrium between cationic and covalent species. Furthermore, the nature of the utilized nucleophile plays an important role on the termination kinetic and mechanism. Water or other soft terminating agents tend to lead to a termination on the kinetically controlled 2-position of the oxazolinium cation, yielding a secondary amine with an ester group on the *ω*-end of the polymer chain. Since the thermodynamically controlled attack on the C5-carbon atom poses an irreversible termination process, providing the desired functional group on the *ω*-end of the polymer, harder terminating agents such as secondary amines are mostly favored choices.

A wide spectrum of suitable terminating agents for the introduction of functional *ω*-end groups has been reported. The overview given in **Figure 1.5** includes various examples of primary and secondary amines, carboxylic acids and various other terminating agents reported in literature.[32,75] The usage of such reagents allows the introduction of amino groups[78-79], hydroxyl groups[80-81], (meth)acrylate groups[20,80], or azides[69,74].

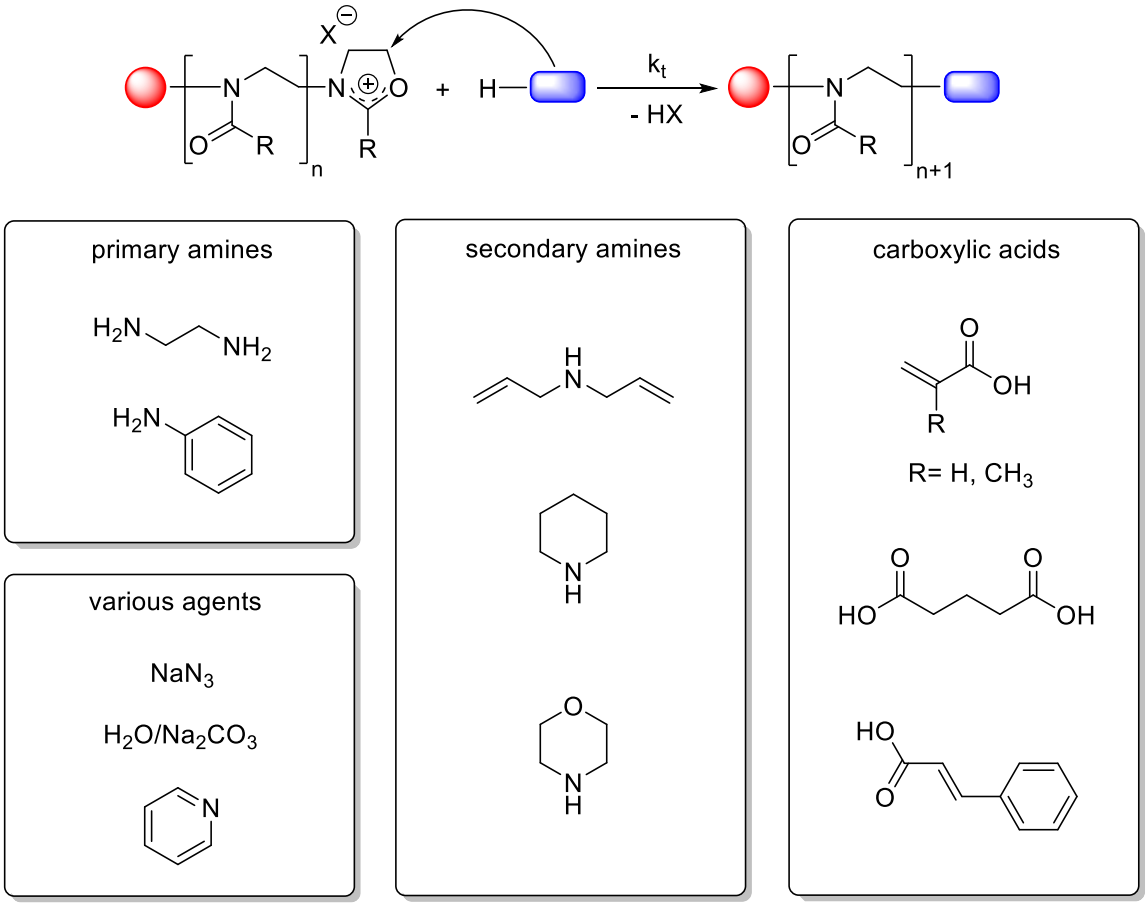

Figure 1.5 Examples of functional terminating agents for the CROP of 2-oxazolines.[32]

Utilization of either one of these end-group functionalization methods or a combination of functionalization *via* initiating and terminating agent is commonly applied to create telechelic polymer structures as depicted in **Figure 1.6**, enabling numerous post-polymerization transformations, coupling reactions or cross-linking strategies.

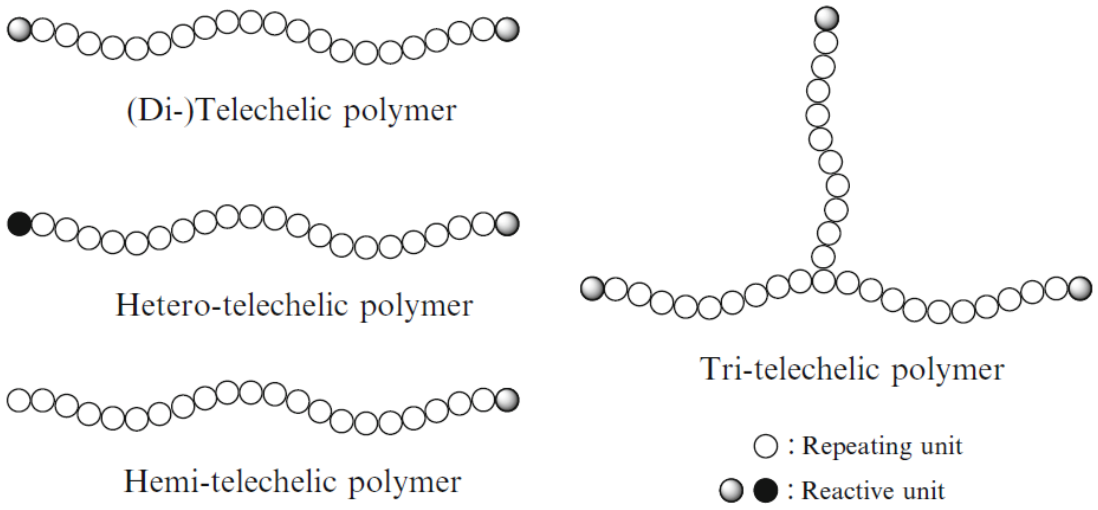

Figure 1.6 Schematic illustration of the different types of telechelic polymer structures [taken from TSUKAHARA and ADACHI[82]].

Introduced by URANECK *et al.*[83] in 1960 to describe end-group linkages of polybutadienes, the term “telechelic” was subsequently widely used to describe end-functional polymers of various types. The designated polymers can have one or multiple of the same functional end-group, described with the terms “hemi-“, “di-“, or “tri-telechelic” depending on the respective number of reactive end-groups. Another example of telechelic polymers exhibits different functional groups on the chain ends, for which the term “hetero-telechelic” is used. The last group of telechelic polymers with more than three reactive end-groups is generally summarized with the term “polytelechelic” polymers.[82]

1.2 Segmented Polymer Networks

Segmented polymer networks (SPNs) represent a sub-class of multicomponent polymer networks in the field of cross-linked polymeric materials. SPNs are network structures assembled through the covalent connection of both polymeric chain ends of the first component to the second polymer, creating nanomaterials with unique attributes.[84] By cross-linking two polymers with varied or even -typically- opposing structures or properties, specific individual characteristics can be merged into one material. Especially the combination of intrinsically immiscible polymers in chemically cross-linked networks enables the design of specific phase morphologies, as the obtained degree of cross-links can lead to forced blending between the polymers.[85-86] In addition to the intrinsic compartibilization of the chosen polymers, the respective polarity has a significant impact on the network structure and further properties. Networks that are built up by the connection of hydrophilic and hydrophobic polymer segments, either through cross-linking of respective homopolymers or cross-linked amphiphilic block or graft copolymers, are called amphiphilic polymer conetworks (APCNs). These promising materials offer exceptional properties through the combination of the contrary characteristics of their macromolecular building blocks, like the ability to swell in polar as well as nonpolar solvents.[87] Although the hydrophilic phase exhibits typical swelling behavior upon contact with water, the swelling is generally restricted by the hydrophobic phase, leading to limited solvent uptake and retained mechanical stability compared to the sole hydrogel.[88] These unique characteristics enable various specific applications, whereas extended-wear soft contact lenses being their most prominent commercial application for over two decades.[89] Other uses involve drug release matrices[90], antimicrobial thin film coatings[91-92], chemical or biochemical sensors[93-94], tissue engineering materials[95], or membranes for chiral separation[96-97]. Besides these examples, APCNs as activating immobilization matrices to retain enzymatic activity in supercritical CO_2[98] or organic solvents[99], as gel polymer electrolyte[100], or as functional membranes[101] have been reported. Further applications of APCNs as chemically[102-103] or enzymatically degradable conetworks[104] have been described.

Besides the selection of the individual network components, the design of the synthetic network formation approach plays a significant role for the physical and structural properties of the resulting APCN. **Figure 1.7** gives an overview over possible APCN design strategies with blue colored hydrophilic and red colored hydrophobic segments illustrated by McLeod and Tew.[105] The illustrated designs differ in their degree of structural definition. While the designs 2 and 6, obtained through random interconnection of linear amphiphilic copolymers, or design 4 by random cross-linking of amphiphilic graft copolymers, lead to lowly defined network structures, other strategies, such as random side interconnection (design 8) or end-linking (design 3) of hydrophilic with hydrophobic linear copolymers, enable increased structural definition of the resulting APCN. Improved structural definition is obtained through the end-linking of two types

of four-arm star homopolymers as depicted in design 7. Lastly, despite the resemblance between the designs 1 and 5, their synthetic strategies differ as design 1 illustrates the terminal cross-linking of linear amphiphilic ABA or BAB triblock copolymer using a low molecular weight tetra-functional cross-linker and design 5 describes the end-linking of AB or BA four-arm amphiphilic star block copolymers.[106-107]

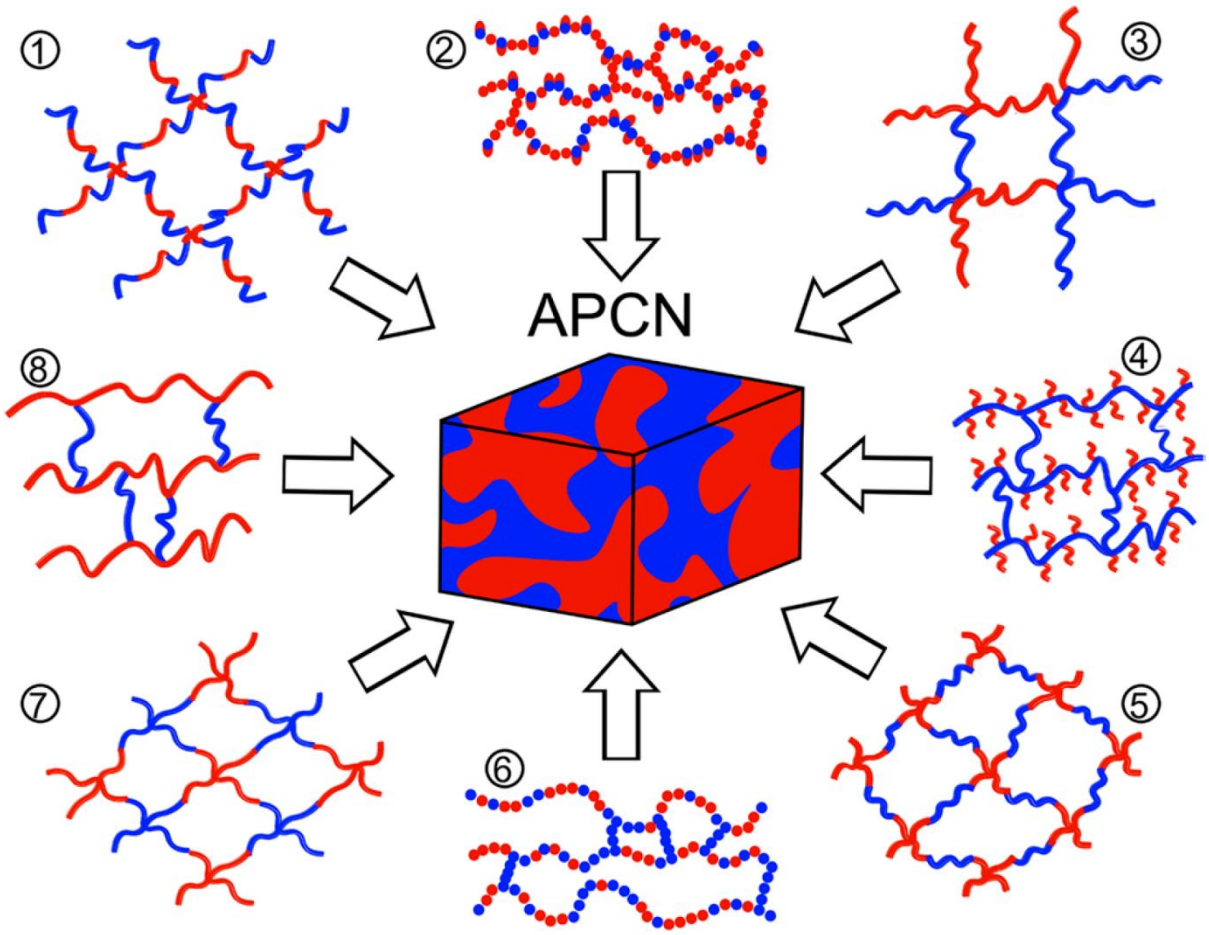

Figure 1.7 Overview of various cross-linking approaches for the formation of amphiphilic polymeric conetworks illustrated by MCLEOD and TEW (red and blue colors indicate hydrophobic and hydrophilic polymers, respectively). (1) Cross-linked ABA triblock polymers. (2) Copolymerized and cross-linked hydrophobic and protected hydrophilic monomers. (3) Cross-linked telechelic polymers. (4) Cross-linked amphiphilic graft copolymers. (5) Cross-linked star polymers with bifunctional macromonomers. (6) Cross-linked amphiphilic copolymers. (7) Cross-linked hydrophobic and hydrophilic star macromonomers. (8) Cross-linked hydrophobic polymers by hydrophilic cross-linkers.[105]

As previously mentioned, the resulting nanostructural morphology of an APCN is mainly determined by the utilized network components and the specific cross-linking strategy. The three main APCN synthesis methods are illustrated by BRUNS *et al.*[101] in **Figure 1.8**.

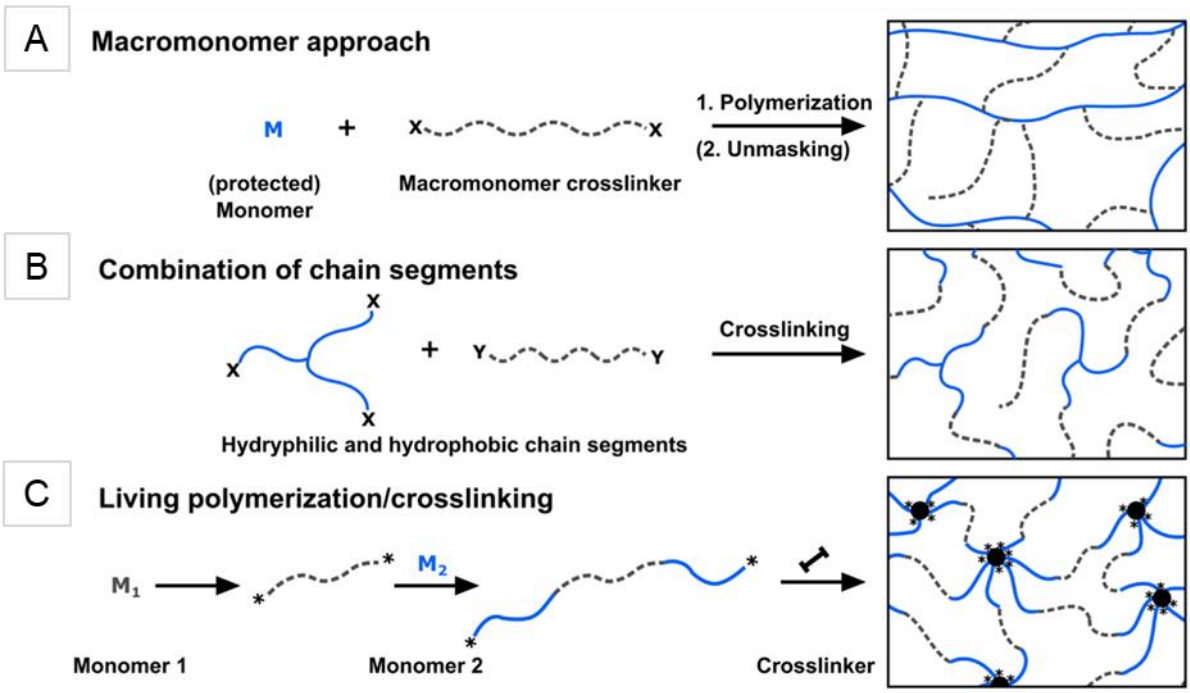

Figure 1.8 Schematic illustration of common APCN synthesis strategies through (A) the macromonomer approach, (B) the combination of chain segments, and (C) the living polymerization with subsequent cross-linking (illustration by ULRICH *et al.*[101]; blue and grey colors indicate the different polarities).

This combination of numerous synthetic approaches and variable usable building blocks poses a great advantage to customize the material properties of the resulting APCN. Due to the utilization of hydrophilic and hydrophobic components, these approaches often require the use of solvent mixtures and/or protection groups to tackle miscibility limitation during network formation.[108] The first and most employed approach is the macromonomer approach (**A**), in which small monomers are copolymerized with a macromonomeric cross-linker of contrary polarity.[109-110] This leads to continuously assembled polymer chains consisting of the chosen monomer randomly interconnected by the commonly well-defined macromonomeric cross-linker with tunable chain length, thus allowing only very limited control over the network architecture.[111] In the second strategy, two types of preformed telechelic chain segments with contrary solubility are cross-linked through their functional end-groups (**B**). In this, structural characteristics of the APCN can be influenced by the number of cross-linkable end-groups and molecular weights of the respective chain segments.[88,112-113] Lastly, the synthesis of APCN structures can be conducted through a living polymerization step to form amphiphilic block copolymers followed by subsequent cross-linking of the terminal living chain ends by the addition of a cross-linking agent (**C**).[107] As living polymerization methods commonly enable good control over the structural definition of the polymeric building blocks, this approach can

yield APCNs with a high degree of structural order adjustable by parameters such as chain lengths, types of monomers, monomer ratios, or type of cross-linker.[114-116]

Although various synthetic strategies for APCN formation with different levels of control over the structural order have been published, many of these APCNs show similarities in their nanostructural morphology. This microstructure is to some extent influenced by the location and number of segments emanating from common junctions in the conetwork[107], but most APCNs exhibit a tendency for microphase separated topologies, at least when in contact with water.[114] In order to characterize APCN microstructures, various techniques commonly used for characterization of phase separated linear block copolymers are utilized, as depicted in **Figure 1.9**.[111]

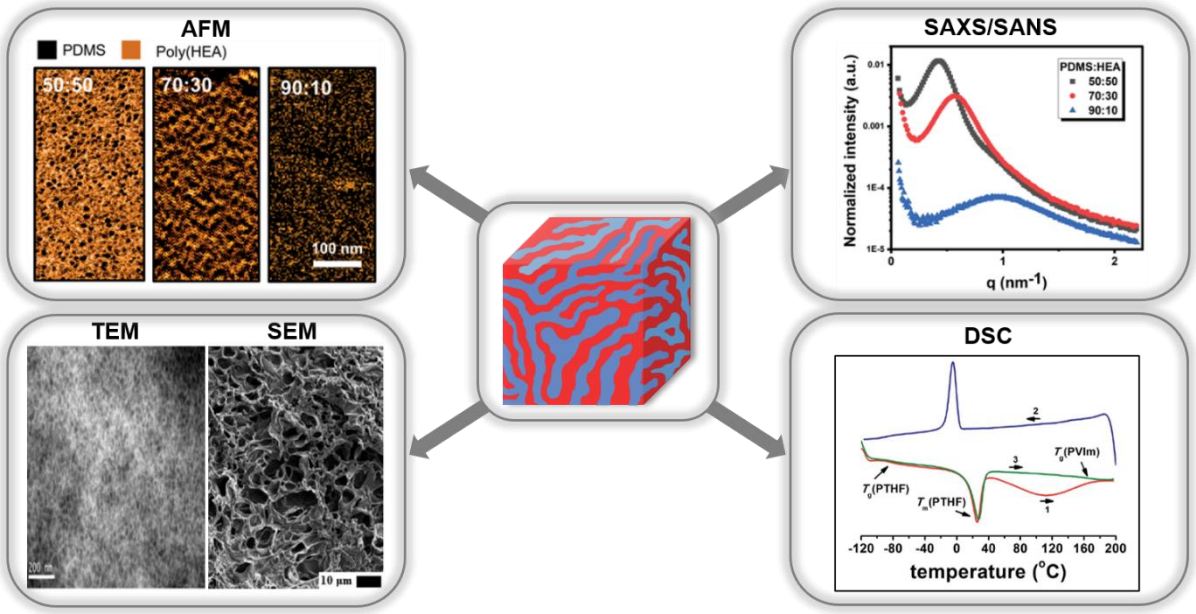

Figure 1.9 Literature examples of typical analytical methods and exemplary respective data for the characterization of APCNs (images taken from: AFM[117]; SAXS[117]; TEM[118]; SEM[119]; DSC[120]; APCN illustration[121]).

The image obtained through atomic force microscopy (AFM) (**Figure 1.9**) shows the typical structure of APCNs with two separated co-continuous phases, with the area ratios generally dependent on the respective ratios of the polymer phases or, in some cases, when performed on a water-swollen sample.[88] Further techniques for the characterization of dry or solvent-swollen samples are scattering methods, such as small-angle X-ray scattering (SAXS) or small-angle neutron scattering (SANS), through which specific scattering patterns can be obtained to gain information about phase thickness, (partial) crystallization or nanophasic swelling potential.[122] The usage of transmission electron microscopy (TEM), cryo-TEM, and

scanning electron microscopy (SEM) has also been reported for topological APCN characterization. Finally, differential scanning calorimetry (DSC) on APCNs has been widely utilized to gain insight into thermal material properties, such as shifted glass transition temperatures T_g compared to the individual polymeric components, or melting temperatures of crystalline areas.[122] Beyond that, more application focused characterization techniques for APCNs can be used, such as dynamic mechanical analysis (DMA)[100,123] or rheology experiments[88,124] for mechanical material data. In recent years, some research works on computer simulations of self-assembly and phase separation of model amphiphilic polymer conetworks have also been published.[125-126]

Since the characteristic nanophasic morphology of APCNs is significantly affected by solvent uptake, this behavior was investigated in various studies. Recently, FRIBICZER *et al.* reported the topographical changes of amphiphilic networks prepared by hetero-complementary coupling of amine-terminated tetra-poly(ethylene glycol) (tetra-PEG) with 2-(4-nitrophenyl)-benzoxazinone terminated tetra-poly(*ε*-caprolactone) (tetra-PCL) upon uptake of selective solvents.[88] For this, the APCNs were swollen either in water as a selective solvent for the hydrophilic PEG-phase, or in toluene to address the PCL-phase, respectively, and the APCN surface was characterized using AFM in phase mode. Comparison of the obtained surface images shows the lack of surface structure in toluene but pronounced microphase-separation for the water-swollen sample, resembling nearly spherical PCL-domains with a size of 20 ± 5 nm. Another example of the effect of solvent uptake on network topology was recently published by LÖSER *et al*., in which the same APCN system composed of tetra-PEG and tetra-PCL star polymers with varying preparation concentrations was swollen in water as a poor solvent for PCL followed by characterization through SAXS measurements.[125] This way, microphase-separated domains with average inter-domain distances of 19 nm and a domain radius of 5-6 nm were determined, indicating the aggregation of 17 to 25 PCL star polymers in the water swollen APCN samples. Furthermore, MUGEMANA *et al*. presented an interesting investigation on the influence of incorporation of metal salts on the nanostructure of an APCN.[127] For this, conetworks composed of poly(*N*-pyridin-4-yl)acrylamide) (PPFPA) and polydimethylsiloxane (PDMS) were synthesized and loaded with $ZnCl_2$ salts by swelling the conetworks in tetrahydrofurane (THF) containing 0.038 M of $ZnCl_2$. The sample films were then dried and characterized using AFM, which revealed that the spherical interconnected PDMS domains of the metal-loaded APCN appear bigger in comparison with the metal-free conetwork. Therefore, in this study the incorporation of metal ions does not change the overall phase morphology, but alters the sizes of the separated domains by cross-linking of the hydrophilic phase. Further examples on this topic are given in **Chapter 3.1**.

These examples show to the unique structural properties of APCNs and their changes upon external influences. Since the understanding of their complex nanostructural behavior requires

comprehensive studies and numerous characterization techniques and the properties differ between each type of APCN (e.g. utilized components, synthesis strategy), further studies on these materials are mandatory to investigate their full potential.

1.3 Polymer-protein Conjugates

In addition to the previously discussed utilization of end-group functionalized polymers as segments in polymer conetworks, well-defined macromolecules with tunable properties can further be used for the conjugation of proteins or enzymes. Since enzymes and biocatalysts in general play an important role in areas such as fermentation processes for industrial food production (e.g. bread, cheese and wine), laundry detergents, or wastewater treatment, the modification and stabilization of proteins has received substantial attention.[128] Due to their high catalytic efficiency and exquisite chemo-, regio-, and enantioselectivity combined with a broad scope of possible chemical transformations, such as C-C-bond formations, hydroxylations, oxidations, and various other functionalization reactions, customized enzymatic biocatalysts are of great industrial interest for the production of pharmaceutical or fine chemical products.[129-130] Besides the naturally occurring post-translational modifications of proteins to control specific properties, such as protein folding, stability or functionality, the conjugation of proteins with synthetic polymers has been proven as an effective toolbox for the modification and customization of biomolecules.[131]

The cornerstone of this field of research was laid by DAVIS and ABUCHOWSKI in 1977 by their report on the conjugation of amino acid side chains with small molecules and polymers to alter the immunological properties of bovine serum albumin (BSA).[132] In this early work, the covalent attachment of polyethylene glycol (PEG) with molecular weights of 1900 and 5000 Da, respectively, to BSA using cyanuric chloride as the coupling agent led to the disappearance of its immunogenicity in rabbits, while increasing protein activity, proteolytic resistance, as well as thermal and pH stability as proven in a further publication.[133] Following this, the covalent conjugation of proteins with the macromolecule PEG became widely known as PEGylation, and is still considered as one of the most impactful protein modification methods.[134-135] As PEG is a commercially available synthetic polymer, typically obtained through the anionic polymerization of ethylene oxide[136], with a good solubility in water as well as numerous organic solvents[137], and further advantages, such as protein-repellent interactions (‘stealth effect’)[136] and non-toxicity[138] upon high molecular weights, the PEGylation became a popular method for the modification of proteins. Most of the published PEG-protein conjugates were targeted towards specific biomedical applications, such as disease treatments/drug delivery[134] or tissue engineering[139]. Commercial drugs based on PEGylated proteins are approved by the US Food and Drug Administration since the 1990s, which owe their success mainly to increased half-life and/or decreased immunogenicity compared to the corresponding native proteins.[140]

In addition to their biomedical applications, PEGylated proteins can also be used in the means of biocatalysis. Among the advantages of PEGylated enzymes over their corresponding native forms are increased stability against denaturation at high temperatures[141] or improved solubility in organic solvents. Organosoluble PEG-protein conjugates have been reported by numerous

research groups, such as lipases[142-143], catalase[142], peroxidase[142,144], or proteases like papain[145] or *α*-chymotrypsin[142]. Typically, the modification is conducted in a grafting-onto coupling approach using the functional *ε*-amino group of proteinogenic lysine residues.[146] This way, PEGylated enzymes could be rendered soluble in common organic solvents, e.g. benzene, dimethylformamide, toluene, or different chlorinated solvents, in combination with an increased enzymatic activity in the unconventional medium compared to the native enzyme.[147] This solubility and enzymatic activity is typically directly influenced by the number of conjugated polymer chains and their respective chain lengths.[142-143] While the activity of PEGylated enzymes is often lower in aqueous environments in comparison to the respective native enzyme due to restricted diffusion of substrates and products, many reports showed retained enzymatic activity in organic media caused by the polymer modification.[143,145-146]

Although PEG has been used successfully for many years to conjugate proteins and enzymes for a wide range of applications, this polymer has its downsides. The repeated usage of therapeutic or diagnostic PEG-protein conjugates has been shown to lead to the generation of anti-PEG antibodies in the human body, often combined with severe accelerated blood clearance phenomenon and hypersensitivity reactions.[148-151] Furthermore, low molecular PEG chains (<400 Da), found as residual impurities in commercial PEG products, can be oxidized *in vivo* into toxic metabolites, posing significant health risks.[152-154] Besides the biomedical disadvantages of PEG usage, this polymer only enables very limited functional or structural modification options to customize polymer or conjugate properties for specific applications.

The previously discussed polymer class of poly(2-alkyl-2-oxazoline)s (POx) represents a promising alternative to PEG for protein conjugation, due to the opportunity to introduce functional groups as terminal or side-chain functionalities. Further advantages of POx are their relatively simple synthesis through living cationic ring-opening polymerization, which allows the synthesis of well-defined polymers in terms of narrow dispersities, well-controllable degrees of polymerization (DP) and a versatile toolbox of different 2-oxazoline monomers to choose from. For biomedical applications, similarities of the important characteristics of PEG, such as good biocompatibility and the protein repellent ‘stealth effect’, were also found for poly(2-methyl-2-oxazoline) (PMOx) and poly(2-ethyl-2-oxazoline) (PEtOx).[4]

The first literature report of a POx-protein conjugate was given by MIYAMOTO *et al.* in 1990.[155] In this early study, the successful conjugation of a catalase with PMOx and PEtOx polymers was reported, followed by the characterization of their enzymatic activity in the organic solvents benzene and chloroform in comparison with the corresponding PEGylated or native enzymes, respectively. Although the POx-protein conjugates showed only limited solubility in benzene (0.077 mg/mL), the enzymatic activity of the conjugates was up to 20 times higher compared to the corresponding native catalase in this solvent. Numerous publications about POx-protein conjugates followed afterwards, mostly with applications as biocatalysts in organic solvents[156-

[157] or as therapeutic agents[158-159]. In many reports, the conjugation is based on amide formation or "click" reactions to connect the respective reactive polymer end-groups (e.g. activated carboxylates[7] or "clickable" groups[55,160]) with the protein.[161] Another coupling strategy was demonstrated by KONIECZNY *et al.* with the utilization of bifunctional pyromellitic acid dianhydride as a linker between the amine end-group of various POx homo- and copolymers and the lysine groups of the respective protein, schematically illustrated in **Figure 1.10**.[162-163]

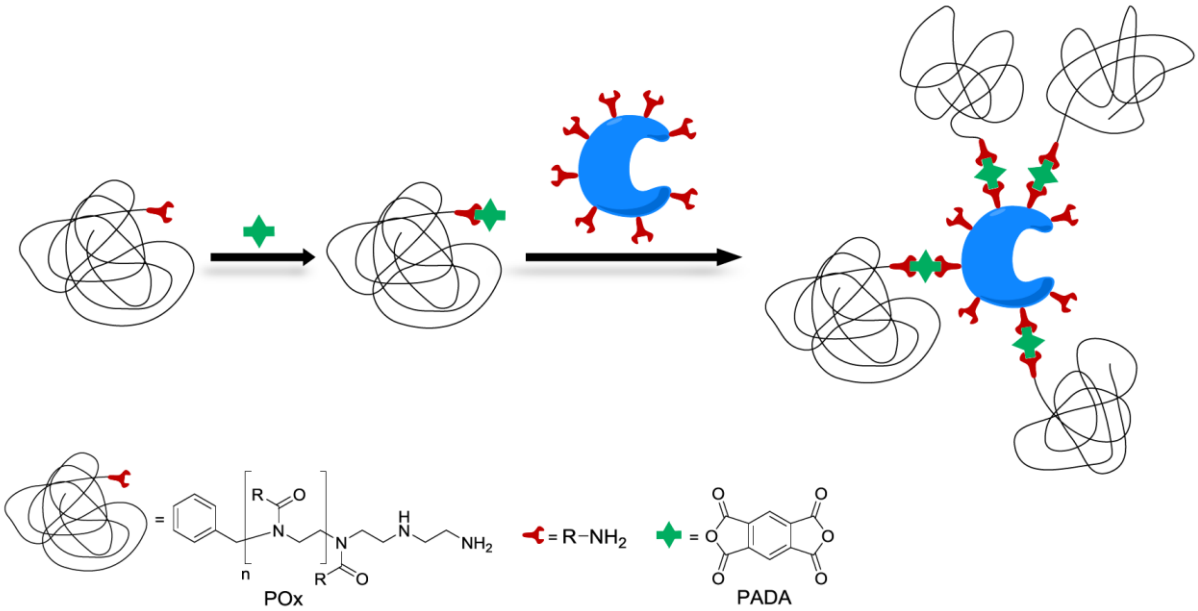

Figure 1.10 Schematic depiction of the enzyme conjugation method *via* the usage of pyromellitic acid dianhydride (PADA)-terminated poly(2-oxazoline)s developed by KONIECZNY *et al.* (illustrated by LEURS[164]).[162-163]

The organo-solubility of the obtained polymer-enzyme conjugates showed high dependence on the type and composition of the attached polymer. While the enzymatic activity of the conjugates in water was generally lower compared to the corresponding native enzymes, high enzymatic activations of up to 153000 in case of a PMOx-laccase conjugate were observed in organic solvents.

Besides covalent conjugation strategies for the development of organo-soluble enzymes through attachment of polymer chains, this aim can further be achieved by noncovalent methods. HIJAZI *et al.* demonstrated this approach by the formation of noncovalent conjugates through the addition of POx terminated with 2,2'-imino diacetic acid (IDA) end-groups to various enzymes.[165] The resulting conjugates were characterized as nano-sized polymer-enzyme aggregates giving clear solutions in organic solvents at concentrations up to 2 mg protein/mL (see **Figure 1.11**). For the respective noncovalent POx-enzyme conjugates with laccase, horseradish peroxidase (HRP), and α-chymotrypsin (CT), enzymatic activity assays

in organic solvents exhibited significantly increased activity compared to the respective corresponding native enzyme.

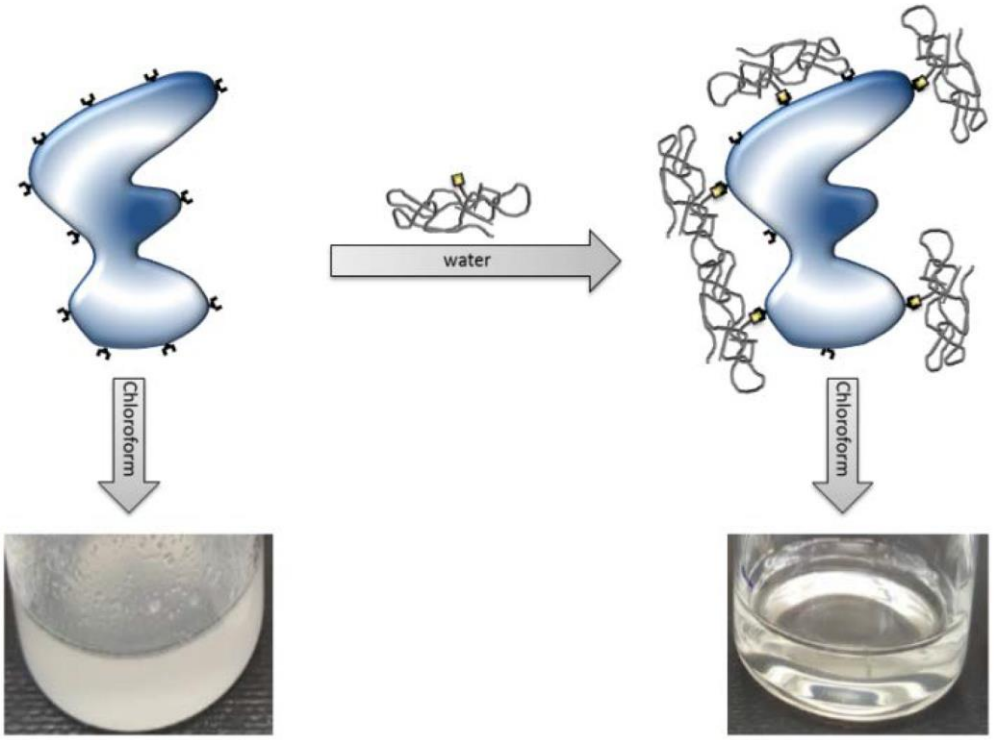

Figure 1.11 Depiction of the formation of organosoluble, non-covalent polymer-enzyme conjugates through the addition of 2,2'-imino diacetic acid terminated poly(2-oxazoline)s by HIJAZI *et al*.[165]

Additional conjugation approaches were conducted using thiol-maleimide Michael addition reactions by the combination of maleimide group end-functionalized POx with thiol group bearing cysteine residues of the respective protein, either by utilizing a protected maleimide-containing initiator[166], or a protected furan-maleimide adduct as termination agent[167] during the CROP of the respective 2-oxazoline monomers, followed by subsequent polymer-analog deprotection reactions.

All these examples demonstrate the great potential of end-group functionalized POx for the conjugation of proteins to increase their stability or solubility in organic solvents. In order to further increase the scope of suitable polymer-protein coupling reactions, the utilization of different POx with terminal acrylate end-groups are investigated in this work in terms of their conjugation potential of proteins *via* aza-Michael addition reaction.

2 Aims and Objectives

The aim of this work was the investigation of the potential of various well-defined, end-group functionalized poly(2-oxazoline)s for two applications in functional nanomaterials; firstly, their suitability and properties as telechelic macromonomers in segmented polymer networks were studied, followed by further investigations of the applicability of functionalized POx for the conjugation of proteins *via* aza-Michael addition reactions. For both applications, these telechelic polymers were equipped with reactive double-bonds on either one or both chain ends, depending on application, *via* the addition of functional termination agents following the CROP of the respective 2-oxazoline monomers.

In the first part of this work, the unique nanophasic morphologies of two novel amphiphilic polymer conetwork families were to be examined based on the preliminary work of BENSKI et *al*.[168] While both APCN families were based on poly(2-(1-ethylpentyl)-2-oxazoline) (PEPOx) as hydrophobic component, the conetworks were varied with regard to their hydrophilic component, whereby either poly(2-hydroxyethyl acrylate) (PHEA) or poly(*N*,*N*-dimethylacrylamide) (PDMA) were chosen as hydrophilic components. The study was aimed towards the characterization of the intrinsic separation behavior of the respective polymer phases of these novel APCNs with varying compositions and the nanophasic changes upon the uptake of orthogonal solvents, since for ideal APCNs no structural alterations should be observable. For this, the suitability of small angle X-ray scattering (SAXS) as a tool for the investigation of the nanophasic structure of APCNs was evaluated.

The second chapter deals with segmented polymer networks composed of the purely hydrophilic polymeric components PEG in combination with either PMOx or PEtOx. Here, the effects of conetwork composition on the structural properties of the resulting SPNs were to be characterized. Furthermore, since the respective polymer components exhibit similar solubility properties, the influence of solvents and temperature on the nanostructural order was to be investigated.

In the last chapter, the potential of the aza-Michael addition as a promising ligation method for the synthesis of polymer-protein conjugates was to be investigated. For this, water soluble polymers with functional acrylate end-groups and varying chain lengths were to be synthesized and characterized. Thereby, PEG was chosen as a polymer commonly applied in protein conjugation, and the protein modification potential should be compared with different functional PMOx and PEtOx to investigate whether the latter pose suitable alternatives for this approach. In order to verify the success of the conjugation reactions, sodium dodecyl sulfate-polyacrylamide gel electrophoresis (SDS-PAGE) should be conducted for the respective varied polymers and reaction conditions.

3 Amphiphilic Polymer Conetworks with ideal and non-ideal Swelling Behavior demonstrated by Small Angle X-ray Scattering

This chapter is based on a publication of SASCHA A. WILHELM[121] as first author.

3.1 Abstract

Amphiphilic polymer conetworks (APCNs) combine two incompatible properties within one material by featuring two interconnected independently swelling nanophases. To simultaneously address both properties, the APCNs need to be swellable in orthogonal solvents without changing their nanostructure. This has not been demonstrated yet. Two novel APCN families applying the macromeric cross-linker approach have been synthesized by cross-linking the hydrophilic poly(2-hydroxyethyl acrylate) (PHEA) or poly(*N*,*N*-dimethylacrylamide) (PDMA), respectively, with the hydrophobic poly(2-(1-ethylpentyl)-2-oxazoline) (PEPOx). For the first time, the APCN PHEA-*l*-PEPOx could be proven to swell in two orthogonal solvents, water and *n*-heptane, retaining its nanostructure in a broad range of compositions by using small-angle X-ray scattering (SAXS). PDMA-*l*-PEPOx seems to show a similar behavior according to swelling experiments, but SAXS revealed that particularly the PDMA phase reversibly changes its nanostructure upon swelling. Thus, the structural integrity of APCNs upon swelling depends on the topology as well as the chemical nature of the polymer phases. Altogether, SAXS experiments are required and well suited to judge changes in nanostructure upon swelling of APCNs.

3.2 Introduction

Since the late 1980s, the concept of amphiphilic polymer conetworks (APCNs) gained a lot of interest among the scientific community. APCNs are generally defined as covalently interconnected networks consisting of both a hydrophilic and a hydrophobic phase.[1] Because of these characteristics, APCNs are distinguished by a specific swelling behavior, exhibiting the ability to swell in polar as well as nonpolar solvents.[107] The unique interaction of covalently connected hydrophilic and hydrophobic domains enables a broad field of different material requirements. This combination of contrasting characteristics leads to a varied microstructural organization of the nanophases, mostly resulting in a distinct segregation between the individual phases. Depending on different parameters such as macromonomer structures (linear, branched or star-shaped) and polymer chain philicities or lengths of the utilized compounds, a multitude of different topologies (e.g. co-continuous, spherical/spheroidal or lamellar phases) and domain sizes can be obtained.[107]

As recently summarized by PATRICKIOS and MATYJASZEWSKI, these kind of structures can be achieved by various synthetic approaches.[169] Suitable strategies include the cross-linking of a

mixture of two different homopolymers[78] or free radical copolymerization of monomers with telechelic macromonomers functioning as macromeric cross-linkers.[170-174] Additionally, endgroup-linking of amphiphilic ABA copolymers[38,175-176] or star block copolymers[177-178] represent possible approaches to obtain APCNs with a high cross-link order and comonomer separation.

Due to a variety of highly tunable properties, APCNs offer many possible applications, with their usage as extended-wear soft contact lenses being the most significant commercial use so far.[89] In addition to that, possible applications as chemical and biochemical sensors[93-94,179-181], activating carriers for enzymatic reactions in supercritical CO_2 [98] or organic solvents[108,182-184] have been reported. Further studies showed the potential of APCNs as matrices for controlled drug release[185-188], membranes for chiral separation[97] or switchable aqueous permeation control[189], and wearable luminescent solar concentrators.[190] The above mentioned applications are successful due to the combination of orthogonal properties within one material, because both APCN nanophases reach throughout the whole material and act independently. However, if an APCN is applied in swollen state, e.g. for contact lenses or separation membranes, these properties, e.g. permeability of oxygen and salts, are only present, if the co-continuous structure is not changed upon swelling. So far no APCN has been reported that is swelling in two orthogonal solvents without changing its nanostructure. Numerous analytical methods have been reported in order to get insight into these complex nanostructures. Among these common methods are atomic force microscopy (AFM)[78,96,120,127,191-192], scanning electron microscopy (SEM)[118-119,182-183,193], solid-state NMR experiments[194-196], transmission electron microscopy (TEM)[118,196-197], small-angle neutron scattering (SANS)[177,198-205] and small-angle X-ray scattering (SAXS).[194,202,206-207] The application of these often combined techniques allows the characterization of the network structure on the nanoscale level, but is commonly limited to usage with dry network samples. Only scattering techniques enable the investigation of swollen APCN samples without the restriction of observing merely the surface of the sample, which is the case for AFM even under liquids. This advantage was utilized by PATRICKIOS *et al.* who used SANS to analyze the architecture of an APCN consisting of methacrylic acid and 2-butyl-1-octylmethacrylate synthesized by group transfer polymerization.[198] They observed single peaks attributed to well separated nanophases with a spacing between the scattering centers calculated from 7.6 to 12.8 nm for different conetwork compositions in D_2O. Another study concerning scattering techniques applied for examination of APCN morphologies was provided by TEW and coworkers.[197] In this work, dry poly(ethylene glycol) and polystyrene conetworks were analyzed by SAXS measurements, yielding clear scattering peaks indicating domain spacings between 22 and 55 nm, which increased with the M_n of the respective precursor polymer. The *d*-spacing values obtained by SAXS were verified by a representative TEM image and displayed good

consistency. In a recent publication by the groups of MÜLHAUPT and IVÁN, the successful alkylation of poly(1-vinylimidazole) in nanophasic poly(1-vinylimidazole)-*l*-poly(tetrahydrofuran) APCNs was reported, leading to nanoconfined poly(ionic liquid) conetworks.[208] The preservation of the bicontinuous nanophasic morphology was validated by AFM and SAXS, in which *d*-spacings of 15-20 nm and average domain sizes of 8.2-8.4 nm were determined. Further studies utilizing SAXS techniques to investigate nanophase-separated functionalized poly(*N*-alkyl acrylamide)-based APCNs were carried out by BRUNS and coworkers, presenting a versatile precursor based strategy for the synthesis and characterization of diversely functionalized nanophasic morphologies.[209] SHIBAYAMA *et al*. conducted another SAXS and SANS-based investigation regarding the microstructure of poly(ethylene glycol)-poly(dimethylsiloxane) amphiphilic conetwork gels.[202] These networks were swollen in toluene, which was subsequently substituted with methanol and water afterwards. This treatment led to a decrease of macroscopic gel size, but clearly displayed arisen first order scattering peaks indicating an intensifying microphase separation. Although APCNs should have two independently swelling nanophases, the swelling of only one phase is investigated in most studies.

Recently, we reported the first study, where the structural changes of an APCN upon swelling was investigated for two orthogonal solvents using SAXS.[168] These APCNs consisted of a hydrophilic, telechelic poly(2-methyl-2-oxazoline) (PMOx) with *N*-[3-(dimethylamino)-propyl]-methacrylamide (DMAP-MAA) end groups as macromolecular cross-linker and poly(2-ethylhexyl acrylate) (PEhAc) as hydrophobic linear component. Swelling this APCN in toluene showed no structural change of the hydrophobic phase, while swelling in water resulted in great structural changes of the hydrophilic phase. Thus, the APCN shows a non-ideal swelling behavior, because the changes of the hydrophilic phase will change the property profile of the material upon swelling and thus limiting the use of the APCN. In the present study, a new macromonomer hydrophobic cross-linker was synthesized and copolymerized with a hydrophilic proton-donor monomer, 2-hydroxyethyl acrylate (HEA), and a hydrophilic proton-acceptor monomer *N*,*N*-dimethylacrylamide (DMA), respectively. The influence of the respective, structural changes upon swelling in selective solvents was explored using SAXS.

3.3 Results and Discussion

Goal of this study was to possibly find an APCN, which does not change its morphology in solvents that selectively swell one of the two polymer nanophases. While a previous study used an APCN with a hydrophobic acrylate-based polymer cross-linked by a hydrophilic poly(2-oxazoline) (POx), the present study will address an APCN with a structure inverse to this. This offers the chance to apply functional groups to the hydrophilic phase, which might have an influence on structural integrity of the APCN by forming hydrogen-bonds. Therefore,

the hydrophilic acrylates DMA and HEA, respectively, were cross-linked by a hydrophobic poly(2-oxazoline). The latter was chosen from a series of non-crystallizing, low *T*g hydrophobic POx, using the least hydrophobic structure to ensure mixing ability with the acrylate in solutions that contain as little solvent as possible. The branched (2-(1-ethylpentyl)-2-oxazoline) (EPOx) was synthesized according to KEMPE *et al.*[210] Based on this monomer, a macromolecular cross-linker was synthesized (32 EPOx repeating units determined by ^{1}H NMR, **Figure 3.13**), bifunctionally initiated with *trans*-1,4-dibromo-2-butene (DBB) and terminally functionalized with DMAP-MAA end groups. This telechelic macromonomer was then copolymerized with either DMA or HEA by free radical photopolymerization as illustrated in **Figure 3.1**, providing the first APCNs based on a purely hydrophobic POx component. The miscibility of the compounds was realized by adding the common solvent 1-methoxy-2-propanol (1M2P) in as small amounts as possible. A poly(2-(1-ethylpentyl)-2-oxazoline) (PEPOx) content between 30 up to 90 wt% was used for both APCN-systems. This led to optically clear APCN films indicating no macroscopic phase separation and the gel content of the dried material was found to be more than 90 wt% with the exception of the networks with 90 wt% cross-linker, which were found to have a gel content in the range of 76-79 wt% (see **Table 3.3**, Experimental Section). In order to get insights in the conversion of the monomers and the potential change of compositions of the APCNs during washing, a freshly prepared non-dried PDMA(50)-*l*-PEPOx(50) was washed with $CDCl_3$ and the mixture was analyzed by ^{1}H NMR. It was found that this mixture is composed of 1M2P, PDMA, and PEPOx, while no residual acrylate monomer was detected (see **Figure 3.14**, Experimental Section). The integrals of the polymers showed that they were present in molar amounts corresponding to equal polymer mass fractions and thus in a similar composition as that of the respective network. Hence, the composition of the APCNs was presumed to be that of the starting concentration in the reaction mixture in all cases. Another typical behavior of nanophase-separated systems is the existence of two T_gs, which can be attributed to each polymer phase. As seen in the **Figures 3.11** and **3.12** (see Experimental Section), this is the case for both APCNs.

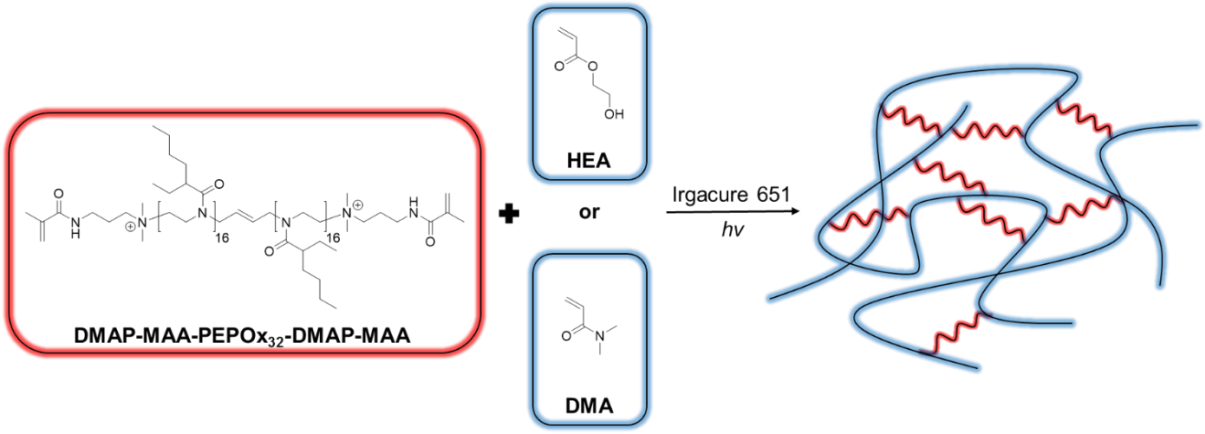

Figure 3.1 Schematic depiction of the investigated amphiphilic polymer conetworks consisting of the hydrophobic macro-crosslinker DMAP-MAA-PEPOx$_{32}$-DMAP-MAA and the respective hydrophilic polymer poly(*N*,*N*-dimethylacrylamide) (PDMA) or poly(2-hydroxyethyl acrylate) (PHEA).[121]

The swelling ratios S_g of these networks were gravimetrically determined for water, toluene, and *n*-heptane, respectively, and compared to those of networks composed of the respective homopolymers (see **Figure 3.2**). As expected, the S_g in water decreases with increasing proportion of the hydrophobic PEPOx for both APCN systems. The swelling ratio drops from 1.8 to 1.2 for PHEA-*l*-PEPOx and from 3.7 to 1.2 for PDMA-*l*-PEPOx when the amount of the hydrophilic component is reduced from 70 to 10 wt%. In case of swelling in toluene, the determined S_g values for the APCNs are found between 1.2 and 2.8 for PHEA-*l*-PEPOx with increasing PEPOx-content. In case of PDMA-*l*-PEPOx S_g nearly linearly increases from S_g = 2.4 to 4.3 with increasing PEPOx content. This may possibly suggest that toluene is not a selective solvent for the PEPOx-phase, but also swells the DMA phase. This is supported by the slight swellability (S_g = 1.3) of the pure PDMA network with a degree of cross-linking similar to PDMA-*l*-PEPOx(70). The divergent $S_{g,\ toluene}$ of the PDMA-*l*-PEPOx networks does not originate from varying degrees of cross-linking (the non-selective solvent $CHCl_3$ swells all PDMA-based APCNs nearly equally, see **Figure 3.15**, Experimental Section), but more likely from different Flory Huggins parameters of the respective toluene/homopolymer systems and from the nanostructures.

In order to find a selective solvent for the hydrophobic phase of both APCN systems, the equilibrium swelling behavior was investigated in *n*-heptane. The APCNs exhibited swelling ratios from S_g = 1.1 to 1.6 (PHEA-*l*-PEPOx) and S_g = 1.0 to 1.4 (PDMA-*l*-PEPOx) with increasing PEPOx mass fraction. This behavior indicates a selective solvent uptake by the PEPOx phase.

The phase size and nanostructure of the APCNs were further characterized by recording SAXS patterns and AFM images of the dry networks.

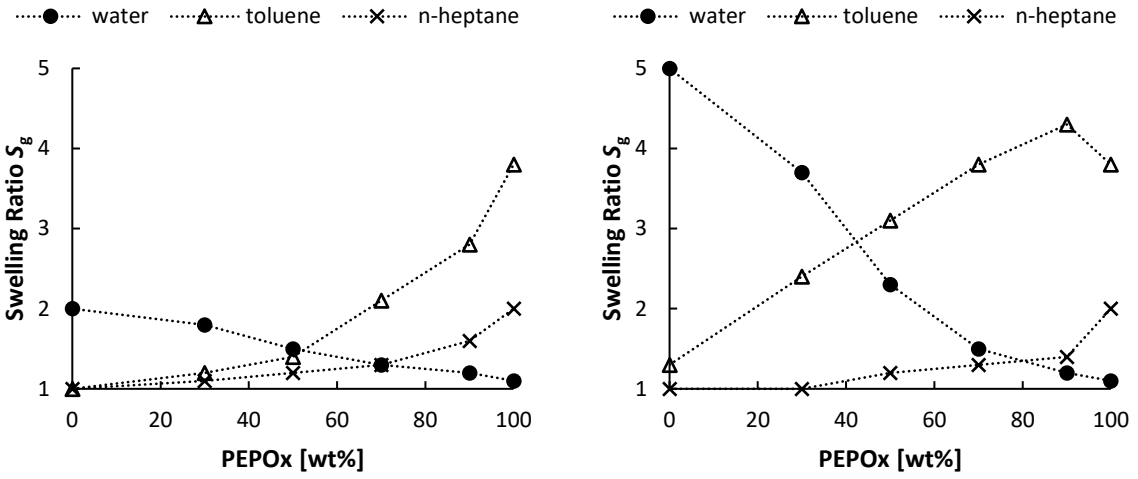

Figure 3.2 Swelling ratios of PHEA-*l*-PEPOx (left) and PDMA-*l*-PEPOx (right) conetworks in different solvents (• water, Δ toluene, x *n*-heptane). All experiments were conducted at least twice, the standard deviations are less than 10% in all cases.[121]

The data of the SAXS measurements of the dry APCN films are presented in **Figure 3.3**. The long-period values *d* were calculated according to $d = 2\pi/q$ with the scattering vector *q* yielding from azimuthal integration of the X-ray scattering patterns. This led to the depicted graphs showing SAXS traces of APCNs with a PEPOx mass fraction between 50 to 90 wt% exhibiting distinct peak maxima *d**. Hereby, well distinguishable data for average long-periods *d** could be determined and thus a highly ordered nanophase separation within the conetworks was confirmed. In contrast, *d** could not be determined for PHEA-*l*-PEPOx(30) and PDMA-*l*-PEPOx(30).

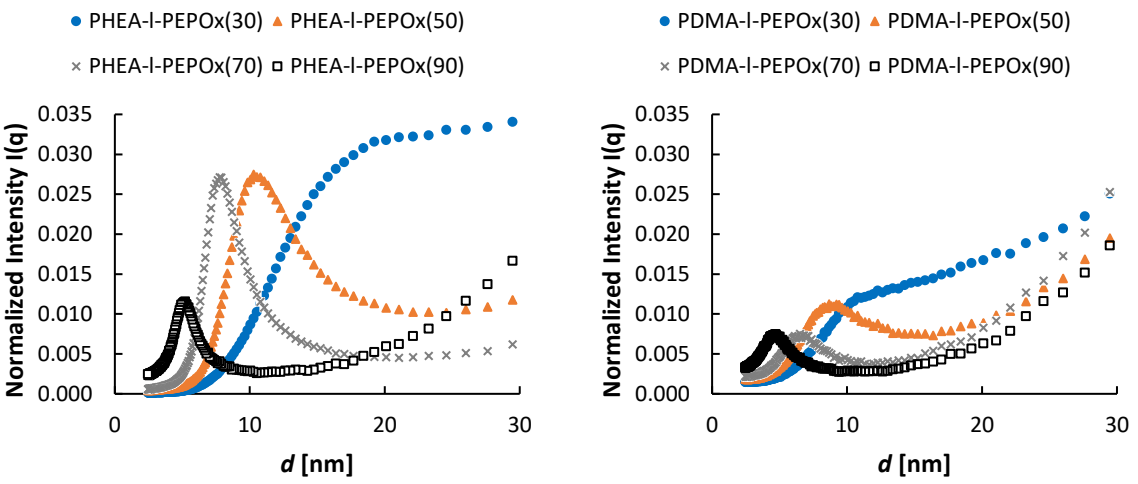

Figure 3.3 Small-angle X-ray scattering (SAXS) traces of dry PHEA-*l*-PEPOx (left) and dry PDMA-*l*-PEPOx (right) conetworks with a variation in PEPOx-content (30 to 90 wt%). All measurements were carried out for 1 h. Intensities were normalized to the total number of counts of the respective measurement and *d* was calculated using $d = 2\pi/q$.[121]

An overview of the identified average long-periods of the different conetworks is given in **Table 3.1**. The d^* values determined for PHEA-*l*-PEPOx conetworks range from 5.2 nm to 19.2 nm with increasing PHEA content in combination with high normalized intensities. In case of the PDMA-*l*-PEPOx films, average long-periods between 4.9 nm successively increasing to 10.5 nm with increasing PDMA amount were detected. The peaks show lower intensities than those found for the PHEA-based APCNs, indicating an either lower scattering contrast or a somewhat lower order of the nanophases compared with the latter conetworks. The average long-period of both APCN systems expands with higher mass fractions of the hydrophilic component. The found long-periods are in good agreement with published results by the group of Patrickios (d^* = 7.6 to 12.8 nm)[198], Iván et al. (d^* = 14.6 and 18.5 nm)[194], Bruns et al. (d^* = 12.2 to 17 nm)[209] and our group (d^* = 6.8 to 12.6 nm)[168], which were also determined utilizing scattering techniques. In all cases, the peaks widen with decreasing PEPOx mass fraction. These findings are in accordance with previously published results of PEhAc-*l*-PMOx networks.[168] In both cases, the 2-alkyl-2-oxazoline-based macro-crosslinker exhibits a defined polymeric structure with a narrow dispersity by utilizing the living cationic polymerization. The second compound however is synthesized by free radical polymerization leading to broad dispersities *Đ*. Since the long-period *d* represents the summarized distance of both phases combined, a higher mass fraction of free radically polymerized phases results in a broader distribution of *d*-values. The domain sizes of the individual APCN polymer phases summarized in **Table 3.1** were calculated by numerically fitting them to the respective network composition in combination with an assumed cubic structure model.

Table 3.1 Summarized domain size data of dry APCNs determined by SAXS analysis.

APCN	d^*_{dry} [nm][a]	d_{PEPOx} [nm][b]	$d_{acrylate}$ [nm][b]
PHEA(70)-*l*-PEPOx(30)	19.2[c]	8.9	10.3
PHEA(50)-*l*-PEPOx(50)	10.5	5.6	4.9
PHEA(30)-*l*-PEPOx(70)	7.8	4.7	3.1
PHEA(10)-*l*-PEPOx(90)	5.2	3.7	1.5
PDMA(70)-*l*-PEPOx(30)	10.5[c]	6.2	4.3
PDMA(50)-*l*-PEPOx(50)	9.0	4.7	4.3
PDMA(30)-*l*-PEPOx(70)	6.8	4.0	2.8
PDMA(10)-*l*-PEPOx(90)	4.9	3.4	1.5

[a] Determined by SAXS traces; [b] calculated by utilizing numerical fitting based on SAXS data to meet the respective conetwork composition assuming a cubic structure model (ρ(PHEA) = 1.31 g cm^{-3} [211]; ρ(PDMA) = 1.09 g cm^{-3} [212]; ρ(PEPOx) = 0.85 g cm^{-3}; for more details see Experimental Section); [c] d^* estimated from shoulder signal.

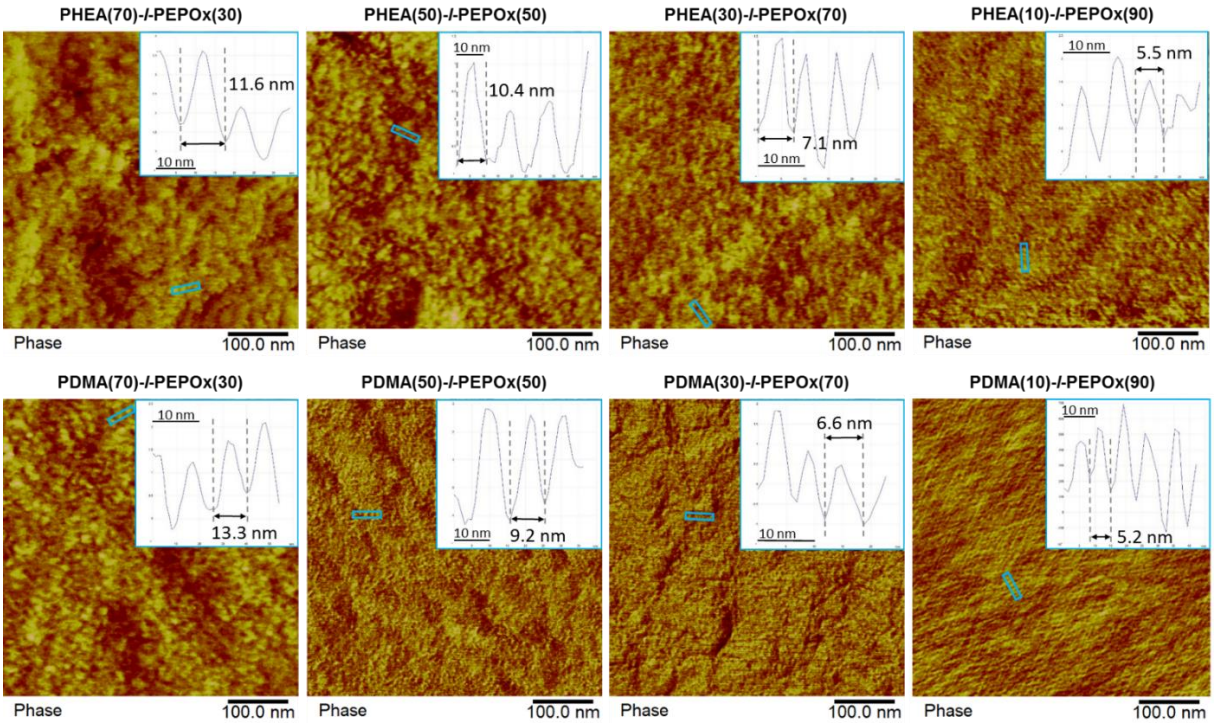

Figure 3.4 AFM phase mode images of cryofractured PHEA-*l*-PEPOx and PDMA-*l*-PEPOx APCNs measured in tapping mode and respective long-period approximations.[121]

All APCN films were cryofractured in order to investigate the nanophase morphology by atomic force microscopy (AFM) imaging shown in **Figure 3.4**. These images demonstrate clearly separated co-continuous nanophases for every conetwork representing typical APCN structures as schematically illustrated in **Figure 3.5**, which match the observations regarding AFM data of comparable systems.[168,184] Among the coherent APCNs with varying PEPOx mass fractions, the phases become thicker with increasing content of the hydrophilic component. This finding coincides perfectly with the SAXS data presented in the last paragraph. Image sectors of both conetwork samples with 90 wt% PEPOx, indicating the most uniform nanophases according to the respective SAXS traces, were representatively investigated regarding long-period data. Average long-periods of 5.5 nm for PHEA(10)-*l*-PEPOx(90) and 5.2 nm in case of PDMA(10)-*l*-PEPOx(90) were determined, approximately matching the domain sizes calculated from the respective SAXS data.

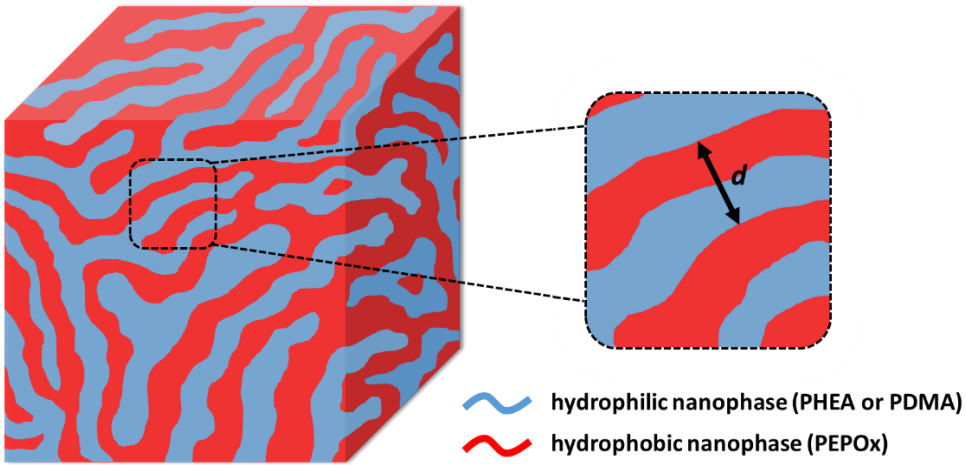

Figure 3.5 Schematic depiction of the co-continuous APCN nanostructure confirmed by AFM measurements with exemplary illustration of long-period *d*.[121]

In order to find out if each of these well-defined nanostructured polymer phases can be swollen independently from the other phase in a selective solvent, the APCN films were transferred to quartz tubes with the respective solvent, sealed and the respective SAXS profiles were recorded. The SAXS traces of the investigated PHEA-*l*-PEPOx conetworks with varying PEPOx content are comparatively depicted in **Figure 3.6**. Each graph shows the respective curves of the network films in the dry and in the swollen state of the respective solvent.

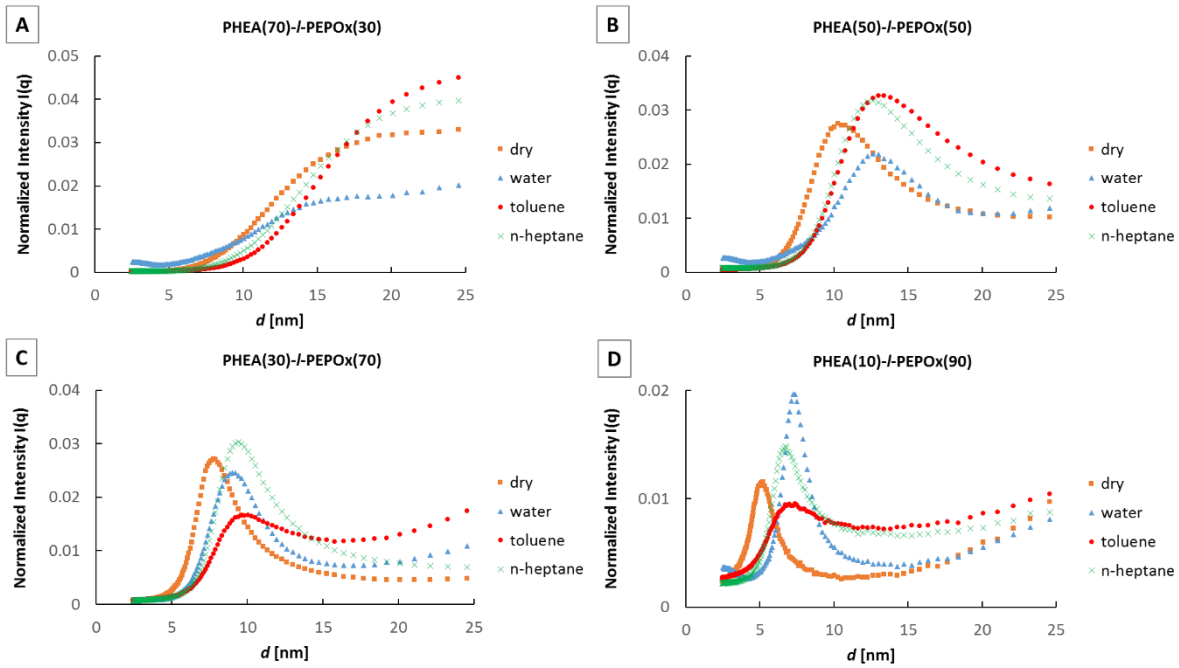

Figure 3.6 SAXS profiles received from PHEA-*l*-PEPOx conetwork samples with varying compositions under dry and swollen conditions (solvents: water, toluene or *n*-heptane). Measurements of dry samples were carried out for 1 h and of swollen samples for 8 h. Intensities were normalized to the total number of counts of the respective measurement and *d* was calculated using $d = 2\pi/q$.[121]

The SAXS profiles of the swollen PHEA-*l*-PEPOx with 50 to 90 wt% of the hydrophobic cross-linker show that the *d** values increase in all cases and the narrow curves indicate that this occurs without losing order of the nanophases (**Figure 3.6 B-D**). This is particularly true for swelling in the most hydrophilic solvent water and the most hydrophobic solvent *n*-heptane. Swelling in toluene seems to result in some loss of order, which could be due to the fact that this solvent is not as selective as the other ones. The results indicate that both nanophases of the APCNs can indeed be swollen independently from each other in a wide range of compositions, as no loss of morphological order is observable in the SAXS traces upon domain size increase due to the solvent uptake, which is a particular advantage suggested for APCN. In case of PHEA(70)-*l*-PEPOx(30) - the sample with the highest hydrophilic content - no peak maximum could be determined. The reason for this characteristic could be that the broadly distributed PHEA-phase at this composition does not allow a higher order. It would not be expected that this can be changed upon swelling. This does not exclude that the however broadly distributed nanophases can be swollen independently (see **Figure 3.6 A**).

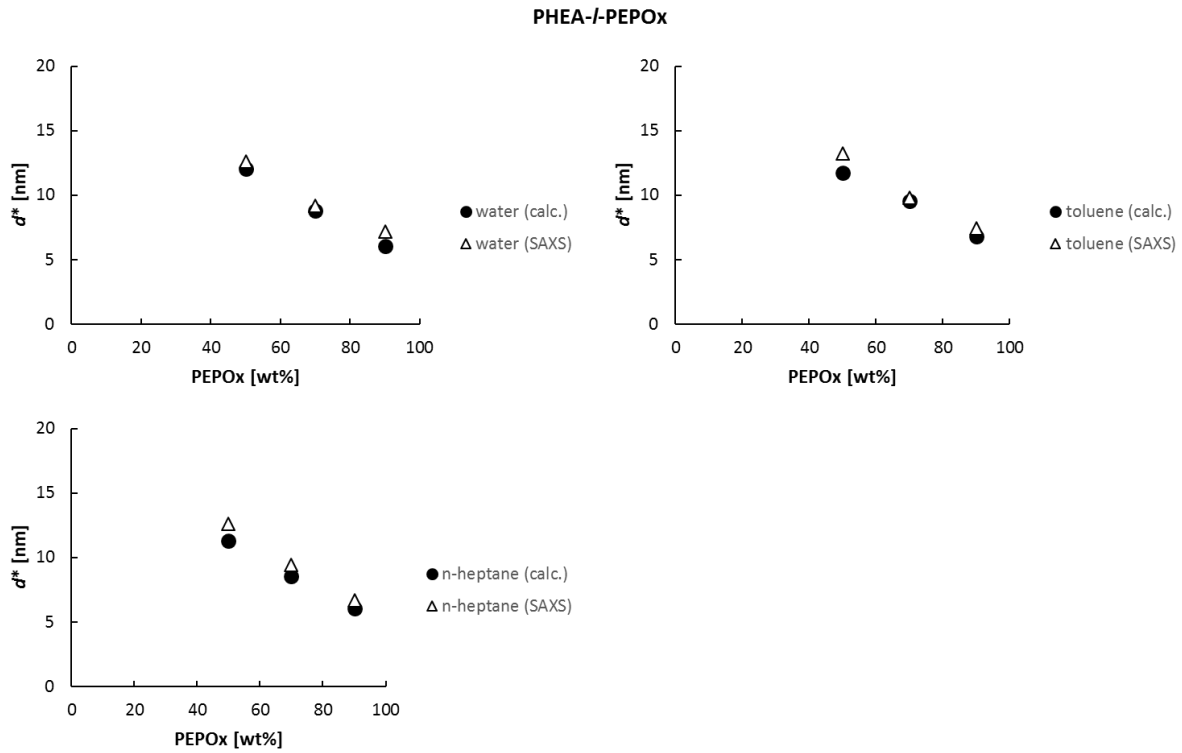

Figure 3.7 Comparison of the average long-periods *d** for PHEA-*l*-PEPOx conetworks with varied PEPOx content in the swollen state between data obtained by SAXS and calculations based on the respective swelling ratios S_g (for more details see Experimental Section 3.5).[121]

In order to validate the proposed ideal swelling behavior of the here presented APCN, the swelling data were used to estimate the volume change of the single polymer phases based on the domain size data summarized in **Table 3.1**. To this end, the volume change of the phases upon swelling was calculated under the simplified presumption that the phases swell selectively and the swollen volume is the simple sum of solvent and polymer volume. As seen in **Figure 3.7**, the estimated and the measured volume changes upon swelling match. Thus, the calculation of the swelling data confirms the statement that the PHEA-*l*-PEPOx APCNs show the individual swelling behavior that has been predicted by many authors.

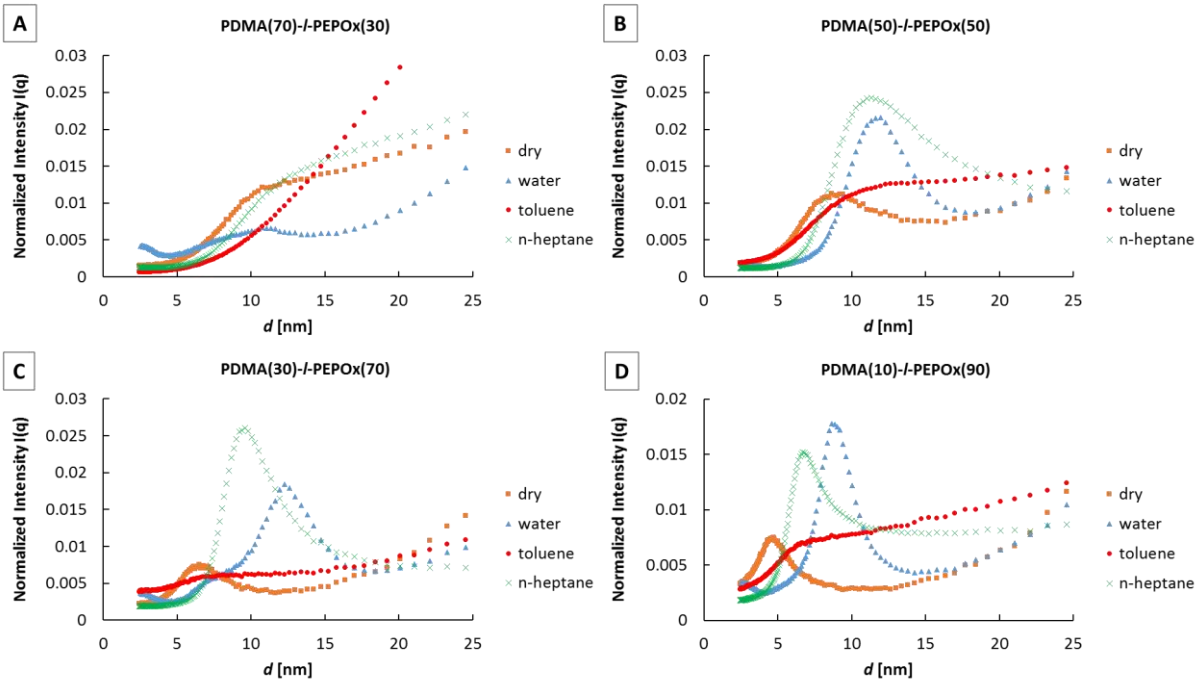

Figure 3.8 Comparative SAXS curves obtained from PDMA-*l*-PEPOx conetwork samples with varying compositions under dry and swollen conditions (solvents: water, toluene or *n*-heptane). Measurements of dry samples were carried out for 1 h and swollen samples for 8 h. Intensities were normalized to the total number of counts of the respective measurement and *d* was calculated using $d = 2\pi/q$.[121]

In contrast to the low T_g PHEA-*l*-PEPOx, the PDMA-*l*-PEPOx APCNs contain a high T_g phase (PDMA) and toluene is not a phase selective solvent. The latter implies that PDMA and PEPOx are not fully immiscible, which might result in a less pronounced nanophase separation and thus in a different swelling behavior. This is supported by the fact that the scattering intensity of the dry PDMA-based ACPNs is about 2-3 times lower than that of the PHEA-based system (see **Figure 3.3**). The SAXS profiles of the swollen PDMA-*l*-PEPOx conetworks in water, toluene and *n*-heptane depicted in **Figure 3.8** are significantly different from those found for the PHEA-*l*-PEPOx system, which is similar in topology, cross-linking, and swelling (see **Figure 3.6**). Again, only APCNs with at least 50 wt% PEPOx exhibit an ordered nanostructure that is regular enough to show d^* values in dry and swollen state.

The swelling in toluene results in a loss of order, which is evident by the broad, weak signal without a distinguishable maximum peak. This is typical for an unselective solvent, because both phases take up solvent reducing the contrast and due to mixing of the polymers, the order of the system will eventually disappear. This is supported by the high swelling ratios in toluene for all compositions.

Swelling in *n*-heptane on the other hand shows the signal shifting typical for selective swelling of a single nanophase in an APCN without losing order. In most cases, the intensity of the

scattering is even enhanced compared to the dry sample. The shift of *d** upon swelling is in the range of the *n*-heptane PHEA-*l*-PEPOx systems. A similar picture is seen for water. However, the peak shifts towards larger *d** values are greater than for all other swelling experiments in the cases of PDMA-*l*-PEPOx APCNs with higher PEPOx content. For example, both APCNs with 90 wt% PEPOx take up 20 wt% of water. While the PHEA system shows an increase in the *d** value of 5.2 to 7.4 nm, the PDMA-system shifts from 4.9 to 9.0 nm.
In order to investigate the influence of previous solvent swelling on the nanophasic structure of the different APCN systems, samples of the respective conetworks were dried and analyzed by SAXS after successive swelling in water, toluene and *n*-heptane. The obtained SAXS traces are shown in **Figure 3.10** (Experimental Section) and respective *d** values are compared in **Table 3.2** (Experimental Section), confirming our expectation that the polymer phases return to their original state after solvent induced swelling.

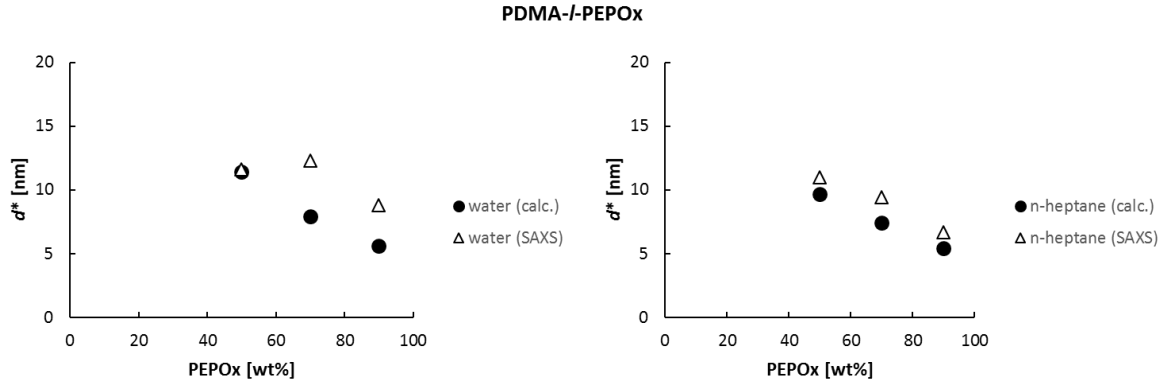

Figure 3.9 Comparison of the average long-periods *d** for PDMA-*l*-PEPOx conetworks with varied PEPOx content in the swollen state between data obtained by SAXS and calculations based on the respective swelling ratios S_g (for more details see Experimental Section 3.5).[121]

The domain size calculations upon swelling for the PDMA-*l*-PEPOx system were carried out as described above and compared to the respective SAXS data in **Figure 3.9**. In contrast to the PHEA-based APCNs, the calculated *d** values for water-swollen PDMA-based APCNs with a PEPOx-content of 70 and 90 wt% are significantly lower than those measured with SAXS. This indicates that there must be a change in nanostructure, e.g., by fusion of separated regions to larger structures, that causes this phenomenon. This might be due to the fact that the polymer phases are partially mixing in the dry state and this mixing is reversed by solvent uptake. This is supported by the generally smaller nanophases found by SAXS for PDMA-*l*-PEPOx. Further, as seen in the SAXS traces of these APCNs in **Figure 3.8 C** and **D**, the SAXS curves of the water-swollen samples show a shoulder at lower *d* values. This could originate from further isolated domains that are not reached by the solvent or swell without being fused

with other domains of the same polymer. The calculated *d** value for water-swollen PDMA(50)-*l*-PEPOx(50) is again matching that of the measured value. This is expected, because the higher content of the swelling PDMA-phase will allow the formation of a fully continuous polymer phase. In case of *n*-heptane swollen PDMA-*l*-PEPOx conetworks, the calculated domain sizes coincide with the measured SAXS data. This is expected due to the high content of the swelling PEPOx-phase resulting in a continuous nanostructure.

3.4 Conclusions

The novel hydrophobic cross-linker PEPOx was copolymerized with the proton-donor monomer HEA or alternatively with the the proton-acceptor monomer DMA to obtain two new families of APCNs. Both networks were swollen in water, toluene, and *n*-heptane and the change in their nanostructure was followed by SAXS. The DMA-based APCN showed significant changes in its nanostructure upon swelling. This would be expected, because a change of the volume ratios of the polymer phases will most likely result in a change in the nanostructure as well. A similar finding was reported in our previous study, which combined the two polymer phases PMOx and PEhAc. Both networks have in common that polymer phases form no strong secondary bonds between the phases. On the other hand, the APCN PHEA-*l*-PEPOx did not show significant nanostructural changes upon swelling in all applied phase-selective solvents for all compositions in the range of 50 to 90 wt% PEPOx. This is the first example of an APCN which was reported with such an ideal swelling behavior. In contrast to the other investigated APCNs, this network contains hydrogen bridges within the HEA-phase as well as between the PHEA and the PEPOx phase. This might be stabilizing the formed nanostructure of the dry APCN. The energy required for breaking these hydrogen bonds will then be higher than that obtainable by changes of the nanophasic structures upon swelling. Further experiments will be required to verify this presumption and to establish APCNs that have a broader range of well-organized independently swelling nanophases.

3.5 Experimental Section / Methods

Instruments:

All ^{1}H NMR experiments were performed on a Agilent DD2-500 spectrometer with 5 mm triple resonance H(C,X) probe operating at 500 MHz and 25 °C with $CDCl_3$ as solvent. Chemical shifts are given in ppm relative to the signal caused by residual nondeuterated solvent.

Polymerizations were conducted in a CEM Discover synthesis microwave equipped with a noninvasive vertically focused IR temperature sensor. Before usage, the polymerization flasks (Schott Duran) were dried at 150 °C overnight and filled under argon atmosphere.

SAXS experiments were carried out at a Bruker NANOSTAR with a VANTEC-2000 detector and an IμS Microfocus source (Incoatec GmbH) with a Cu-anode (wavelength λ = 0.154 nm)

and integrated Montel Optic. The distance between sample and detector was 107 cm and calibration was performed with a silver behenate standard. All measurements were carried out under vacuum at room temperature. Swollen network samples were placed with the respective solvent in quartz glass capillaries (1 mm diameter), which were sealed on both ends. SAXS patterns of dry samples were accumulated over 1 h and swollen networks over 8 h, followed by azimuthal integration to obtain the scattered intensities as a function of the magnitude of the scattering vector $q = 4\pi\sin(\theta)/\lambda$ (2θ = diffraction angle).

Table 3.2 Comparison of domain size data determined by SAXS analysis of dry APCN films before and after swelling experiments.

APCN	d^*_{dry} [nm][a]	d^*_{dry} [nm][b]
PHEA(70)-*l*-PEPOx(30)	19.2[c]	20.1[c]
PHEA(50)-*l*-PEPOx(50)	10.5	10.5
PHEA(30)-*l*-PEPOx(70)	7.8	8.0
PHEA(10)-*l*-PEPOx(90)	5.2	5.1
PDMA(70)-*l*-PEPOx(30)	10.5[c]	12.0[c]
PDMA(50)-*l*-PEPOx(50)	9.0	8.8
PDMA(30)-*l*-PEPOx(70)	6.8	6.7
PDMA(10)-*l*-PEPOx(90)	4.9	4.9

[a] washed and dried conetwork samples; [b] washed and dried samples measured after successive swelling experiments in water, toluene and *n*-heptane; [c] d^* estimated from shoulder signal.

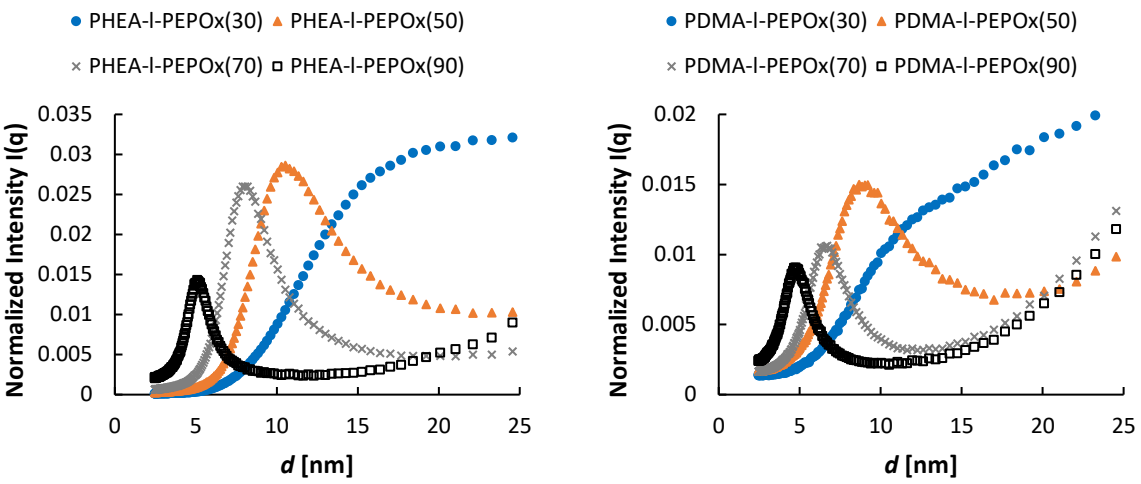

Figure 3.10 SAXS profiles of dry PHEA-*l*-PEPOx (left) and dry PDMA-*l*-PEPOx (right) conetwork films after successive swelling in water, toluene and *n*-heptane. All measurements were carried out for 1 h. Intensities were normalized to the total number of counts of the respective measurement and *d* was calculated using $d = 2\pi/q$.[121]

Calculations based on SAXS-data:

Domain size data (**Table 3.1**):

The presented values were calculated based on equation (1). Densities ρ of the respective polymers are given under **Table 3.1**. For this calculation, a cubic structure model was assumed and the domain sizes of the PEPOx-phase d_{PEPOx} were calculated as according to equation (1).

$$d_{PEPOx} = \frac{d^*_{dry}}{1+((wt\%_{polyacrylate}*\rho_{PEPOx})/((100-wt\%_{polyacrylate})*\rho_{polyacrylate}))^{1/3}} \qquad (1)$$

Calculated long-periods *d** based on swelling ratios S_g (**Figure 3.7** + **Figure 3.9**):

Theoretical long-periods $d^*_{swollen}$ of swollen APCNs based on the domain sizes of the polymer phases obtained by equation (1) were calculated according to equation (5) by utilizing the respective gravimetric swelling ratio S_g of the network in the solvent (see **Figure 3.2**) and the density of the respective solvent ρ_{solv}. This was calculated under the assumption that the solvent uptake of the respective polymer phase is exclusive (PHEA or PDMA in water; PEPOx in toluene or *n*-heptane) and the swelling of these phases is simply an addition of the volumes of solvent and polymer. First, the mass swelling ratio S_g is transferred to the respective volume swelling ratio S_V:

$$S_V = \frac{\frac{(S_g-1)}{\rho_{solv}}+\frac{wt\%_{phase1}}{\rho_{phase1}}+\frac{wt\%_{phase2}}{\rho_{phase2}}}{\frac{wt\%_{phase1}}{\rho_{phase1}}+\frac{wt\%_{phase2}}{\rho_{phase2}}} \qquad (2)$$

Then the effective volume swelling ratio of the respective, selectively swelling polymer phase is calculated by:

$$S_{v,phase} = \frac{(S_v - 1)}{vol\%_{phase}} + 1 \quad (3)$$

The *d* of the swollen phase is calculated by:

$$d_{phase,swollen} = d_{phase,dry} * (S_{V,phase})^{\frac{1}{3}} \quad (4)$$

The new long-period is calculated by:

$$d^*_{swollen} = d_{phase1,swollen} + d_{phase2,dry} \quad (5)$$

Atomic force microscopy (AFM) was performed with a Veeco Dimension Icon Scanning Probe Microscope (Veeco Instruments) equipped with a Nanoscope V Controller and an AVH-1000 Workstation. All network samples were cryofractured and measured in tapping mode using commercial tapping mode etched silicon probe (TESPA) cantilevers with resonance frequencies between 300 and 400 kHz. Phase images were recorded at 5% below the fundamental resonance frequency of the cantilever with a typical scan speed of 1 Hz and a resolution of 512 samples per line for a 300-400 nm scan size. Images were processed with the software NanoScope Analysis 1.5 (Bruker).

A dynamic mechanical analyzer DMA850 (TA Instruments, Inc.) was used to investigate the glass transition temperatures of the APCNs. Samples with dimensions of 30 mm x 5 mm x 0.4 mm (length, width, and thickness) were therefore prepared, dried and mounted to a film tension clamp. The conetworks were then analyzed up to a temperature of 150 °C with a heating rate of 3 K min^{-1}, a frequency of 1 Hz, an amplitude of 20 µm, and a preload force of 0.01 N.

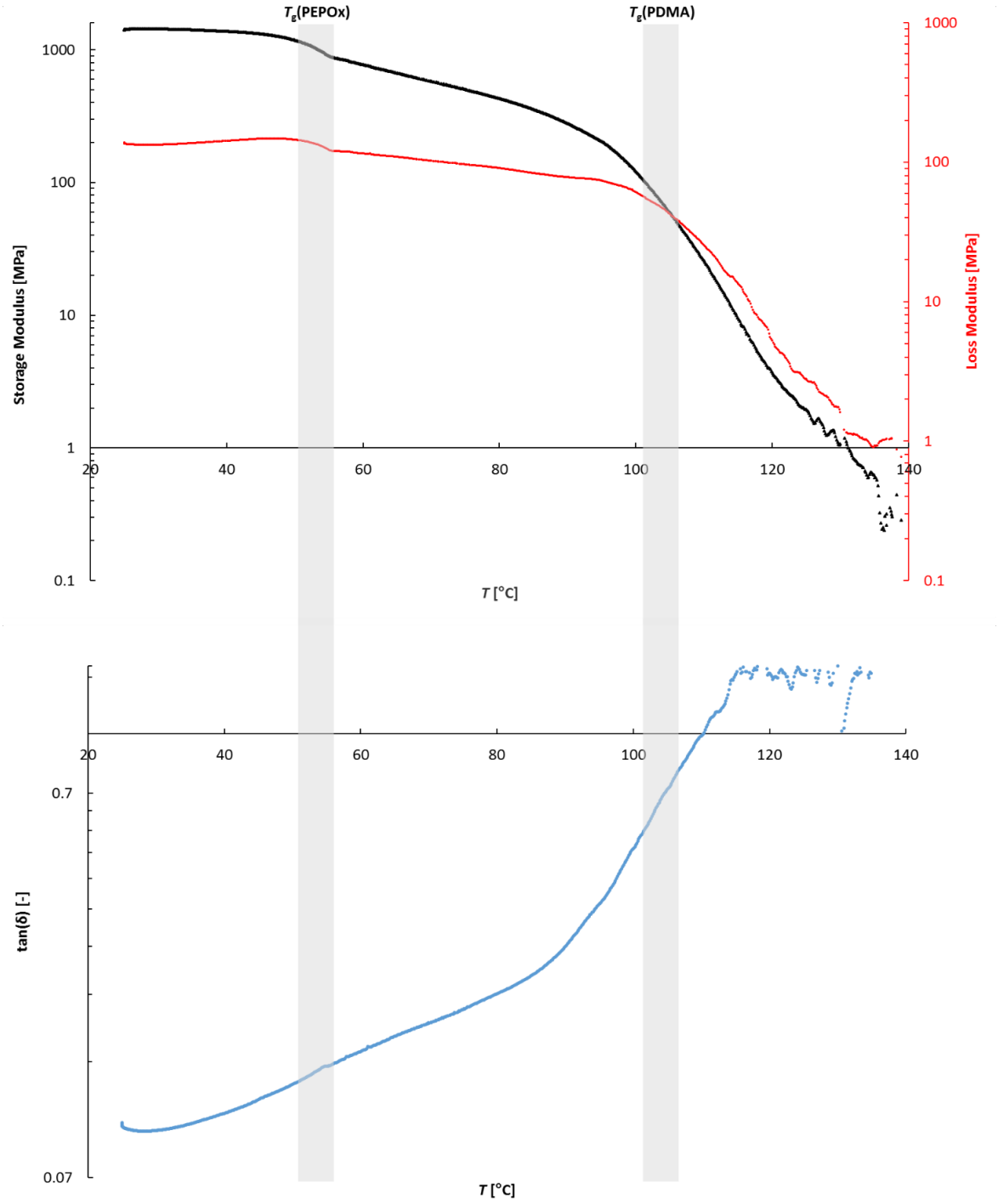

Figure 3.11 DMA data plots of PDMA(50)-*l*-PEPOx(50).[121]

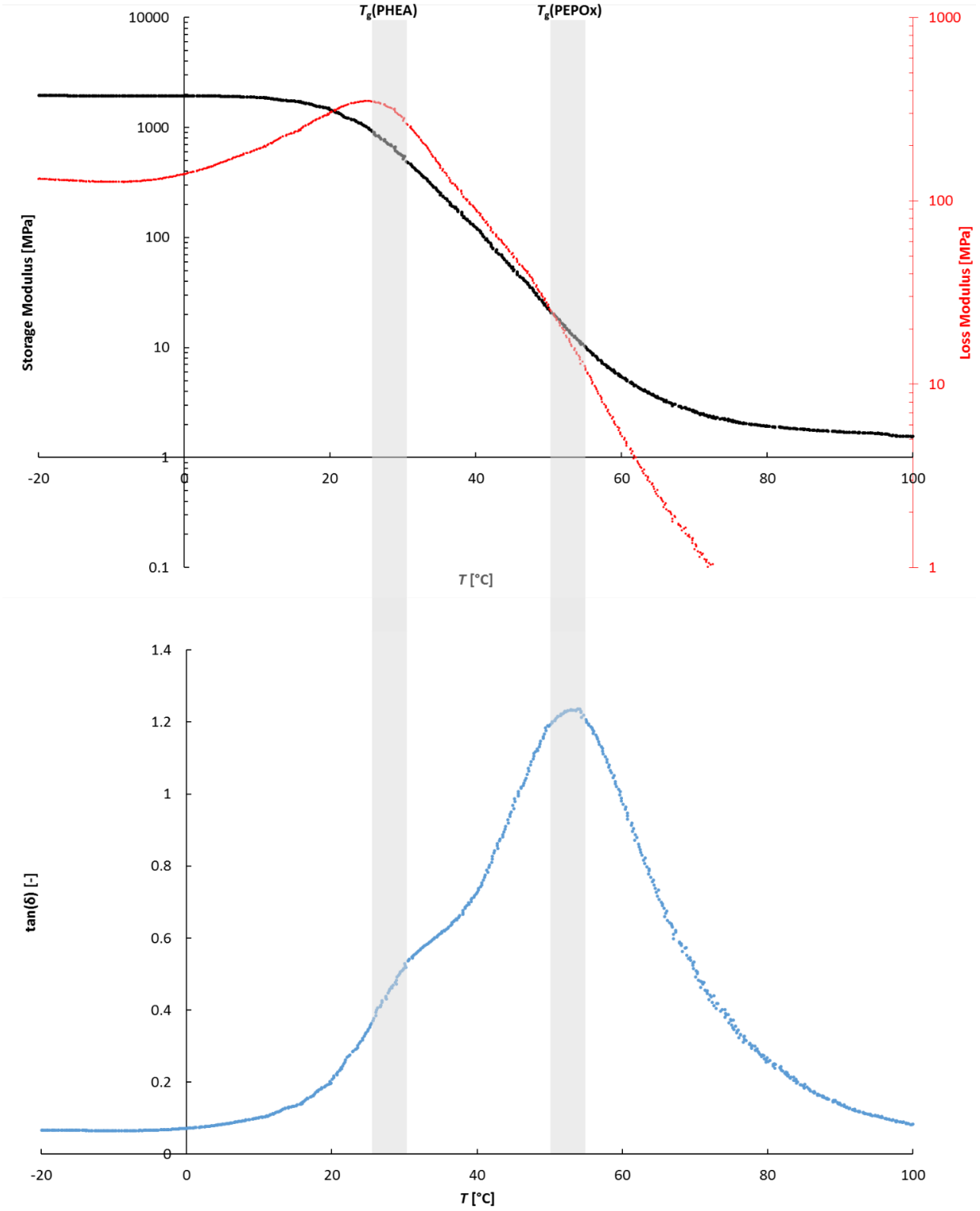

Figure 3.12 DMA data plots of PHEA(70)-*l*-PEPOx(30).[121]

Materials:

Acetonitrile (Fisher Chemical) was purified using a MB SPS Compact (M. Braun GmbH) solvent purification system. The initiator *trans*-1,4-dibromo-2-butene (DBB, Acros Organics) was recrystallized twice from *n*-heptane (VWR) and stored under argon atmosphere at −20 °C. *N*-[3-(Dimethylamino)-propyl]-methacrylamide (DMAP-MAA, Sigma-Aldrich), 2-hydroxyethyl acrylate (HEA, Alfa Aesar) and *N*,*N*-dimethylacrylamide (DMA, Sigma-Aldrich) were distilled for purification and stored under argon atmosphere at −20 °C. All solvents were purified by distillation under reduced pressure. 2-Ethylhexanoyl chloride (TCI), 2-chloroethylammonium chloride (Acros Organics) and other chemicals were used without further purification. Irgacure® 651 was kindly provided by Ciba Specialty Chemicals (now part of BASF).

Synthesis of N-(2-Chloroethyl)-2-ethylhexanamide:

The two step synthesis of the monomer 2-(1-ethylpentyl)-2-oxazoline (EPOx) was carried out according to literature.[210] After cooling a suspension of 13.49 g (14.37 mL, 0.083 mol, 1 eq.) 2-ethylhexanoyl chloride and 9.75 g (0.084 mol, 1 eq.) 2-chloroethylammonium chloride in 200 mL dichloromethane under argon atmosphere to −5 °C, 26.6 mL (19.37 g, 191 mmol, 2.3 eq.) triethylamine were added dropwise over a period of 45 min and the reaction mixture was stirred for 3 h at −5 °C. The reaction was terminated by addition of 70 mL water, the aqueous phase was extracted twice with 50 mL dichloromethane and the combined organic phases were washed with water and brine. The organic phase was then dried over $MgSO_4$, and after removal of the solvent under reduced pressure, the crude product was used in the following reaction step without further purification.

Synthesis of 2-(1-Ethylpentyl)-2-oxazoline (EPOx):

The crude product of N-(2-Chloroethyl)-2-ethylhexanamide was suspended in 50 mL tetrahydrofuran and added dropwise to 100 mL of a 25 wt% solution of KOH in water. After heating the reaction mixture to 50 °C for 16 h, it was cooled to ambient temperature and the aqueous phase was extracted twice with diethyl ether. The combined organic phases were washed three times with water and once with brine. The organic phase was subsequently dried over $MgSO_4$, the solvent was removed under reduced pressure and after distillation (81 °C oilbath temperature, 0.1 mbar) 8.69 g (0.051 mol) of the product in 62% yield (relative to 2-ethylhexanoyl chloride) was obtained as a colorless oil and stored under argon atmosphere at −20 °C.

Synthesis of Poly(2-(1-ethylpentyl)-2-oxazoline) (PEPOx) with DMAP-MAA End Groups:

2.61 ml (2.50 g, 14.79 mmol, 30 eq.) EPOx and 105.5 mg (0.49 mmol, 1 eq.) DBB as initiator were dissolved in 10 mL of dry acetonitrile under argon atmosphere and heated to 140 °C for

3.5 h in a synthesis microwave reactor. Subsequently, the living polymerization was terminated with a 12-fold molar excess of DMAP-MAA (1.07 mL, 5.92 mmol) at 45 °C for 72 h. After removal of the solvent under reduced pressure, the crude product was dialyzed against methanol for 20 h using benzoylated cellulose membranes (1000 MWCO). The solvent was removed under reduced pressure and 1.9 g of the purified slightly orange polymer was obtained in a yield of 71% and with 96% acrylamide end group functionalization.

^{1}H NMR (500 MHz, $CDCl_3$-*d*) δ = 0.87 (br. s., 190 H, $CH_2-C\mathbf{H_3}$) 1.28 (br. s., 127 H, $C\mathbf{H_2}-C\mathbf{H_2}-CH_3$) 1.51-1.59 (br. s., 127 H, $CH-(\mathbf{CH_2})_2$) 1.99 (s., 6 H, $C\mathbf{H_3}$-CCH_2) 2.16 (br. s., 4 H, CH_2-$C\mathbf{H_2}$-CH_2-NH) 2.37 – 2.82 (br. m., 38 H, $C\mathbf{H_2}$-CH_2-$C\mathbf{H_2}$-NH and $C\mathbf{H}$-$(CH_2)_2$) 3.27 (m., 12 H, N-$(C\mathbf{H_3})_2$) 3.35 – 3.90 (br. s., 129 H, N-$(C\mathbf{H_2})_2$) 3.99 (br. s., 4 H, $C\mathbf{H_2}$-CH) 5.36 (br. s., 2 H, $CC\mathbf{H_2}$) 5.57 (br. s., 2 H, CH_2-$C\mathbf{H}$) 5.93 (br. s., 2 H, $CC\mathbf{H_2}$) ppm.

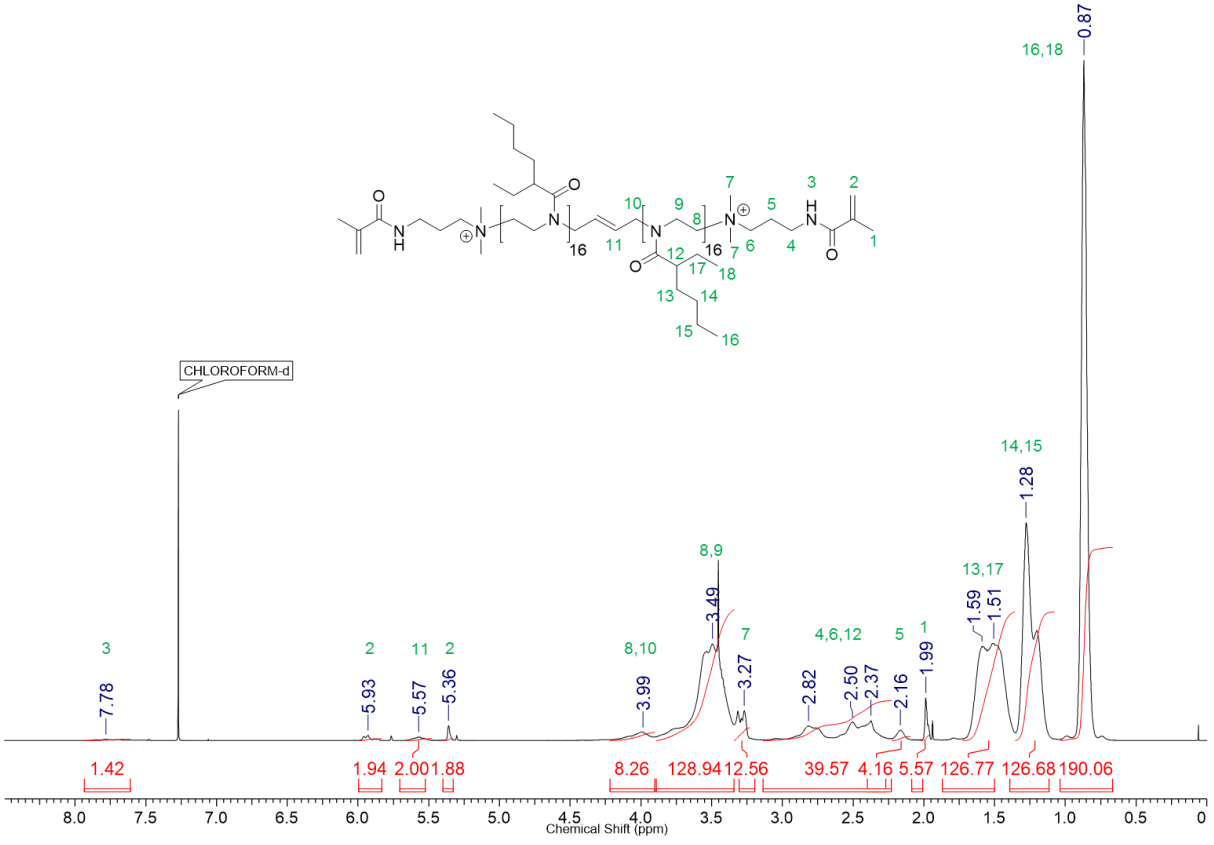

Figure 3.13 ^{1}H NMR spectrum of the macromeric cross-linker DMAP-MAA-PEPOx_{32}-DMAP-MAA in $CDCl_3$.[121]

Synthesis of PHEA-*l*-PEPOx, PDMA-*l*-PEPOx APCNs, and respective homopolymer networks:

The macromolecular crosslinker MAA-DMAP-PEPOx_{32}-DMAP-MAA was dissolved in either the respective monomer (HEA or DMA) or a mixture of the monomer and a small amount of 1-methoxy-2-propanol (see **Table 3.2**) to obtain a homogeneous solution by vortex mixing.

Subsequently, 2 mg of the initiator Irgacure 651 were dissolved and the reaction mixture was placed between two microscope slides covered with adhesive poly(propylene)-tape (Tesafilm). Beforehand, two additional strips of adhesive tape were placed on each end of one of the glass slides in order to control the thickness of the polymer film (about 50 µm per layer). The polymerization was carried out for 2 x 180 s under UV flash light (Heraflash, Heraeus Kulzer, Germany, λ = 340 nm) on each side. Afterwards, the network films were removed from the microscope slides and washed in chloroform for 20 h to calculate the sol/gel content of each network by the mass loss after the washing procedure. The homopolymer networks were prepared by photopolymerization of the pure PEPOx macromonomer; the PDMA and PHEA networks were photopolymerized using tetra(ethylene glycol) diacrylate (TTEGDA, 4.0 mol% for PDMA, 4.5 mol% for PHEA) as cross-linker.

Table 3.3 Listing of the compositions of the respective reaction mixtures used in APCN synthesis and gravimetrically determined gel content of each conetwork.

APCN	PEPOx [wt%]	PEPOx [mg]	HEA [µL]	DMA [µL]	1M2P [µL]	Gel content [wt%]
PHEA-*l*-PEPOx(30)	30	59.8	126.6	-	-	98.1
PHEA-*l*-PEPOx(50)	50	60.1	54.2	-	50	94.2
PHEA-*l*-PEPOx(70)	70	60.4	23.2	-	70	89.8
PHEA-*l*-PEPOx(90)	90	60.0	6.0	-	100	78.9
PDMA-*l*-PEPOx(30)	30	61.0	-	147.8	-	96.8
PDMA-*l*-PEPOx(50)	50	60.8	-	63.0	50	93.3
PDMA-*l*-PEPOx(70)	70	58.4	-	26.0	70	95.2
PDMA-*l*-PEPOx(90)	90	60.2	-	6.9	100	76.4

Determination of washed-out residues after swelling the raw conetworks in $CHCl_3$:

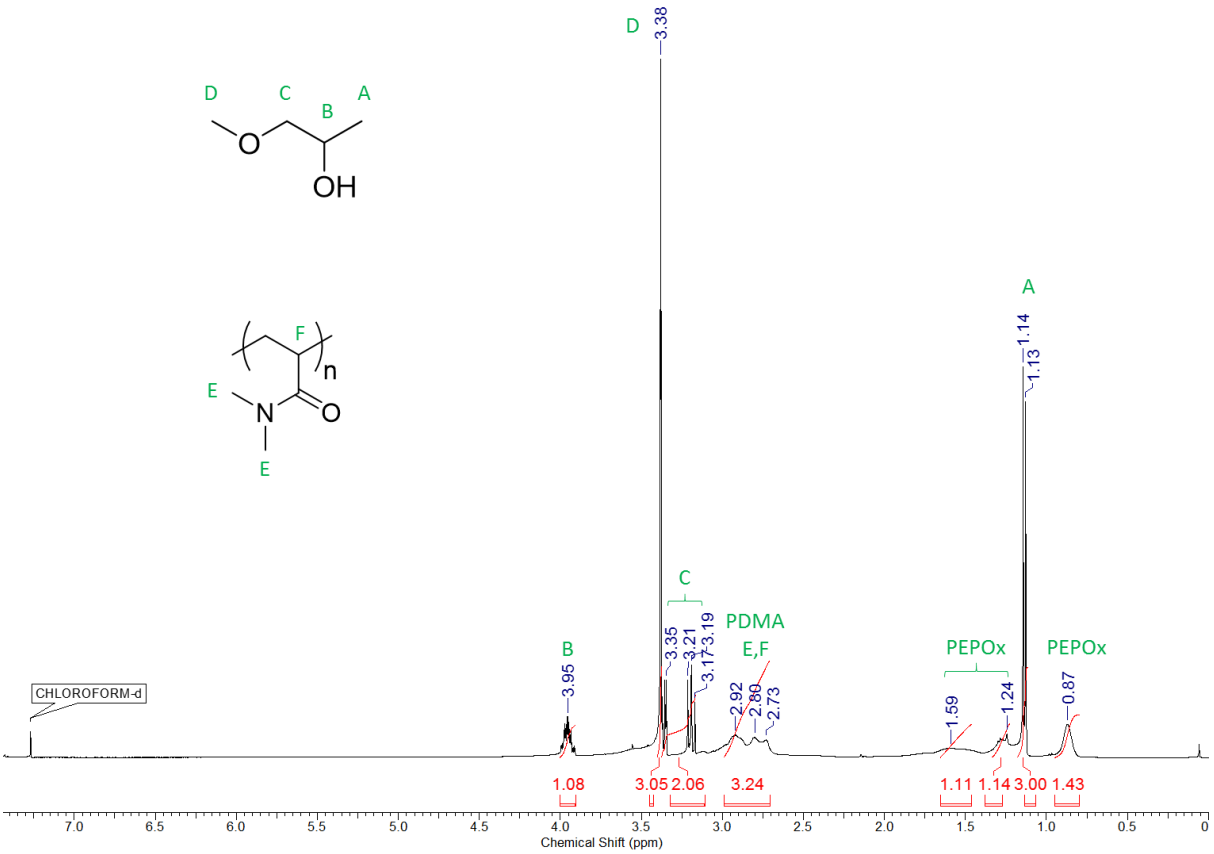

Figure 3.14 ^{1}H NMR spectrum of the washed-out residues of a raw PDMA(50)-*l*-PEPOx(50) conetwork in $CDCl_3$.[121]

Determination of the Swelling Behavior:

The equilibrium swelling ratios (swelling ratio $S_g = m_{swollen}/m_{dry}$) of the different network films were investigated gravimetrically. Therefore, a washed and dried sample was swollen in the respective solvent for 20 h and weighed. The network was successively pre-dried using a stream of compressed air followed by heating the sample to 60 °C under reduced pressure for at least 3 h and weighed again.

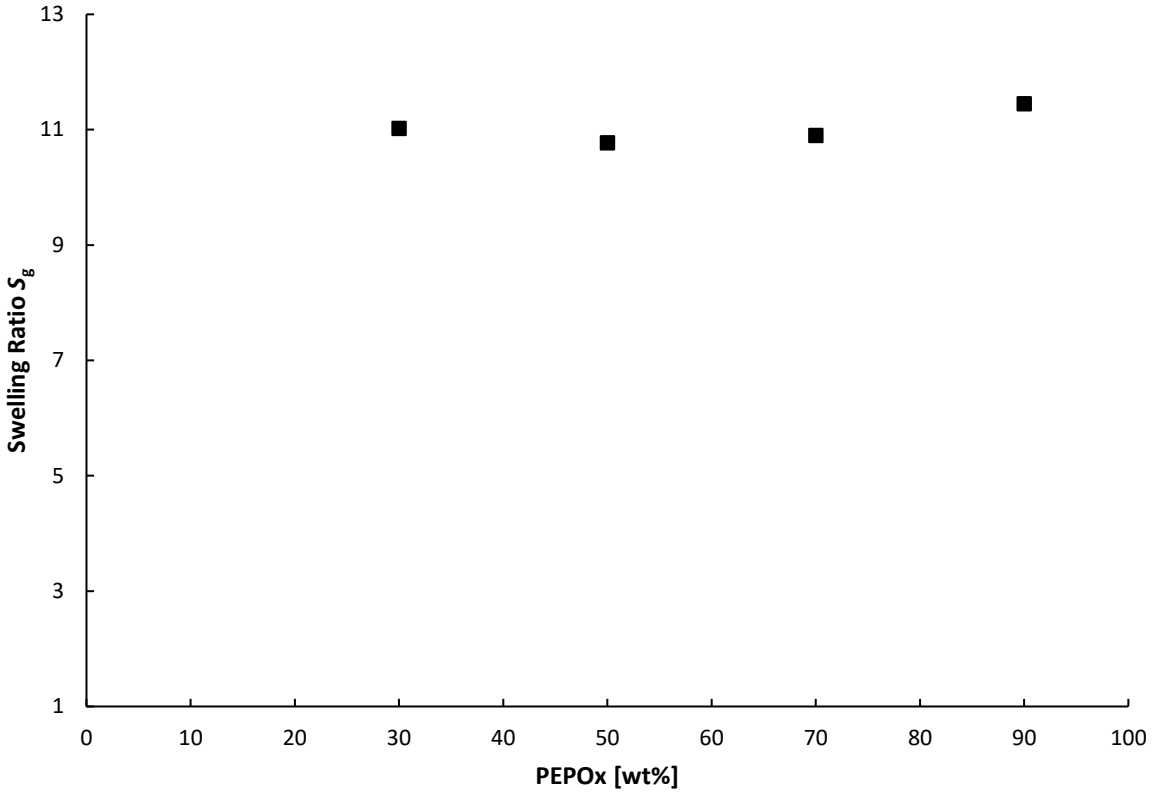

Figure 3.15 Swelling ratios of washed PDMA-*l*-PEPOx conetworks in $CHCl_3$ (swollen for 20 h at RT).[121]

4 Solvent Induced Nanophase Formation in Hydrophilic Segmented Polymer Networks based on Poly(ethylene glycol) and Poly(2-alkyl-2-oxazoline)s

4.1 Abstract

Segmented polymer networks (SPNs) can be considered as stabilized homogeneous blends of different polymers. They are mostly designed by polymers of very different polarity, e.g., in amphiphilic polymer conetworks (APCNs). These networks exhibit a well-ordered nanophase separation, but require a challenging synthesis procedure. The present study aims towards SPNs that are prepared by polymers with similar structure and polarity in order to investigate if they are still forming defined nanophases. Therefore, the similar hydrophilic polymers polyethylene glycol (PEG), poly(2-methyl-2-oxazoline) (PMOx), and poly(2-ethyl-2-oxazoline) (PEtOx) were chosen as polymer segments. The polymers were mixed and cross-linked *via* their acrylate end groups. The resulting SPNs were investigated with small-angle X-ray scattering (SAXS) and atomic force microscopy (AFM) regarding their nanostructures in dry and swollen state. PEG-PEtOx-SPNs are found to not form ordered nanostructures due to the partial miscibility of the polymers. PEG-PMOx-SPNs show a highly ordered nanophase separation depending on the degree of cross-linking and the mass ratio of the respective polymers. X-ray diffraction (XRD) measurements revealed that this is due to the influence of the cross-linking on the formation of PEG crystals. Thermal or toluene-induced melting of these PEG-crystals in lowly cross-linked PEG-PMOx-SPNs can be used to reversibly switch between a nanophase separated structure and a non-ordered structure composed of PEG crystals and PMOx, while the PEG crystals in the higher cross-linked SPNs seem to form within the boundaries of the PEG-nanophases. Additionally, the enzyme horseradish peroxidase entrapped in a PEG-PMOx-SPN with 50 wt% PMOx was activated in toluene, similar to a more elaborately produced APCN, to demonstrate a potential application of the developed SPN system.

4.2 Introduction

Blending different homopolymers is a common way to obtain materials with tailored properties. Cross-linking such blends to a low degree leads to so-called segmented polymer networks (SPNs). If the segments have a sufficient size in combination with a narrow size distribution, these materials can have two independently addressable interconnected polymer nanophases due to phase separation of immiscible polymers. The best known class of SPNs are amphiphilic polymer conetworks (APCNs), which generally merge hydrophilic and hydrophobic and thus immiscible polymers in a single material, enabling various specific applications. Such APCNs are capable of being swellable in orthogonal solvents such as water and heptane[213-

[214], or water and perfluorinated solvents.[192] Each of these orthogonal solvents is selectively swelling a polymeric nanophase, which allows to specifically include enzymes[215], sensing molecules[94,181], inorganic nanoclusters[213], or photocatalytic molecules[117] in these phases or to use them as separation membranes.[85,97] Entrapped this way, enzymes such as lipases[184] or chymotrypsin[183] can be greatly activated in organic solvents, either as thin films[216] or as nanoseparated microparticles.[170] Photocatalytic substances allow the improvement of solar cells by using fluorescence resonance energy transfer (FRET) between the two polymeric nanophases.[117] Another important application of APCNs is the use of the gas permeability of the organic phase in case of polydimethylsiloxane (PDMS), which allows applications such as extended-wear soft contact lenses[89] and gas sensors.[93] They can also be equipped with self-healing properties[127] or controllable thermo-responsiveness.[217] Another application that derives from these properties is the controlled release of antimicrobials[218] or other pharmaceuticals.[214] The nanophasic structure of the APCNs and also SPNs is generally formed in dry state and can be either retained upon swelling in a selective solvent[121] or erased when using a common solvent.[219]

The synthesis of SPNs is often quite elaborate, because usually polymers with contrary properties, e.g. PDMS and PEG, need to be forced into a homogeneous nanostructure to enable a uniform cross-linking reaction between both components. The verification of nanophase separation by atomic force microscopy (AFM)[78,96,120,127,191-192], solid-state NMR experiments[84,194-196,220], transmission electron microscopy (TEM)[118,196-197,221], scattering methods like small-angle neutron scattering (SANS)[177,198-205] and small-angle X-ray scattering (SAXS)[121,125,168,194,202,206-207,222-223] or simply by determination of two T_g values is often used as a proof for a successful synthesis.[214,224] The much simpler preparation utilizing polymers with similar properties is usually not considered. Since only very few polymers are fully miscible[225], as determined by, *inter alia*, properties like different stereoregularity[226], or distinction between homopolymer and respective blockcopolymer interactions[227], even such SPNs should still form a distinguished nanophase separation. An interesting example on this topic is given by DU PREZ and coworkers through the investigation of SPNs composed of hydrophilic poly(2-alkyl-2-oxazoline)s (PMOx or PEtOx) and hydrophobic poly(methyl methacrylate) (PMMA) in different ratios.[228] While the conducted swelling experiments with water or acetone clearly show the amphiphilic character of the formed conetworks, DSC analysis reveals shifted or even mixed glass transition temperatures for these SPN samples contrary to the corresponding polymer blends, which only exhibit complete polymer phase separation by means of two separate T_g values. These findings underline the complex morphological behavior of multi-component polymer networks.

In order to shed more light on the role of cross-linking on the behavior of blends of hydrophilic polymers, we chose to synthesize SPNs based on the combination of the purely hydrophilic

polymers PEG and either PMOx or PEtOx, respectively. These components were chosen for two reasons: Firstly, the network synthesis can be conducted in water as a suitable shared solvent for each polymer, avoiding elaborate compatibilizing protection strategies as part of the conetwork synthesis.[213] Secondly, although the chosen polymers are known to have very similar solubility characteristics[7,229], PEG is, in contrast to both POx polymers, soluble in toluene. This difference in solubility might be the key to selectively address a nanophase in SPNs based on entirely hydrophilic polymers.

4.3 Results and Discussion

SPNs can be designed in various ways[107], including the copolymerization of monomers with appropriate macromonomeric crosslinkers[230-231] or direct cross-linking of different functionalized homopolymers.[78,232] The latter way was chosen to prepare SPNs by photo-cross-linking of *α*,*ω*-functionalized macromonomers with either acrylate end groups (commercially available PEG-diacrylate; M_n = 4000 g/mol) or methacrylamide end groups (MAA-DMAP-PEtOx$_{40}$-DMAP-MAA, M_n(SEC) = 4200 g/mol, $Đ$ = 1.13, end group functionality > 96% (^{1}H NMR, see **Figure 4.16**, Experimental Section). These polymers were deployed in the conetwork synthesis utilizing a free radical copolymerization reaction initiated by UV radiation as illustrated in **Figure 4.1**. Conetworks with three different PEG:PEtOx compositions were synthesized, varying between 70 to 30 wt% PEG content (see **Table 4.1**, Experimental Section). Soluble residues were removed by washing the obtained conetwork films in chloroform after cross-linking, and the respective gel content was determined gravimetrically, yielding the gel content values shown in **Table 4.1**. A gel content between 84 and 96 wt% was found for the dried PEG-PEtOx conetwork samples, indicating successful conetwork formation in all cases.

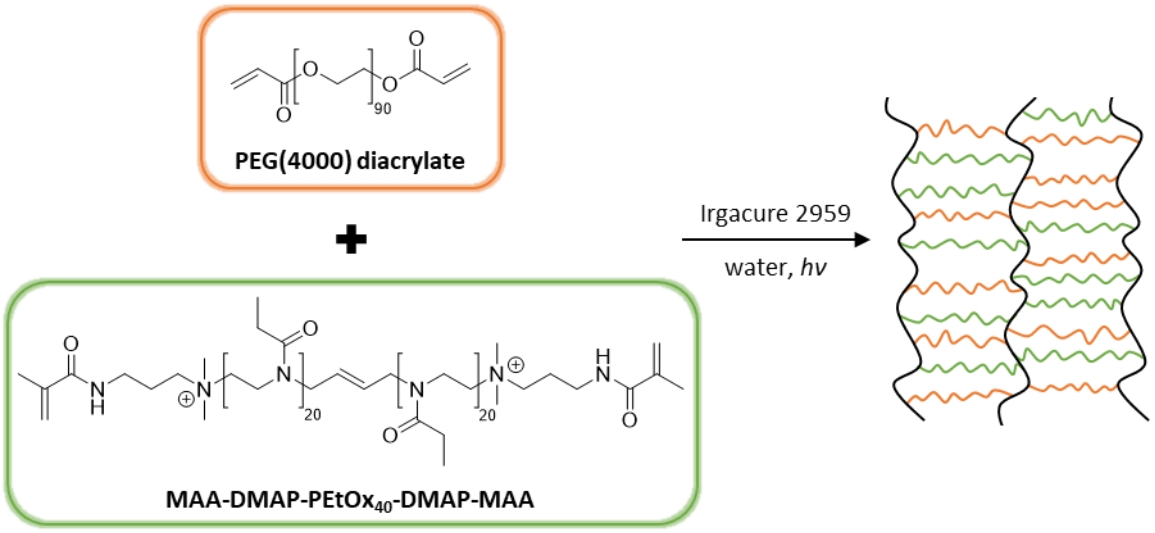

Figure 4.1 Schematic illustration of the SPN synthesis *via* free radical photopolymerization of AA-PEG$_{90}$-AA and MAA-DMAP-PEtOx$_{40}$-DMAP-MAA.

The images of the dried SPN samples presented in **Figure 4.2**(**A**) show a significant difference in the optical appearance. Conetworks with 30 wt% PEG content are entirely transparent, but rising the PEG fraction to 50 or 70 wt% led to observably cloudy network samples. A similar finding was reported by Clarke and Tew.[122] Bottlebrush APCNs based on PEG and poly(dimethyl siloxane) (PDMS) with varying PEG content were studied in this work and a correlation between the PEG content and the optical appearance of the conetworks was discussed. Further investigations of these APCNs revealed high degrees of crystallinity in the PEG domains up to 82.4 % according to DSC. By performing similar DSC analyses of the here presented SPNs, degrees of crystallinity (X_C) of the PEG phases between 14.35 (50 wt% PEG) and 49.6% (70 wt% PEG) were calculated [ΔH_f(PEG) = 137 J/g[122], see **Figure 4.13**, Experimental Section). The existence of the crystalline PEG domains was also confirmed by X-ray diffraction (see **Figure 4.15**, Experimental Section). Furthermore, in order to confirm that the crystallization of PEG chains is the only origin of the observed cloudiness in the conetworks with at least 50 wt% PEG content, the dried samples were heated to 50 °C. The crystalline segments should be melting at this temperature according to DSC. The heated SPN films display full transparency, indicating that not only the PEG crystals are molten, but the amorphous PEG also forms smaller phases than the crystals (see **Figure 4.2**(**B**)).

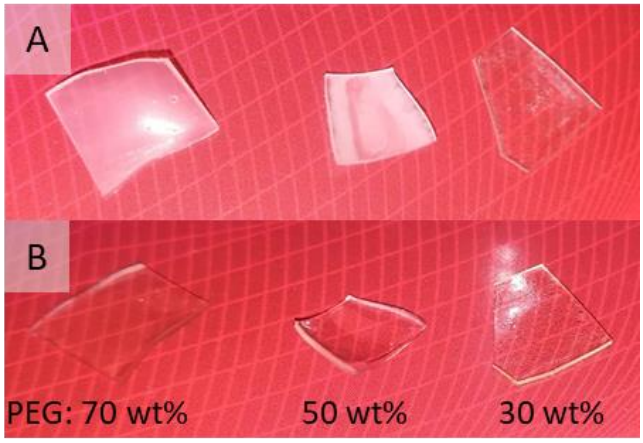

Figure 4.2 Comparison of the optical appearance of the washed and dried PEG-PEtOx SPNs with observable cloudiness for samples with at least 50 wt% PEG at room temperature (A) and heated to 50 °C (B).

In **Figure 4.3**, the gravimetrically determined swelling ratios S_g of the PEG-PEtOx conetworks in toluene or water are shown in respect to the PEtOx mass fractions. As expected, the swelling ratio in toluene decreases from S_g = 2.3 to 1.5 with increasing PEtOx content, underlining the swelling selectivity of toluene for PEG. A similar decrease in swelling ratios corresponding to increasing PEtOx mass fractions is seen for water as a common solvent for both polymers, however leading to much higher swelling ratios in the range from S_g = 4.4 to 3.6 due to the solvent uptake of both polymer components. This observation could either be explained by a somewhat lower hydrophilicity of PEtOx compared to PEG or by a higher slightly higher cross-link density in conetworks with increased PEtOx content.

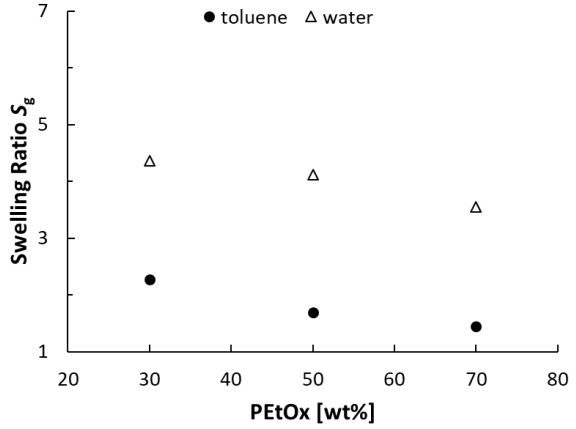

Figure 4.3 Gravimetrical swelling ratios S_g of PEG-PEtOx-SPNs with varying PEtOx content swollen in toluene or water. All experiments were performed in triplicate with standard deviations of less than 5%.

For a better understanding of the nanostructural morphology of the SPNs, various SAXS patterns of dry and swollen conetwork samples were recorded. In order to analyze the swollen networks, the respective sample film was transferred to a quartz tube filled with the respective solvent, which was afterwards sealed by melting the quartz tube tip. The obtained SAXS traces showing the normalized intensity $I(q)$ against long-period d calculated as $d = 2\pi/q$ with the scattering vector q obtained by azimuthal integration of the X-ray scattering patterns are presented in **Figure 4.4**. In case of the dried SPN samples, no nanophase separation between the PEG and the PEtOx chains can be identified for each respective composition due to the lack of distinguishable trace maxima. Therefore, it can be presumed that both polymers are at least to some extent miscible independent from the respective polymer mass fractions. Thus, no expected distinguished phase separation occurs. The SAXS traces of the PEG-PEtOx-SPNs swollen in toluene display no differing trends in regard to the varying polymer mass fractions as well. However, despite toluene being a selective solvent for PEG, no recognizable peak maxima d^* could be determined for these samples. The mere presence of shoulder-signals in the range of d = 10 nm indicates prevailing miscibility between the polymer chains along the network, possibly due to a higher contribution from the enthalpy of polymer mixing than from the enthalpy of PEG solution in toluene. In further SAXS experiments, the morphological influence of additional solvents (benzene, *p*-xylene, methyl *tert*-butyl ether, or tetrachloromethane) on the SPNs were tested, but according to these findings, it was not possible to induce distinct nanophase separation through uptake of a selective solvent for the studied SPN system based on PEG and PEtOx (spectra not shown). The predominant miscibility of the two polymers was confirmed by DSC measurements of the cross-linked and the non-cross-linked PEG/PEtOx mixtures, both indicating mixed T_g areas (see supplementary **Figures S3** and **S4**).

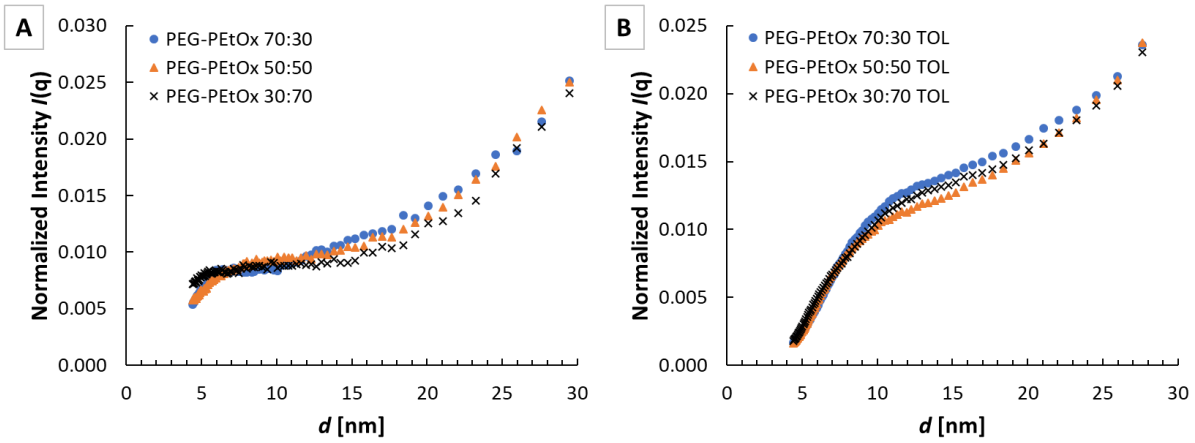

Figure 4.4 Graphical comparison of the SAXS traces of PEG-PEtOx-SPNs with different compositions in the dried state (A) and swollen in toluene (B). Scattering data was collected for 1 h for dried samples and 8 h for swollen networks. All intensities were normalized to the total number of counts of the respective measurement and d was calculated as $d = 2\pi/q$.

Since PEG and PEtOx are obviously too well miscible to result in a clear recognizable phase separation, further SPNs were synthesized, in which the PEtOx fraction was replaced by the more hydrophilic $PMOx_{39}$ with DMAP-MAA end groups ((MAA-DMAP-$PMOx_{39}$-DMAP-MAA, Mn(SEC) = 3500 g/mol, $Đ$ = 1.19, end group functionality > 98% (determined by ^{1}H NMR, see **Figure 4.17**, Experimental Section). The PEG-PMOx-SPNs were derived in the same conetwork compositions and under similar synthesis conditions (see Experimental Section, **Table 4.1**). In order to vary the degree of cross-linking, a second set of SPNs was prepared from a diluted solution to give the polymer chains more freedom to separate. In the following, these two sets of SPNs are named highly cross-linked (HC)-PEG-PMOx-SPNs and lowly cross-linked (LC)-PEG-PMOx-SPNs for easier differentiation. All obtained PEG-PMOx conetworks exhibit very high gel mass fractions between 96 and 99 wt%. Further, the HC- as well as the LC-PEG-PMOx-SPN films display a similar optical appearance with observable cloudiness in samples with a PEG mass fraction of at least 50 wt% (see **Figure 4.5**). This cloudiness was analogously identified as formation of crystalline PEG-domains in the dried networks utilizing DSC measurements and observing the change in optical appearance upon heating the cloudy samples above 50 °C and thus melting crystalline domains (T_m(DSC) = 43 °C; **Figure 4.5**(**B**); for X-ray diffraction see **Figure 4.15**).

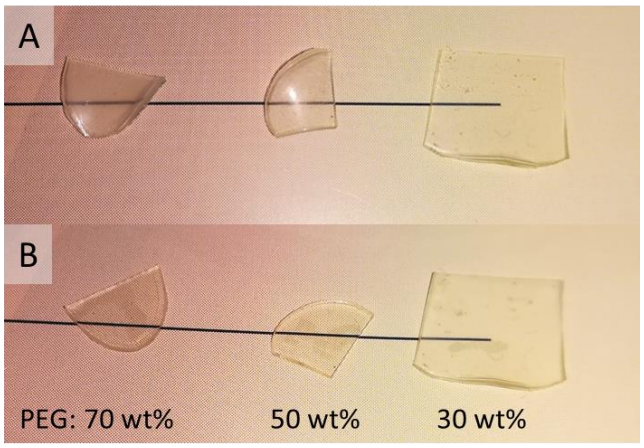

Figure 4.5 Comparison of the optical appearance of the washed and dried HC-PEG-PMOx network films at room temperature (A) and heated to 50 °C (B) to melt the crystalline domains.

Characterization of the gravimetrical solvent uptake of the different PEG-PMOx conetworks was conducted in toluene and water, respectively (**Figure 4.6**). In case of toluene, nearly identical gravimetrical swelling ratios S_g ranging between S_g = 2.1 and 1.3 were determined for the HC-PEG-PMOx SPNs in comparison with the previously discussed PEG-PEtOx conetworks (see **Figure 4.3**). These swelling ratios are similar for the lower cross-linked SPNs, indicating that the PEG phase is selectively swollen by toluene, because the degreee of cross-linking plays no role. The S_g values for HC-PEG-PMOx-SPNs swollen in water as mutual solvent for both polymeric components are significantly higher than those of the PEG-PEtOx SPNs, and contrary display an increase from S_g = 5.4 to 6.3 with PMOx mass fractions increasing from 30 to 70 wt% (**Figure 4.6**(**A**)). Considering the same points as discussed for the PEG-PEtOx-SPN above, it is suggested that PMOx exhibits an even higher hydrophilicity than PEG. The S_g values for the LC-PEG-PMOx-SPNs derived from diluted aqueous solutions show the same trend, but are about 50% higher, proving that these SPNs are indeed cross-linked to a lower degree.

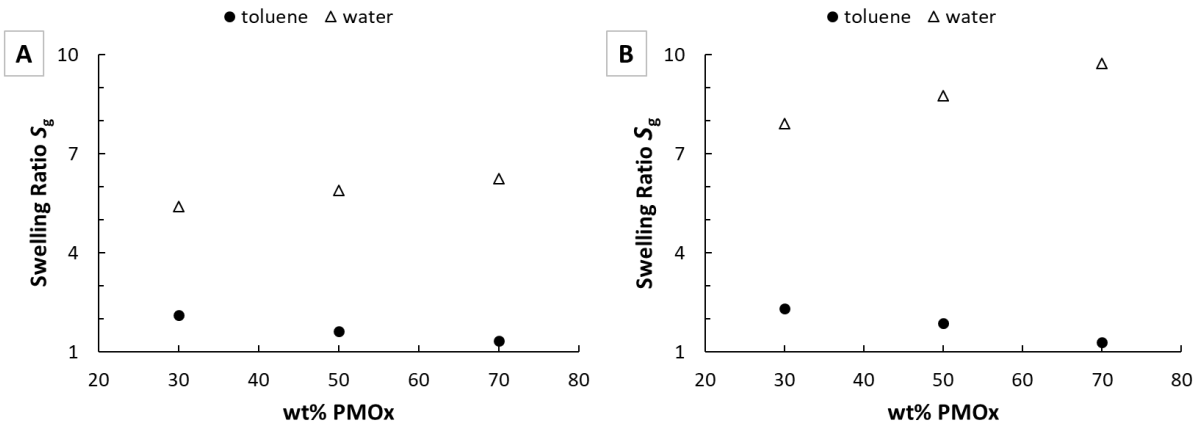

Figure 4.6 Gravimetrical swelling ratios S_g of PEG-PMOx-SPNs with varying PMOx content swollen in toluene or water. The SPNs are derived from aqueous solutions with respective total polymer masses of 1 g (A) or 215 µg (B) per mL of water. All experiments were performed in triplicate with standard deviations less than 5%.

As shown in **Figure 4.7**, all SAXS patterns of dry HC-PEG-PMOx SPNs display distinctly separated nanophases with peak maxima indicating respective long-periods of d^* = 9.4 nm, 10.8 nm and 11.6 nm with increasing PMOx mass fraction. When the networks are swollen in water – a mutual solvent for both hydrophilic polymers - the long-period peaks are only recognizable as low-intensity shoulder signals in the respectively similar nanometer range. This was expected, because the uptake of water leads to the swelling of both polymer phases simultaneously, leading to a loss of order and decreased scattering contrast within the networks. Contrary to this, the nanophasic structure is retained upon swelling in the selective solvent toluene, causing a shift in the respective scattering peak of each SPN composition to greater long-period values.

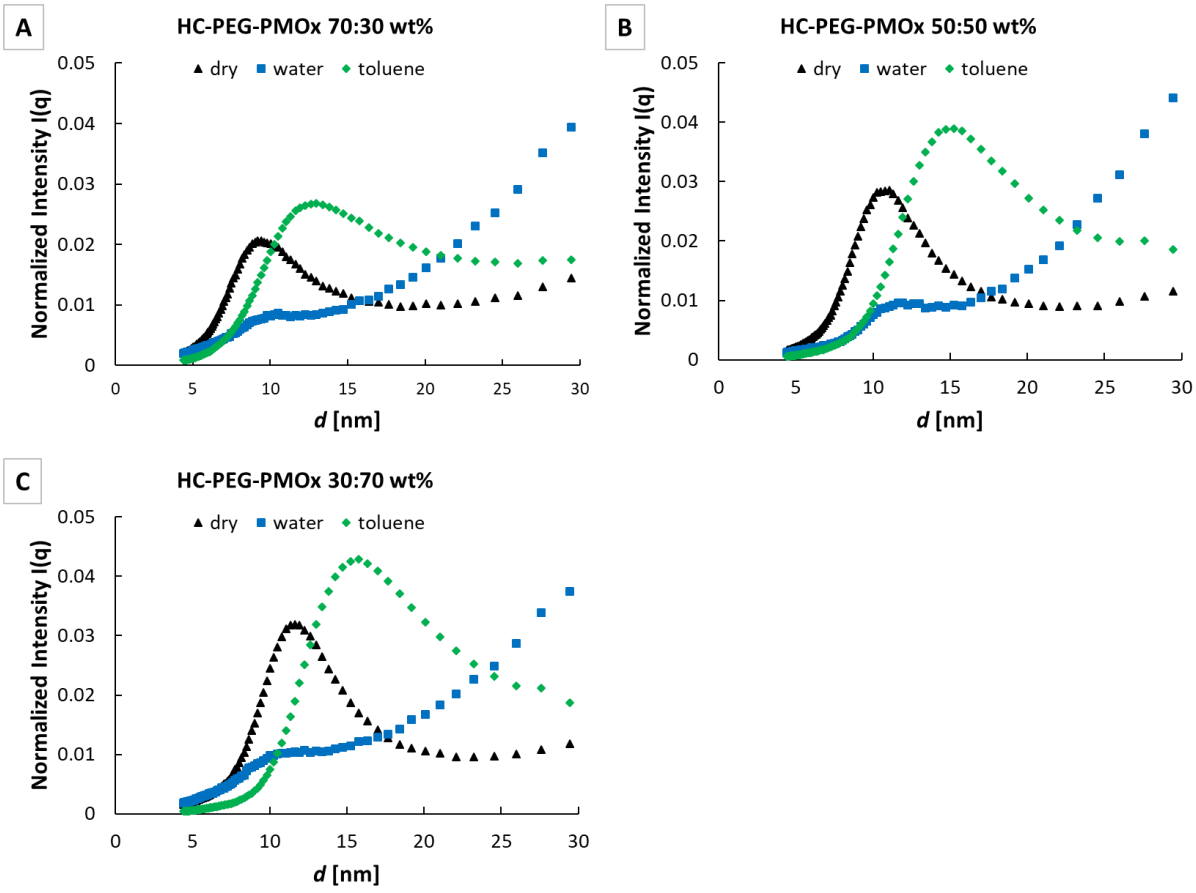

Figure 4.7 Scattering traces of HC-PEG-PMOx SPNs with different compositions in the dried state and swollen in toluene or water, respectively. Scattering data was collected for 1 h for dried samples and 8 h for swollen networks. All intensities were normalized to the total number of counts of the respective measurement and *d* was calculated as $d = 2\pi/q$.

The SAXS traces found for the LC-PEG-PMOx SPNs in dry and swollen state are shown in **Figure 4.8**. In case of the LC-PEG-PMOx with a PMOx content of 70 wt%, the SAXS traces of the dry material presented in **Figure 4.8**(**C**) suggest a similar, highly ordered structure as found for the higher cross-linked sample (**Figure 4.7**(**C**)). The influence of cross-linking can be seen as the *d* value increases from 12.2 nm (for HC) to 13.8 nm (for LC). Expectedly, the greater freedom in the lowly cross-linked sample leads to a stronger phase separation. The corresponding toluene swollen samples exhibit the same cross-linking dependent *d*-shifts. The dry sample LC-PEG-PMOx with 50 wt% PMOx shows, in contrast to the higher cross-linked sample, no nanostructural order in the SAXS pattern (**Figure 4.8**(**B**)). This can either be due to miscibility of the polymers or to the formation of a rather non-ordered state.

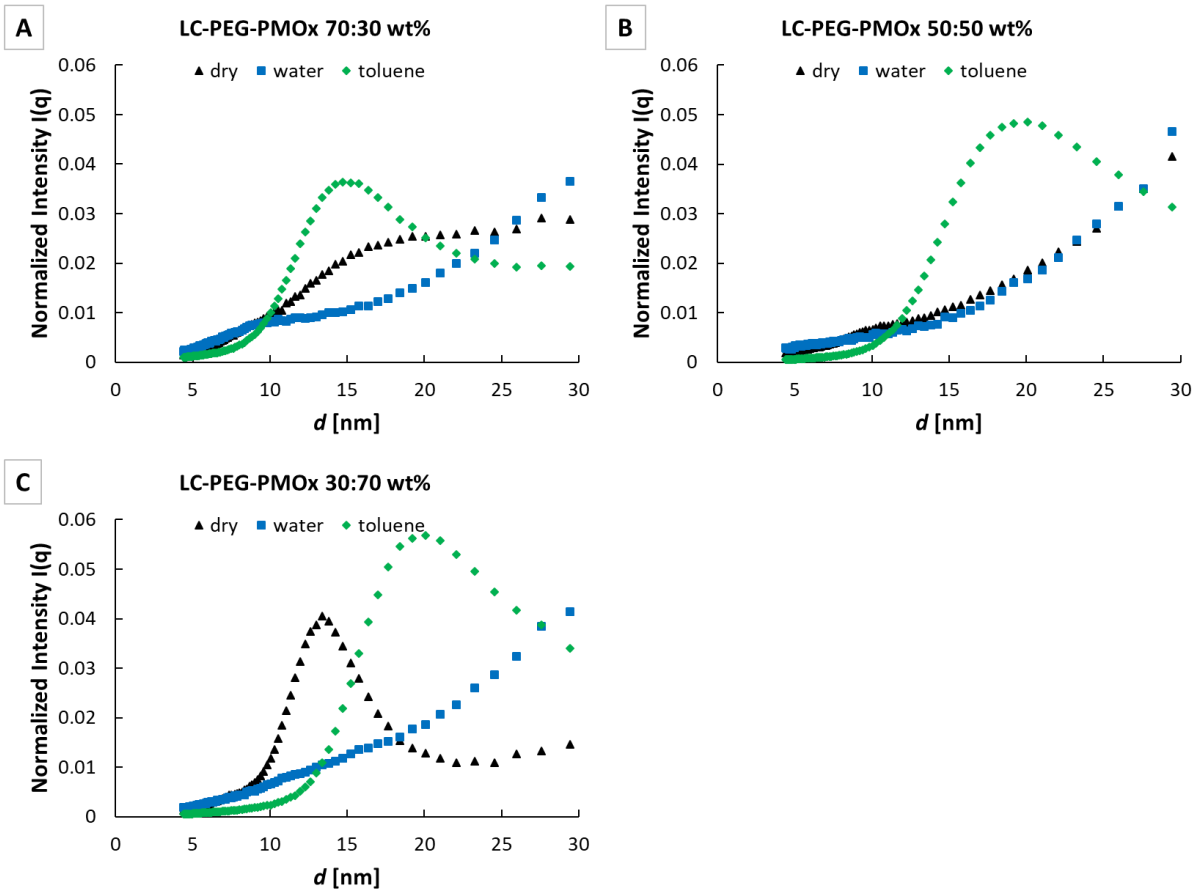

Figure 4.8 SAXS traces of LC-PEG-PMOx SPNs with different compositions in the dried state and swollen in toluene or water, respectively. Scattering data was collected for 1 h for dried samples and 8 h for swollen networks. All intensities were normalized to the total number of counts of the respective measurement and *d* was calculated as $d = 2\pi/q$.

Comparison of the AFM images of both samples suggest that both materials are nanophase separated (**Figure 4.9**). However, the LC-PEG-PMOx-SPN (50) (**Figure 4.8**(**B**)) shows a somewhat less regular structure than the respective highly-cross-linked SPN (**Figure 4.7**(**B**)). According to DSC analysis, both, the lower and the higher cross-linked PEG-PMOx (50) show crystallinity of PEG domains as also confirmed by X-ray diffraction measurements (see **Figure 4.15**). It is known to literature, that the formation of crystals can substantially alter the nanostructure in non-cross-linked blockcopolymers.[233-234] This is due to the fact that the driving force that leads to polymer crystals overcomes the minimized surface energy obtained by the formation of the ordered nanostructure and thus the crystallizing polymer chains are driven out of the initial structure into the crystals, which leads to a rather unordered structure. Cross-linking hinders the mobility of the polymer chains within the material. If the degree of cross-linking is high enough, the nanostructure of the phase separated polymer segments is retained as in the case of HC-PEG-PMOx-SPNs. In case of the LC-PEG-PMOx-SPNs this might not be

the case and the cross-linked material acts similar to non-cross-linked blockcopolymers. If the LC-PEG-PMOx-SPN is swollen in toluene, which is known the destroy the PEG crystals, an ordered nanostructure is formed as indicated by the SAXS trace in **Figure 4.7**(**B**). Decreasing the PMOx content in the LC-PEG-PMOx to 30 wt% results in a less ordered structure in comparison with the respective higher cross-linked sample, which becomes more ordered when swollen in toluene (**Figure 4.8**(**A**)). Thus, crystal formation of PEG within the LC-PEG-PMOx SPNs seems to result in non- or less-ordered nanostructures, which become more regular upon swelling in the PEG-selective solvent toluene as the PEG crystals are dissolved, but not in the non-selective solvent water. This difference in the respective nanostructures is also noticeable by comparison of the AFM images depicted in **Figure 4.9**. The conetwork sample of HC-PEG-PMOx (**B**) with 50 wt% PMOx shows a distinct nanostructure in contrast to the lowly crosslinked analogue (**A**). The respective DSC curves shown in **Figure 4.10** reveal a significantly higher crystallinity in the LC-PEG-PMOx SPN due to less hindrance through cross-links. It is also evident that the melting point of the PEG crystals is much lower in the highly cross-linked network. Thus, it might be possible that the PEG crystals are majorly formed in the confinement of the nanostructure. The PEG crystals in the lowly cross-linked APCNs might grow beyond that confinement due to higher flexibility of the polymer chains resulting in larger crystals and somewhat reduced order.

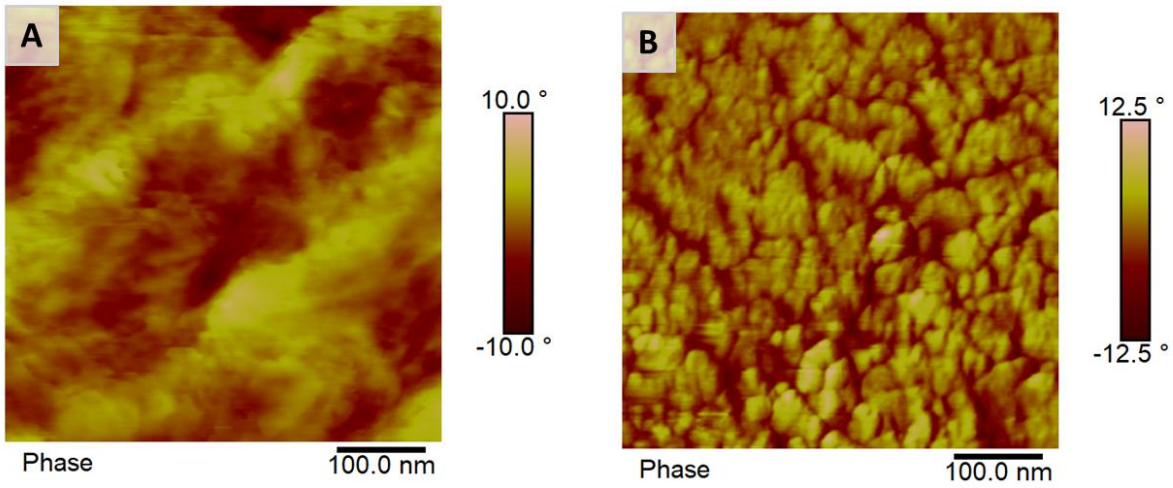

Figure 4.9 AFM phase mode images of LC-PEG-PMOx-SPN with 50 wt% PMOx (A) and HC-PEG-PMOx-SPN with 50 wt% PMOx (B) measured in tapping mode under nitrogen atmosphere at room temperature. The samples were prepared as described in the experimental part, dried and cryofractured.

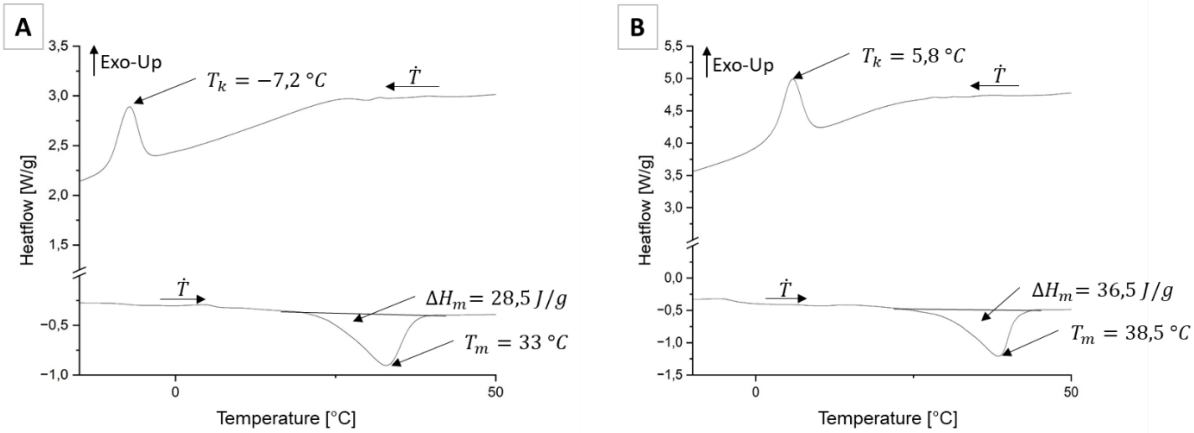

Figure 4.10 DSC curves of HC-PEG-PMOx-SPN with 50 wt% PMOx (A) and LC-PEG-PMOx-SPN with 50 wt% PMOx (B) obtained with a heating rate of 10 K/min. The samples were prepared as described in the experimental part and dried before measurement.

It was presumed that toluene leads to the formation of a regular nanostructure in LC-PEG-PMOx due to solvent induced “melting” of the PEG crystals. In order to confirm this, it was now explored if this effect can also be achieved by termperature-induced melting of the PEG crystals. To this end, LC-PEG-PMOx-SPN with 50 wt% PMOx was placed in the SAXS aperture, heated to 50 °C and 70 °C, respectively, and then the SAXS patterns were recorded. The temperatures were chosen, because 50 °C lies above the melting temperature of the PEG crystals (T_m = 41 °C) and 70 °C exceeds the T_g of PMOx ($T_{g,PMOx}$ ~ 61 °C). As seen in

Figure 4.11, no ordered nanostructure is obtained after heating the sample to 50 °C, while a highly ordered nanostructure can be found upon heating to 70 °C. The nanostructured SPN heated to 70 °C was then (quickly) cooled to room temperature by switching of the heating source in the SAXS aperture. This resulted in a still ordered nanostructured material. We suppose, this is due to the fact that the stiff PMOx phase, as soon as the temperature falls below the T_g, partly hinders the PEG from crystallizing and thus freezes the obtained nanostructure. In order to shed more light on this phenomenon, the sample was annealed at 60 °C overnight prior to cooling it to room temperature, because here the PEG crystals are not formed, but the PMOx chains are still flexible. Interestingly, the resulting material shows a non-ordered structure, thus the loss in structure occurs prior to formation of the PEG crystals. The same loss in order is obtained by swelling the SPN in the common solvent water and drying it afterwards.

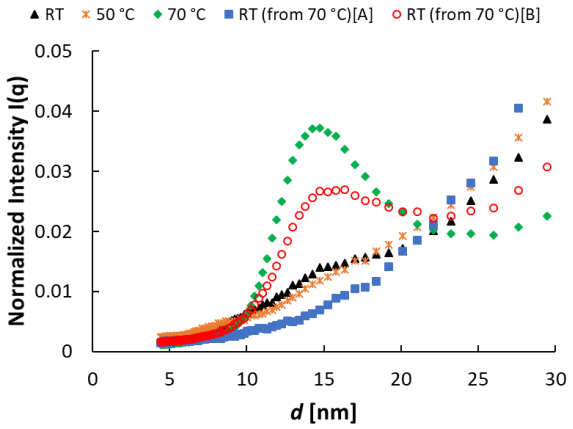

Figure 4.11. SAXS traces of the LC-PEG-PMOx-SPN with 50 wt% PMOx in the dried state measured subsequently at the listed temperatures. Procedure for Trace A (blue squares): heating to 70 °C for 1 h, annealing at 60 °C for 16 h followed by cooling to room temperature. Trace B (red circles) was collected at RT after the sample was cooled from 70 °C by switching off the heating source at the aperture. Respective scattering data were collected for 1 h. All intensities were normalized to the total number of counts of the respective measurement and d was calculated as $d = 2\pi/q$.

As shown above, SPNs prepared from very similar polymers, such as the water-soluble PMOx and PEG, form distinguished nanophases that can be addressed by a selective solvent. We were wondering if such a network can be loaded with an enzyme by simply adding the latter to the aqueous macromonomer solution prior to photopolymerization. It would be expected that the protein in such an SPN would have an affinity to the PMOx phase as known from previously found interactions between PMOx and proteins.[235-236] This way, the enzyme would be addressable *via* the selectively toluene-swellable PEG phase while being immobilized in the

non-swollen PMOx phase. The advantage of such a system would be the simple encapsulation of a wide range of enzymes due to the common water solubility of the components in contrast to, e.g., APCNs.[215] For this experiment, the enzyme horseradish peroxidase (HRP) was immobilized in a HC-PEG-PMOx-SPN with 50 wt% of each polymer. This was achieved by dissolving both macromonomers in an aqueous buffer solution containing the enzyme HRP followed by the addition of the initiator and the network synthesis was analogously conducted by photopolymerization.

The activity of the enzyme in the organic solvent toluene was determined by the peroxidase-catalyzed oxidative coupling reaction of *N*,*N*-dimethyl-*p*-phenylene diamine and phenol with *tert*-butyl hydroperoxide. The absorbance increase - a measure for the formation of the violet colored product - is shown in **Figure 4.12** and compared the activity of a slurry of the HRP powder in the same educt solution. A significantly increased enzymatic activity of the immobilized HRP compared to the suspended native enzyme was detected. While the native HRP powder shows no activity in the toluene, the specific activity of the SPN-immobilized HRP was calculated from the linear slope of the absorbance versus time plot, yielding a specific activity of 115 mU μg^{-1} (with U defined as the increase in absorbance of 0.001 per minute at 546 nm at room temperature and a reaction volume of 2.4 mL). No noticeable inactivation of the immobilized HRP could be detected in the monitored reaction time interval as indicated by the nearly linear increase of absorbance. This observation nicely corresponds to the results reported by BRUNS *et al.*, in which HRP was network-loaded by swelling a PHEA-*l*-PDMS APCN in an enzyme loaded buffer solution, followed by monitoring the activity of the immobilized enzyme in *n*-heptane.[108] Thus, the fully water swellable SPN can act similar to an APCN with selectively addressable polymer phases for enzyme activation combined with a simpler one-step synthesis of the enzyme loaded conetworks.

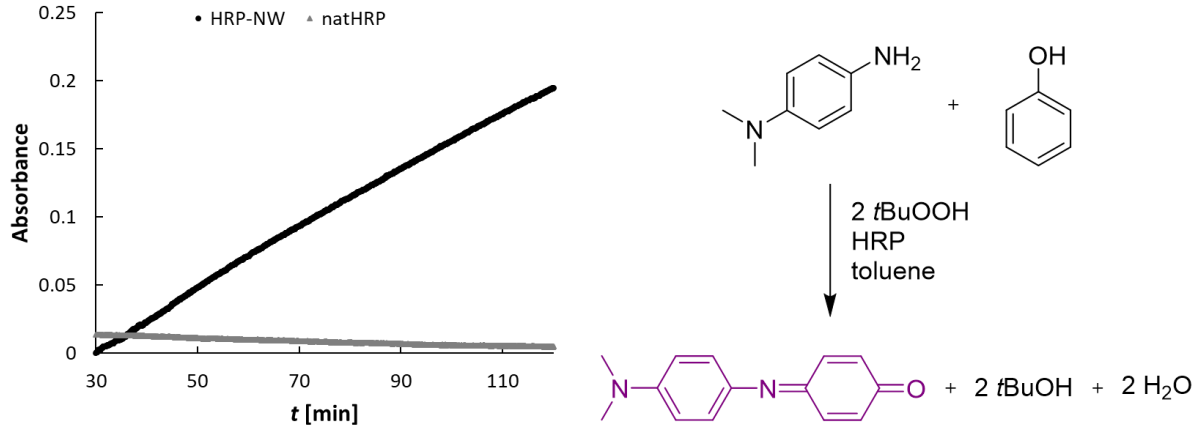

Figure 4.12 Oxidative coupling reaction of *N*,*N*-dimethyl-*p*-phenylene diamine (DMPDA) with phenol catalyzed by horseradish peroxidase (HRP) in toluene. Product formation was monitored by the increase in absorbance at λ = 546 nm. The reaction was catalyzed by 20 µg of HRP immobilized in a PEG-PMOx-film (black trace) and 2 mg of suspended native HRP (grey trace), respectively, in 2.4 mL of reaction medium.

4.4 Conclusions

This study was dedicated to the behavior of segmented polymer networks composed of PEG and the similar, also water-soluble, polymers PEtOx and PMOx, respectively. The swelling data in water indicates that PEtOx is somewhat more hydrophobic and PMOx more hydrophilic compared to PEG. While SAXS measurements in PEG-PEtOx-SPNs suggest that they do not nanophase separate, similarly prepared SPNs composed of PEG and PMOx show a distinguished nanophase separation. Decreasing the degree of cross-linking of the latter SPNs results in an apparent miscibility of conetworks with a PEG:PMOx mass fraction of 50:50 wt%. Swelling such SPNs in the PEG-selective solvent toluene, surprisingly results in a distinguished nanophase separation. DSC, X-ray diffraction, and AFM measurements revealed that this behavior is based on the fact that PEG can crystallize across the nanophases disrupting the overall order of the two polymer phases. Melting these crystals recovers the intrinsic phase separation. The generally selective addressability of polymer nanophases in SPNs composed of hydrophilic polymers offers a number of application possibilities in fields such as drug release or membrane technology. Further, the SPNs, although prepared from similar polymers, exhibit great resemblance to characteristics typically shown by APCNs in most cases, which often are elaborately prepared by cross-linking homopolymers with very different solubility. Thus, the vast field of applications of APCNs might be partly addressed by SPNs with simpler preparation protocols combined with specific nanostructural properties. This was shown on the example of activating the included enzyme HRP in the organic solvent toluene in a similar manner as previously performed with an APCN.[108]

4.5 Experimental Section / Methods

Instruments

All polymer syntheses were performed in a CEM Discover synthesis microwave equipped with a non-invasive vertically focused IR temperature sensor. The polymerization flasks (Schott Duran) were dried before usage at 150 °C overnight and handled under argon atmosphere.

The ^{1}H NMR spectra were recorded on an Agilent DD2 spectrometer with 5 mm triple resonance H(C,X) probe operating at 500 MHz and 25 °C with $CDCl_3$ as sample solvent. Chemical shifts are given in ppm relative to the signal caused by residual non-deuterated solvent.

The molecular weight (M_n, M_w) and the dispersity ($Đ$) of the polymers were obtained by size exclusion chromatography (SEC). The SEC was performed on a Viscotek GPCMax with a refractive index detector at 55 °C and saline *N*,*N*-dimethylformamide (DMF with 20 mmol LiBr) as eluent. Polystyrene standards (Viscotek) with narrow dispersities were used for column calibration.

A DSC 2910 (TA Instruments, Inc.) was used to determine thermal transitions of the polymer blends and networks (around 10 mg sample weight). Therefore, the DSC temperature was equilibrated at −50 °C and a temperature range between −50 and 100 °C was analyzed using a heating and cooling rate of 10 K/min for two consecutive runs. The depicted DSC traces show the results of the second run and indicated T_g values were based on the second heating curve.

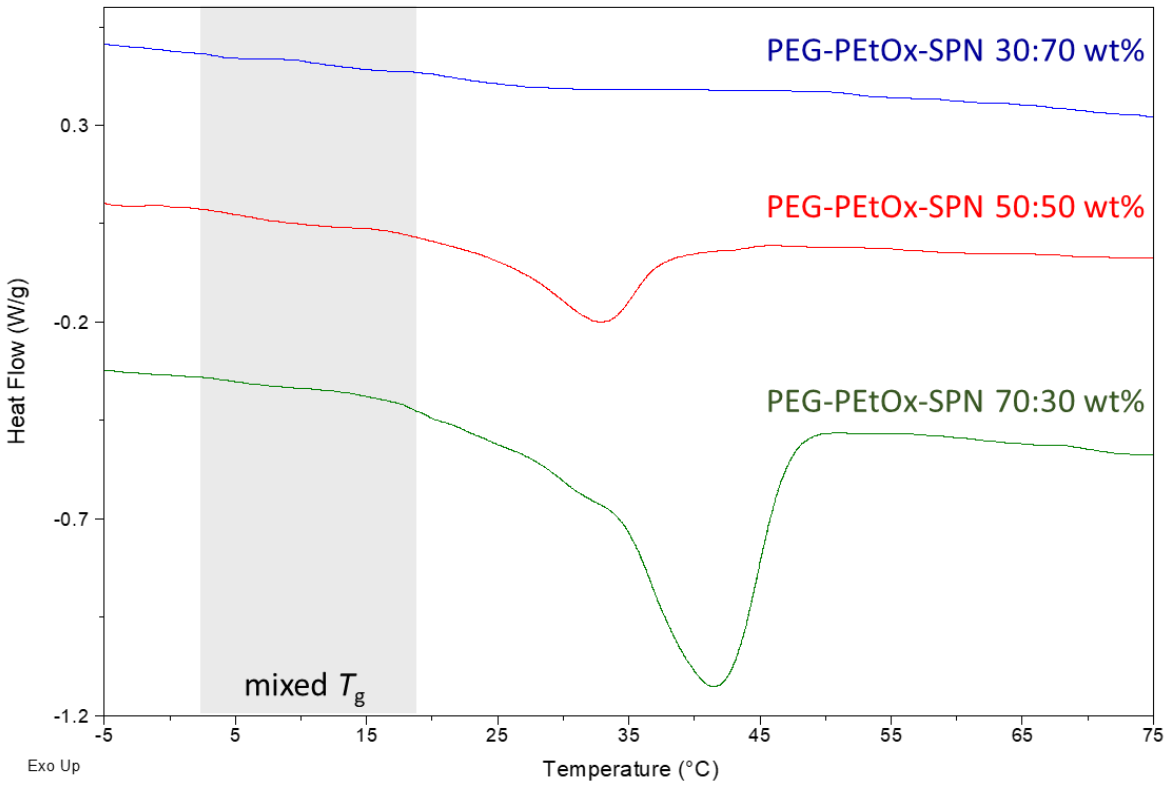

Figure 4.13 DSC graphs of PEG-PEtOx-SPN samples with varying composition (composition values given in wt%; traces shown with y-offset).

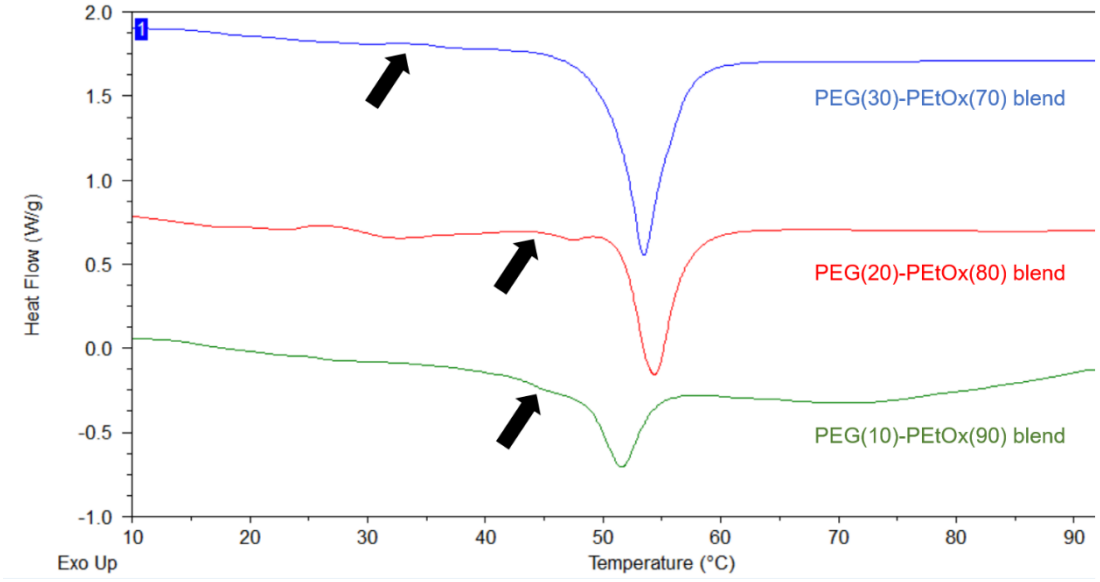

Figure 4.14 DSC graphs of uncross-linked blends of PEG and PEtOx (blend compositions given in wt%; traces shown with y-offset).

Atomic force microscopy (AFM) images were recorded on a Veeco Dimension Icon Scanning Probe Microscope (Veeco Instruments) equipped with a Nanoscope V Controller and an AVH-1000 Workstation. All examined SPNs were cryofractured, dried and measured under nitrogen atmosphere in tapping mode with commercial tapping mode etched silicon probe (TESPA) cantilevers at resonance frequencies between 300 and 400 kHz. The phase images were recorded at 5% below the fundamental resonance frequency of the cantilever with a typical scan speed of 1 Hz and a resolution of 512 samples per line for a 300 to 400 nm scan size. Recorded images were processed using the software NanoScope Analysis 1.5 (Bruker).

SAXS measurements were performed on a Bruker NANOSTAR with a VANTEC-2000 detector and an IμS Microfocus source (Incoatec GmbH) with a Cu-anode (wavelength λ = 0.154 nm) and integrated Montel Optic. The distance between sample and detector was 107 cm and a silver behenate standard was used for calibration. All experiments were carried out under vacuum and at room temperature unless stated otherwise. Swollen network samples were placed in quartz glass capillaries (diameter 1 mm) with the respective solvent and sealed prior to the measurement. The scattering data of dry samples was accumulated over 1 h and swollen networks over 8 h, followed by azimuthal integration to obtain the scattered intensities as a function of the magnitude of the scattering vector $q = 4\pi\sin(\Theta)/\lambda$ (with 2Θ = diffraction angle).

X-ray diffractograms (XRD) were recorded in symmetrical reflection mode at room temperature using a Philips PW 1140/90 goniometer (1D detector) and Ni-filtered CuK_α radiation.

Ultraviolet-visible spectroscopy (UV-VIS) measurements to monitor enzyme activity were conducted on a double-beam spectrophotometer Specord 210 from Analytik Jena and the samples were measured in quartz glass cuvettes (optical path length: 10 mm) at room temperature.

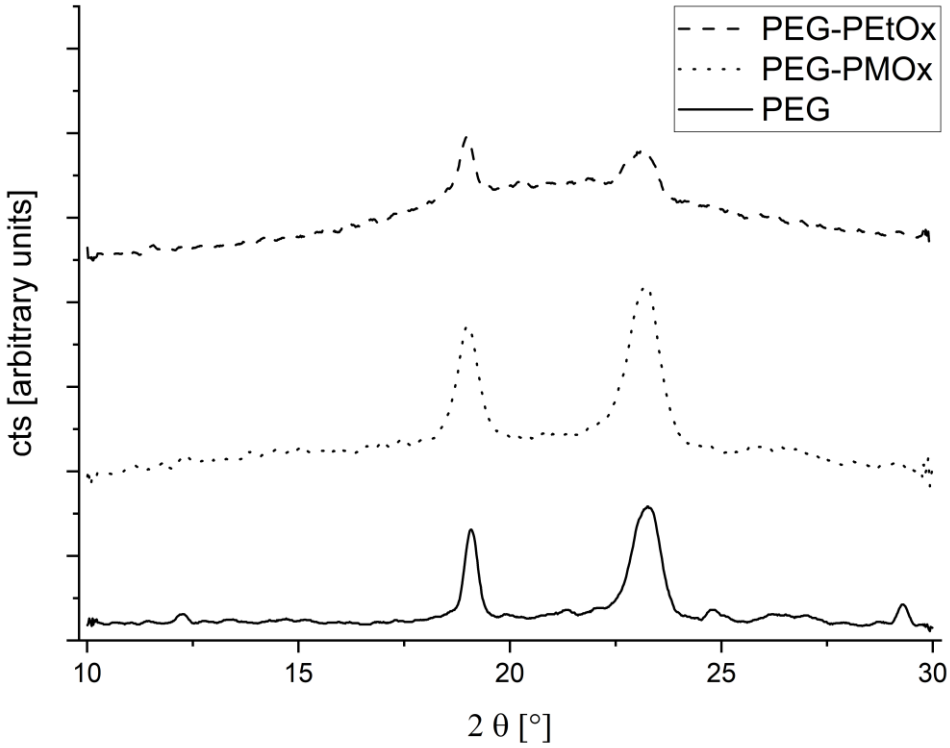

Figure 4.15 X-ray diffraction of SPNs composed of HC-PEG-PMOx-SPN (50:50 wt%), PEG-PEtOx-SPN (50:50 wt%) and pure PEG.

Materials

All solvents were distilled under reduced pressure before usage. For the polymerizations, chloroform was distilled from activated aluminum oxide (Merck) and acetonitrile (Fisher Scientific) was purified using a MB SPS Compact (M. Braun GmbH) solvent purification system. Both solvents were purified and stored under argon atmosphere at −20 °C with molecular sieves (3 Å). The initiator *trans*-1,4-dibromo-2-butene (DBB, Acros Organics) was recrystallized twice from *n*-heptane (Fisher Scientific), dried and stored at −20 °C under argon atmosphere. 2-Methyl-2-oxazoline (MOx, Acros Organics) and 2-ethyl-2-oxazoline (EtOx, Acros Organics) were purified by distillation over CaH_2 (Acros Organics) under argon atmosphere and stored at −20 °C before usage. *N*-[3-(Dimethylamino)-propyl]-methacrylamide (DMAP-MAA, Merck) was distilled before usage and poly(ethylene glycol)4000 diacrylate (PEG4000DA, Merck) was used as received. Irgacure 2959 (2-hydroxy-4'-(2-hydroxyethoxy)-2-methylpropiophenone) was kindly provided by Ciba Specialty Chemicals (now part of BASF). Horseradish peroxidase (HRP, EC 1.11.1.7) was purchased from Sigma Aldrich, *N*,*N*-dimethyl-*p*-phenylene diamine (DMPDA) and phenol were purchased from Acros Organics and used as received.

Syntheses of poly(2-oxazoline) macromonomers with DMAP-MAA end groups

The telechelic PMOx and PEtOx were synthesized based on previous polymerization protocols from our group.[123] In case of PMOx, 5.0 mL (5.0 g, 58.75 mmol, 40 eq.) 2-methyl-2-oxazoline and 314.2 mg (1.47 mmol, 1 eq.) DBB as initiator were dissolved in 20.0 mL of dry acetonitrile under argon atmosphere. The polymerization vessel was then heated to 100 °C for 4 h in a synthesis microwave reactor. Afterwards, the living polymerization was terminated by adding an 8-fold molar excess (in respect of initiator) of DMAP-MAA (1.9 mL, 11.75 mmol) and further heating at 45 °C for 72 h. The solvent was then removed under reduced pressure and the crude product was solved in chloroform and subsequently precipitated in ice-cold diethyl ether followed by centrifugation at 5000 rpm. This was repeated two times and the polymer was further dialyzed against methanol for 16 h using benzoylated cellulose membranes (MWCO = 1000 Da). After removal of the methanol under reduced pressure, the polymer was solved in water and lyophilized to obtain the dried polymer with 98% acrylamide end group functionalization.

The synthesis of the PEtOx-based macromonomer was performed analogously, but chloroform as polymerization solvent and a 10-fold molar excess of the termination agent DMAP-MAA (2.4 mL, 14.68 mmol) yielded a higher end group functionalization rate. Following this protocol, the telechelic PEtOx-acrylamide was obtained with 96% acrylamide end group functionalization.

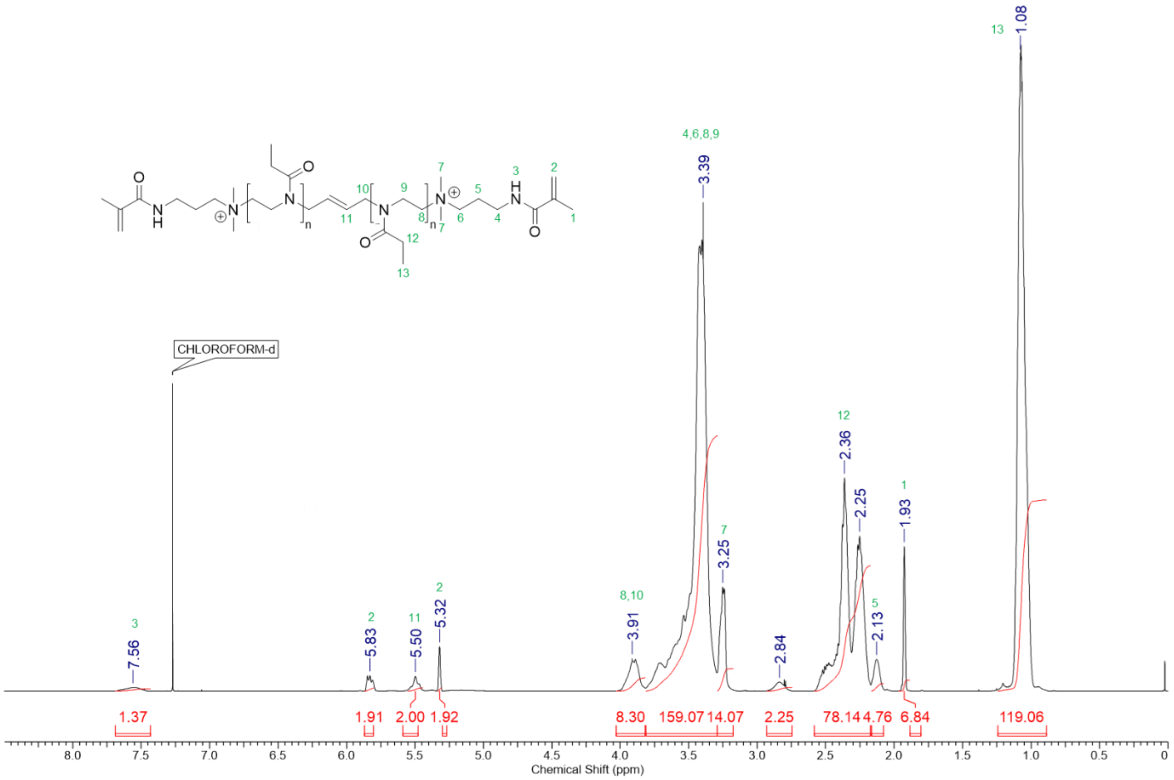

Figure 4.16. ^{1}H NMR spectrum of the bifunctional polymer MAA-DMAP-PEtOx$_{40}$-DMAP-MAA in $CDCl_3$.

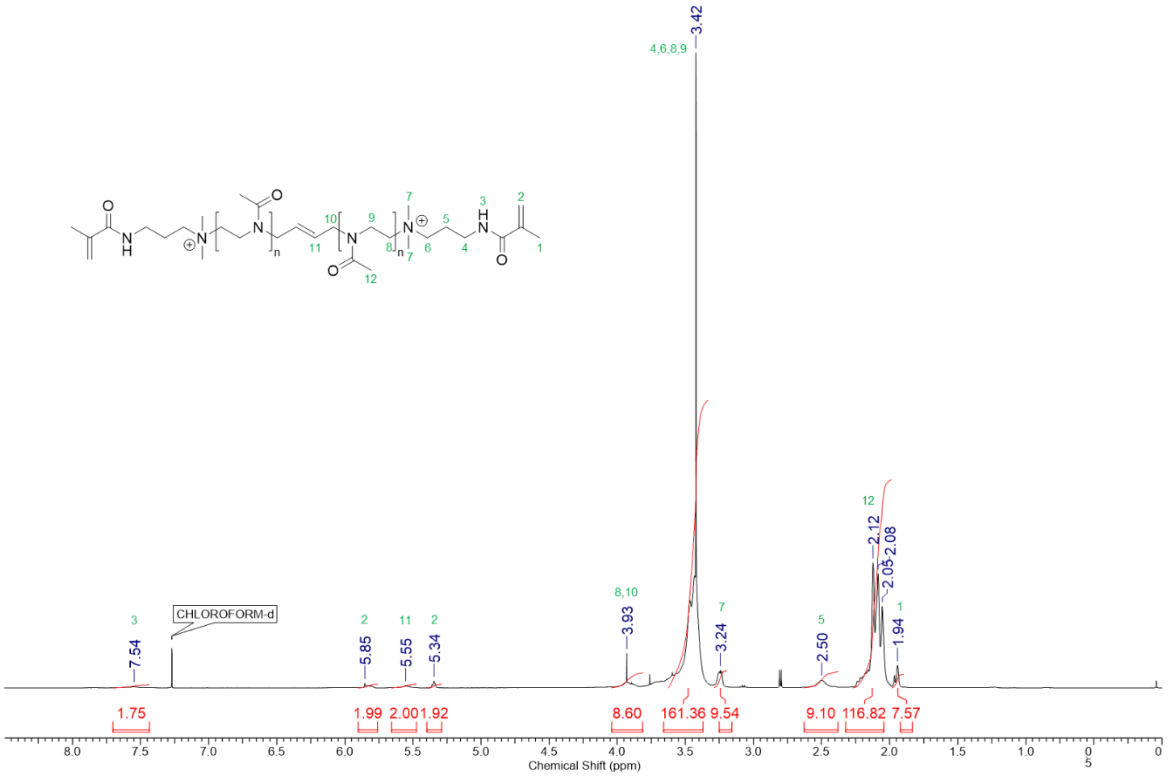

Figure 4.17 ^{1}H NMR spectrum of the bifunctional polymer MAA-DMAP-PMOx$_{39}$-DMAP-MAA in $CDCl_3$.

Synthesis of PEG-POx-SPNs

Both telechelic polymers PEG(4000)DA and the respective POx-DA were dissolved in water in the intended mass composition (see **Table 4.1**) and mixed until a clear solution was obtained. Afterwards, 2 mg of the photoinitiator Irgacure 2959 were dissolved in the reaction mixture. The solution was then placed on a microscope slide covered with adhesive poly(propylene)-tape (Tesafilm, tesa SE) and additional strips of adhesive tape placed on each end on the glass slide in order to control the thickness of the resulting network film (about 50 µm per tape layer). Afterwards, a second glass slide covered with adhesive tape was placed on top of the first slide and the photopolymerization was performed for 2 x 180 s under UV flash light (Heraflash, Heraeus Kulzer, λ = 340 nm) on each side. The obtained network films were then removed from the glass slides, dried and washed in chloroform for 20 h to remove remaining extractables and calculate the sol/gel content of the respective network.

Table 4.1 Overview of the reaction conditions of the synthesized SPNs and respective gel content and resulting thickness values of the obtained washed and dried polymer films.

SPN	PEG(4000)-DA [mg]	PEtOx-DA [mg]	PMOx-DA [mg]	Water [µl]	Gel content [wt%]	Thick-ness [µm]
PEG(70)-PEtOx(30)	70	30	-	100	92.8	400
PEG(50)-PEtOx(50)	50	50	-	100	83.6	400
PEG(30)-PEtOx(70)	30	70	-	100	95.8	400
HC-PEG(70)-PMOx(30)	70	-	30	100	96.8	400
HC-PEG(50)-PMOx(50)	50	-	50	100	98.7	400
HC-PEG(30)-PMOx(70)	30	-	70	100	95.7	400
LC-PEG(70)-PMOx(30)	70	-	30	466	93.2	200
LC-PEG(50)-PMOx(50)	50	-	50	466	90.5	200
LC-PEG(30)-PMOx(70)	30	-	70	466	92.8	200

In case of the HRP-loaded SPN, a 50:50 wt% mixture of PEG(4000)-DA and PMOx-DA (30 mg respectively) was dissolved in 100 µL of a solution of HRP (1 mg mL^{-1}) in 100 mM phosphate buffer (pH 7.0). The initiator Irgacure 2959 (1.5 mg) was added to the reaction mixture and the photopolymerization was conducted as previously described for PEG-PMOx networks. The resulting network film was rinsed with water to remove non-immobilized enzyme, dried with a stream of compressed air for 30 min and stored at 4 °C.

Determination of gravimetrical swelling ratios

All equilibrium swelling ratios of the SPN films with various compositions were determined gravimetrically by swelling a washed and dried network sample in the respective solvent for 20 h. The swollen sample was then weighed to determine $m_{swollen}$, dried (first by a stream of compressed air, then by heating the sample to 60 °C under reduced pressure for 3 h) and afterwards weighed again to obtain m_{dry} to calculate the respective gravimetrical swelling ratio $S_g = m_{swollen}/m_{dry}$.

Enzymatic activity study of the immobilized HRP in the PEG-PMOx-SPN

Enzymatic activity of the immobilized HRP in the organic solvent was measured based on an experimental protocol by BRUNS *et al*.[108] For this, the enzymatic activity of HRP in toluene was determined *via* the peroxidase catalyzed oxidative coupling of *N*,*N*-dimethyl-*p*-phenylene diamine (1.67 mM) and phenol (1.67 mM) using *tert*-butyl hydroperoxide (0.83 mM) as oxidizing agent. The enzyme-loaded network film was fixated in the beam path with a sample holder inside the cuvette and 2.2 mL of the substrate solution without *tert*-butyl hydroperoxide were given in the cuvette. For reference in the two-beam spectrophotometer, a non-loaded network film with the same polymer composition and thickness was fixated in a second cuvette and 2.2 mL of the substrate solution were added. The reaction was then started by the addition of 200 µL of a 10 mM *tert*-butyl hydroperoxide solution in toluene and stirring the reaction mixture at room temperature. After an initial delay of 30 min, an increase in absorbance at a wavelength of 546 nm was displayed. Using the linear slopes after the initial delay, the specific catalytical activity of the immobilized HRP was calculated defined as the increase in absorbance of 0.001 per minute at 546 nm at room temperature with a total reaction volume of 2.4 mL.

For comparison, the native, free enzyme HRP was suspended as a lyophilized powder in the substrate solution. The measurement was started by adding the oxidizing agent and stirring the reaction mixture at room temperature with the substrate solution as reference. **Figure 4.18** shows the respective reaction mixture with free and immobilized HRP after 150 min reaction time.

Figure 4.18 Cuvettes filled with the reaction mixture and the native (left) or immobilized HRP (right) after reaction times of 150 min at RT.

5 Comparative Study of Acrylate-functionalized Polyethylene Glycol and Poly(2-alkyl-2-oxazoline)s for the Conjugation of Proteins *via* Michael Addition Reactions

Parts of the data presented in this chapter are based on the results obtained during a practical course by L. NEUKIRCH[237] under the supervision of the author.

5.1 Abstract

The chemical conjugation of proteins offers the opportunity to improve or modify different properties of these biomolecules through covalent coupling of the protein with another molecule. By this means, the conjugation of proteins with various (macro)molecules creates bioconjugates with commonly modular properties determined by the respective components. This study gives a deeper insight into the aza-Michael addition reaction as a promising strategy for the conjugation of proteins with terminally acrylate-functionalized polymers. For this, three different unilaterally functionalized polymers (polyethylene glycol (PEG), poly(2-methyl-2-oxazoline) (PMOx) and poly(2-ethyl-2-oxazoline) (PEtOx)) with various molar masses were synthesized. The obtained macromolecules were utilized in a series of aza-Michael addition reactions with solvent exposed lysine residues of a model enzyme to determine polymer-specific differences. We demonstrated polymer-specific deviations in the efficiency of the conjugation reaction of the respective polymers and lysozyme as a model protein. Gelelectrophoretic analysis of the respective conjugate samples revealed higher degrees of polymer conjugation of lysozyme were established in case of the PEG-acrylate compared to the poly(2-oxazoline)-based conjugation agents. Further investigations showed different reaction kinetics for the aza-Michael addition reaction of the acrylate-functionalized polymers with piperidine as a small-molecule model substrate, displaying the lowest reaction rate for the PEG-acrylate. Based on these results, protein-polymer-interactions between bound POx chains and the protein surface were assumed as the determining factor resulting in the higher protein conjugation efficiency using functionalized polyethylene glycol compared to poly(2-alkyl-2-oxazoline)s.

5.2 Introduction

Since the reports of the pioneering work of ABUCHOWSKI *et al.*[132] in the late 1970s, the research field of proteins covalently modified with synthetic polymers gained significant scientific and industrial interest. Conjugation of biopolymers drastically alters their properties, which can be tailored by the combination with a suitable polymeric compound. Reported physico-chemical characteristics of modified proteins comprise enhanced solubility, stability, or so-called ‘stealth’

properties, which lead to significantly increased circulatory lifetimes of therapeutic protein drugs in the body.[238] Besides diagnostic and therapeutic applications of polymer-protein conjugates representing the industrially most important sectors[161,239], further reported utilizations include organosoluble rendered enzymes for highly active and selective biocatalytic transformations in organic media.[146,162-163,165]

Many of the previously mentioned properties of polymer-modified proteins can be either tuned by the type and characteristics of the chosen polymer or the employed conjugation approach.[161] As for the former option, PEG has been considered the leading polymer in this area. While PEG provides essential advantages for the conjugation of biomolecules, such as commercial availability, good solubility in numerous solvents, and a protein-repellent effect, this polymer offers only limited potential for the customization of the polymer structure or solubility.[240] Besides further concerning downsides of PEG, e.g. the formation of toxic degradation products upon *in vivo* oxidation reactions[241] or anti-PEG antibodies[242], other polymers moved more into the scientific focus as PEG alternatives for the conjugation of proteins.[152] Among these, poly(2-alkyl-2-oxazoline)s (POx) have been verified as a versatile and promising alternative for the modification of biomolecules.[5]

In addition to the effect of the chosen polymeric components, the chemistry of the coupling reaction has a significant impact on the properties of the resulting bioconjugate. Since native proteins only offer limited potential for intrinsic chemical modifications due to structural instability under harsh reaction conditions, most conjugation strategies target the available nucleophilic groups of proteinogenic amino acids, such as thiol groups of cysteine residues[166], carboxylate groups[243], or amine groups of lysine residues[162-163].[244] Furthermore, highly selective and efficient ligation methods have been demonstrated, which often are utilizing Michael-type addition reactions for selective targeting proteinogenic thiol groups, but the number of bound polymers is usually limited by the number of available cysteine residues.[166,244] Therefore, polymer coupling *via* the more prevalent amino groups of proteinogenic lysine residues would enable protein conjugation with numerous functional polymers, which is typically crucial to obtain organosolubility of proteins.[162-163] This approach was demonstrated in 1984 by MATSUSHIMA *et al.* by investigating the modification of chymotrypsin with 2,4-bis(*O*-methoxypolyethylene glycol)-6-chloro-*s*-triazine, successfully coupling the activated PEG to 12 out of the total of 15 amino groups in the chymotrypsinogen molecule.[245] The obtained PEG-protein conjugates retained an enzymatic activity of 57%, were soluble in various organic solvents and even catalyzed hydrolysis and aminolysis reactions in benzene.

For this reason, this study aimed to explore the potential of the aza-Michael addition reaction as a tool for the conjugation of proteins with synthetic polymers. In this process, the influence

of the polymer type will also be considered, as the two well-known conjugation polymers PEG and POx will be investigated in this comparative study.

5.3 Results and Discussion

In this work, the conjugation potential of the often similarly utilized hydrophilic polymers PEG, and the poly(2-alkyl-2-oxazoline)s PMOx and PEtOx *via* Michael-type addition reactions was investigated using lysozyme as a model protein. Since the aza-Michael addition, considered as one of the most widely used reactions in organic syntheses[246], describes the addition of a nucleophilic nitrogen center to electron deficient alkenes, all explored polymers had to be modified with reactive acrylate end-groups, either by polymer analogue end-group functionalization (mPEG) or termination of the CROP with a functional termination agent (POx). For this, two commercially available monomethoxy polyethylene glycols with molar masses of 2000 (mPEG2000) or 5000 Da (mPEG5000), respectively, were terminally acrylate-functionalized based on a literature protocol by LUTOLF *et al.*[247] For this, both polymers were dried in a vacuum heating oven at 40 °C over night and the respective acrylate-functionalization was achieved by conversion with acryloyl chloride after prior deprotonation of the terminal hydroxyl group using triethylamine. This way, the respective acrylate-functionalized monomethoxy PEG-acrylates (mPEG-AA) with degrees of functionalization of 96% for mPEG2000-AA and 100% in case of mPEG5000-AA were obtained, as determined by ^{1}H NMR spectroscopy (see **Figure 5.8**, Experimental Section).

Table 5.1 Overview of the obtained data for the acrylate functionalized polymers used for conjugation reactions (DP: degree of polymerization; DF: degree of functionalization).

Polymer	DP_{set}	DP (NMR)	M_n (NMR) [g/mol]	M_n (GPC) [g/mol]	$Đ$	DF [%]
mPEG2000-AA	-	44	2066	4260	1.0	96
mPEG5000-AA	-	113	5058	11050	1.0	100
$PMOx_{35}$-AA	25.0	35	3064	4210	1.1	100
$PMOx_{47}$-AA	50.0	47	4086	5530	1.1	100
$PEtOx_{24}$-AA	21.5	24	2465	3570	1.1	90
$PEtOx_{41}$-AA	43.0	41	4150	6160	1.1	96

Furthermore, telechelic PMOx and PEtOx with varying degrees of polymerization (see **Table 5.1**) were prepared *via* cationic ring-opening polymerizations and subsequent end-group

functionalization through the addition of acrylic acid (AA) as nucleophilic termination agent. The acrylate-functionalized poly(2-oxazolines) (POx-AA) were characterized by ^{1}H NMR spectroscopy (see **Figures 5.9** and **5.10**, Experimental Section) and yielded high degrees of end-group functionalization between 90 to 100% to ensure high coupling potential for the following conjugation step depicted in **Figure 5.1**. GPC measurements were conducted to verify narrow dispersities, however the values for the molar masses found for the PEG polymers were twice as high as confirmed by ^{1}H NMR analysis, even when unfunctionalized precursors were used to exclude the reactive acrylate end-groups. This indicates a discrepancy in the hydrodynamic volume of the two polymer types, since the same polystyrene standard was used for the calibration to obtain the relative molar masses. For the subsequent conjugation reaction, lysozyme was chosen as a commercially available model protein with a molar mass of 14.4 kDa and 6+1 free primary amino groups.[248]

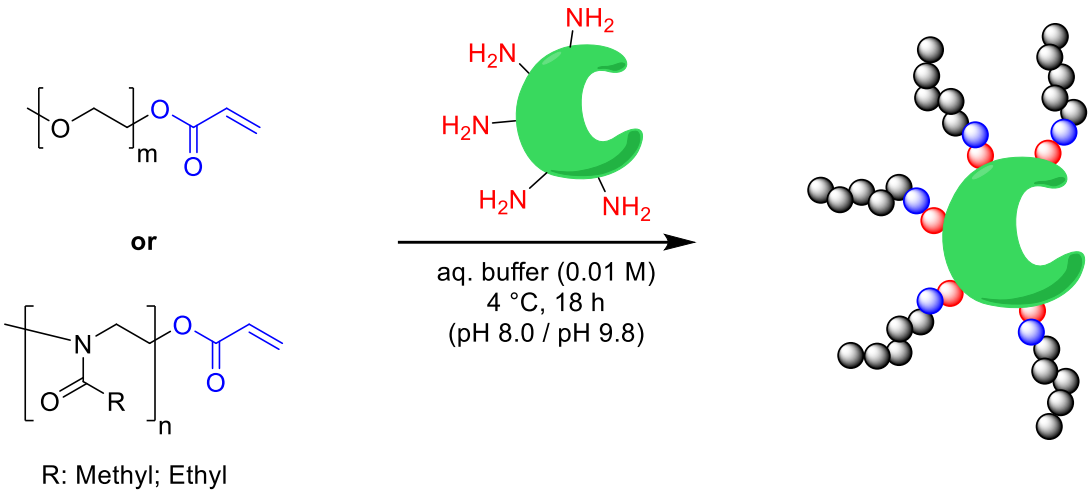

Figure 5.1 Schematic illustration of the modification of proteinogenic amino groups with acrylate functionalized polymers *via* the Michael addition reaction.

In 2007, RANU *et al.* reported the conduction of various addition reactions of amines and conjugated alkenes, which were carried out in water at room temperature, resulting in significant reaction rate acceleration compared to organic solvents, with small molecule substrates yielding between 85% and 95% conversion after short reaction times of 20 to 50 min.[249] This finding poses a promising approach for protein modification, as the reaction solvent for these conjugations is typically limited to water. Since the successful formation of peptide-PEG conjugates utilizing acrylate-functionalized PEG (3400 g/mol) and various synthetic thiol-containing peptides *via* Michael-type addition reactions has been demonstrated by LUTOLF *et al.*[247], even under neutral pH values (pH 7.3), this study was designed to investigate the coupling potential of acrylates and proteinogenic amino groups. Therefore, pH

values of 8.0 and 9.8 were chosen due to the expectedly lower reactivity of the amino groups, covering a basic pH range below and above the isoelectric point of lysine residues (pH(I) 9.6[250]) while avoiding pH induced protein denaturation[251]. Based on the previous results of ROTH[252], the acrylate-functionalized polymers were added in a molar excess of 20:1 with respect to the primary amino groups of the lysozyme in an aqueous carbonate buffer as reaction medium.

After stirring the reaction mixtures at 4 °C for 18 h, they were lyophilized and the success of the respective conjugation reaction was afterwards determined using sodium dodecyl-sulfate polyacrylamide gel electrophoresis (SDS-PAGE), a common method for the separation of proteins based on their molecular weight developed by LAEMMLI[253], as the addition of polymer chains to the protein increases the molar mass resulting in additional observable bands in the gels after staining with Coomassie blue. The gel shown in **Figure 5.2** demonstrates the results of the Michael addition reactions between lysozyme and the respective acrylate-functionalized polymers performed at pH 8.0.

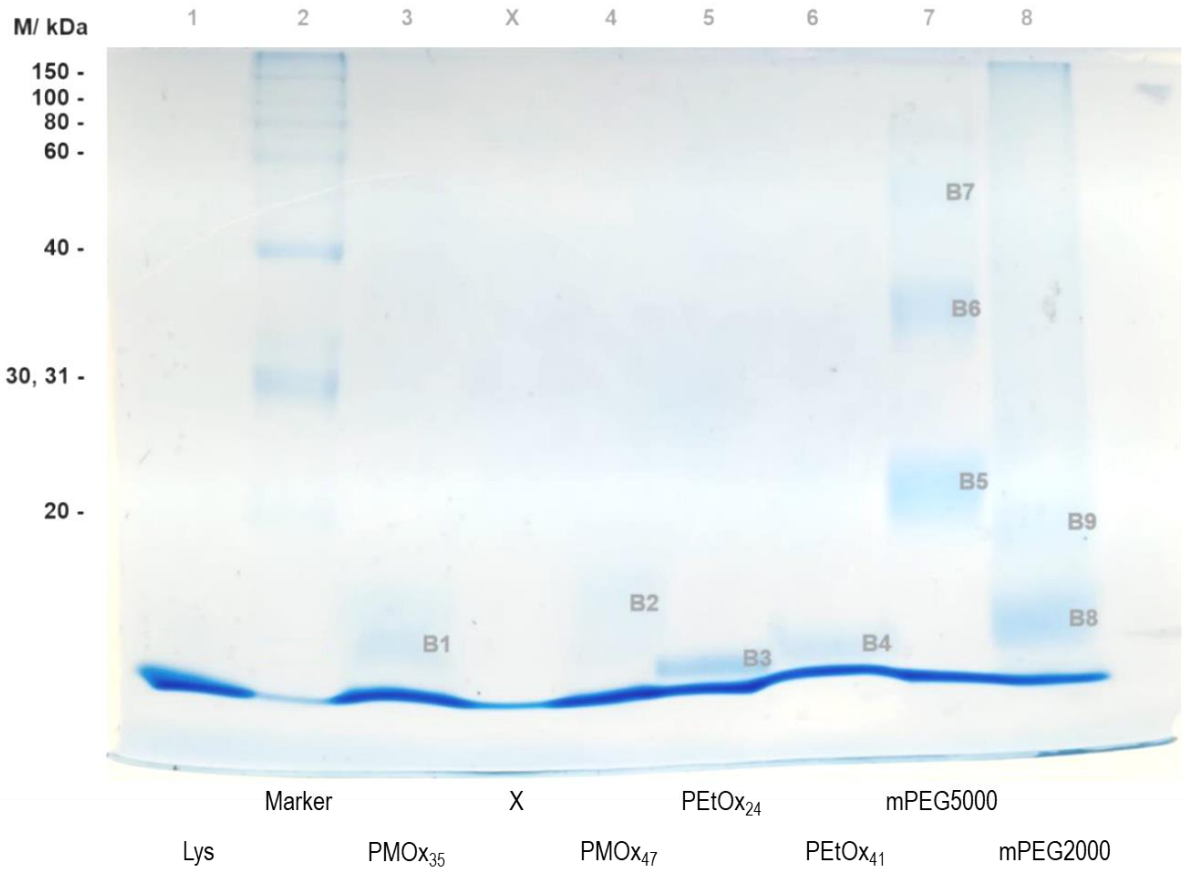

Figure 5.2 SDS-PAGE analysis gel of the conjugation samples conducted at pH 8.0. Lane 1: Lysozyme; lane 2: Protein ladder marker; lane 3: Lysozyme + $PMOx_{35}$-AA; lane X: blank; lane 4: Lysozyme + $PMOx_{47}$-AA; lane 5: Lysozyme + $PEtOx_{24}$-AA; lane 6: Lysozyme + $PEtOx_{41}$-AA; lane 7: Lysozyme + mPEG5000-AA; lane 8: Lysozyme + mPEG2000-AA [modified from [237]].

In lane 1 only one defined band of the native lysozyme is observable, while the lanes 3 to 6 of the POx-modified proteins exhibit additional bands between the clearly visible bands of the respective unmodified proteins and the 20 kDa band of the protein ladder (lane 2). Due to the weak intensities of the stained bands B1, B2 and B4, only partial formation of POx-lysozyme conjugates is indicated, with only one or two respective polymers coupled to the protein (B1 – B4). Contrary to the low band intensities and low molecular weight region of the POx-modified lysozyme, the lanes 7 and 8 of the PEG-lysozyme conjugates exhibit several clearly visible product bands in addition to the band of the remaining unmodified protein. In lane 7 (lysozyme conjugated with mPEG5000-AA), the distinct bands B5 (~20 kDa) and B6 (~35 kDa) indicate the single or quadruple addition of PEG chains to the protein, respectively, while the weaker band B7 could be caused by fully PEG5000-conjugated lysozyme. Lane 8 displays the two recognizable bands B8 and B9, both located in the region under the 20 kDa marker band, suggesting the respective single or twofold addition of mPEG2000-AA chains to the lysozyme.

Figure 5.3 shows the stained SDS-PAGE gel of the polymer-lysozyme conjugate samples obtained after changing the pH value of the carbonate buffer for the addition reaction to pH 9.8 under otherwise identical reaction conditions. It is generally noticeable that all lanes with applied conjugation samples exhibit more intensive product bands above the respective bands of the remaining unmodified lysozyme. The lanes 3, 4, 5 and 8, where POx-lysozyme conjugate samples were applied, display similar results as previously discussed for the conjugate synthesis at pH 8.0, each with only one clearly visible distinct band slightly above the native lysozyme band indicating low degrees of modification. Therefore, even the elevated pH value during the addition reaction could not provide lysozyme conjugates with numerous POx chains, but the ratio of modified to unmodified protein seems to be increased. Direct comparison between PMOx and PEtOx reveals more distinct bands for the PEtOx-lysozyme conjugates (B2 and B3), while the modification with PMOx leads to a broadening of the conjugate bands (B1 and B11). The characterization of the PEG-modified samples (lane 6 and 7) indicates comparable modification efficiency as obtained from the addition reaction conducted at pH 8.0, although both lanes display low intensity bands at even higher molar masses, possibly originating from protein aggregates (B7 at ~70 kDa) or higher modified PEG-lysozyme conjugates (B10 at ~24 kDa; 5x mPEG2000-modification) compared to the conjugation at pH 8.0.

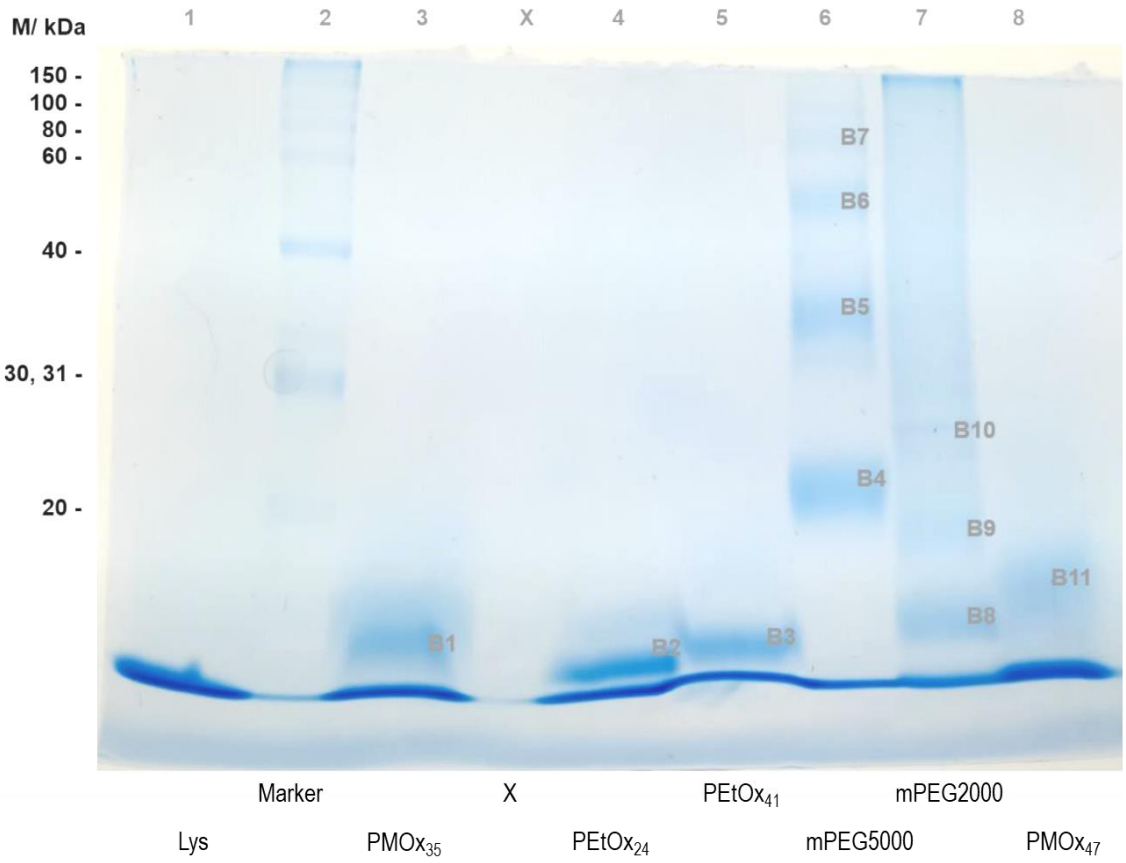

Figure 5.3 SDS-PAGE analysis gel of the conjugation samples conducted at pH 9.8. Lane 1: Lysozyme; lane 2: Protein ladder marker; lane 3: Lysozyme + $PMOx_{35}$-AA; lane X: blank; lane 4: Lysozyme + $PEtOx_{24}$-AA; lane 5: Lysozyme + $PEtOx_{41}$-AA; lane 6: Lysozyme + mPEG5000-AA; lane 7: Lysozyme + mPEG2000-AA; lane 8: Lysozyme + $PMOx_{47}$-AA [modified from [237]].

Altogether, direct comparison of the results obtained by SDS-PAGE for the investigated polymer-lysozyme conjugates *via* Michael addition reactions performed at pH 8.0 or pH 9.8, respectively, indicates similar numbers of bound POx chains for both pH values, while the conjugation with mPEG chains shows additional bands upon increasing the pH value of the buffer solution. Although all respective gel lanes where conjugation products were applied display significant bands of unmodified lysozyme, the pH value increase to 9.8 resulted in an overall higher intensity for the bands allocated to polymer-protein-conjugates. This way, more polymer-modified lysozyme could be obtained, however the number of bound polymer chains to one respective protein molecule remained limited. According to this, the increase of pH value did not lead to significantly higher conjugation efficiency, but the type of polymer turned out to play an important role in the Michael addition reaction with proteins. These findings were further confirmed in two additional sets of polymer-lysozyme conjugation reactions under analogous conditions using mainly various acrylic acid terminated PMOx (DP (NMR) = 25; 93)

and PEtOx (DP (NMR) = 28; 42; 68) polymers (for polymer data see **Table 5.2**, Experimental Section) for the conjugation and mPEG2000-AA for comparison of the influence of polymer type on the conjugation efficiency. The obtained gels after SDS-PAGE displayed in **Figures 5.4** and **5.5** confirm the previously discussed results (see **Figures 5.2** and **5.3)**, showing significant higher conjugation efficiency in case of modification with the acrylate functionalized PEG.

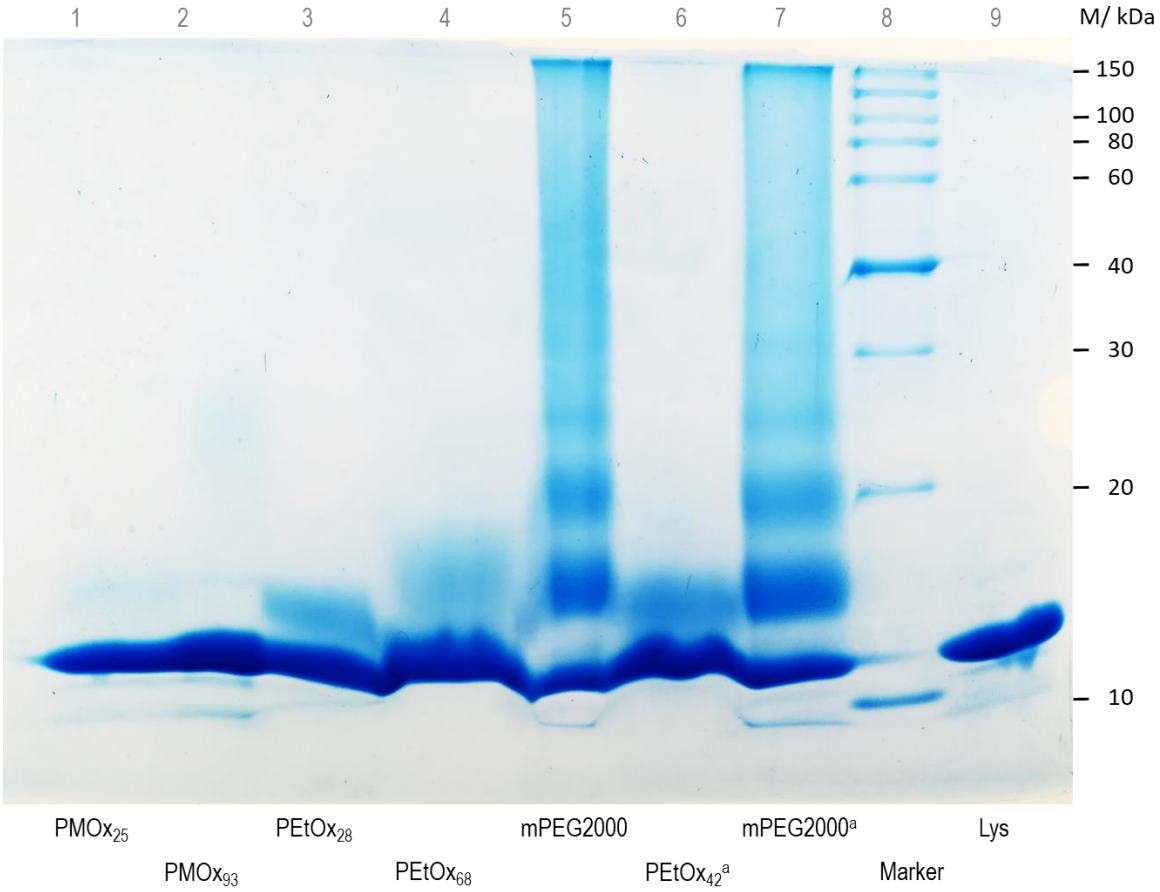

Figure 5.4 SDS-PAGE analysis gel of the conjugation samples conducted at pH 8.0. Lane 1: Lysozyme + $PMOx_{25}$-AA; lane 2: Lysozyme + $PMOx_{93}$-AA; lane 3: Lysozyme + $PEtOx_{28}$-AA; lane 4: Lysozyme + $PEtOx_{68}$-AA; lane 5: Lysozyme + mPEG2000-AA; lane 6: Lysozyme + $PEtOx_{42}$-AA[a]; lane 7: Lysozyme + mPEG2000-AA[a]; lane 8: Protein ladder marker; lane 9: Lysozyme ([a]: doubled conjugate concentration in analysis sample).

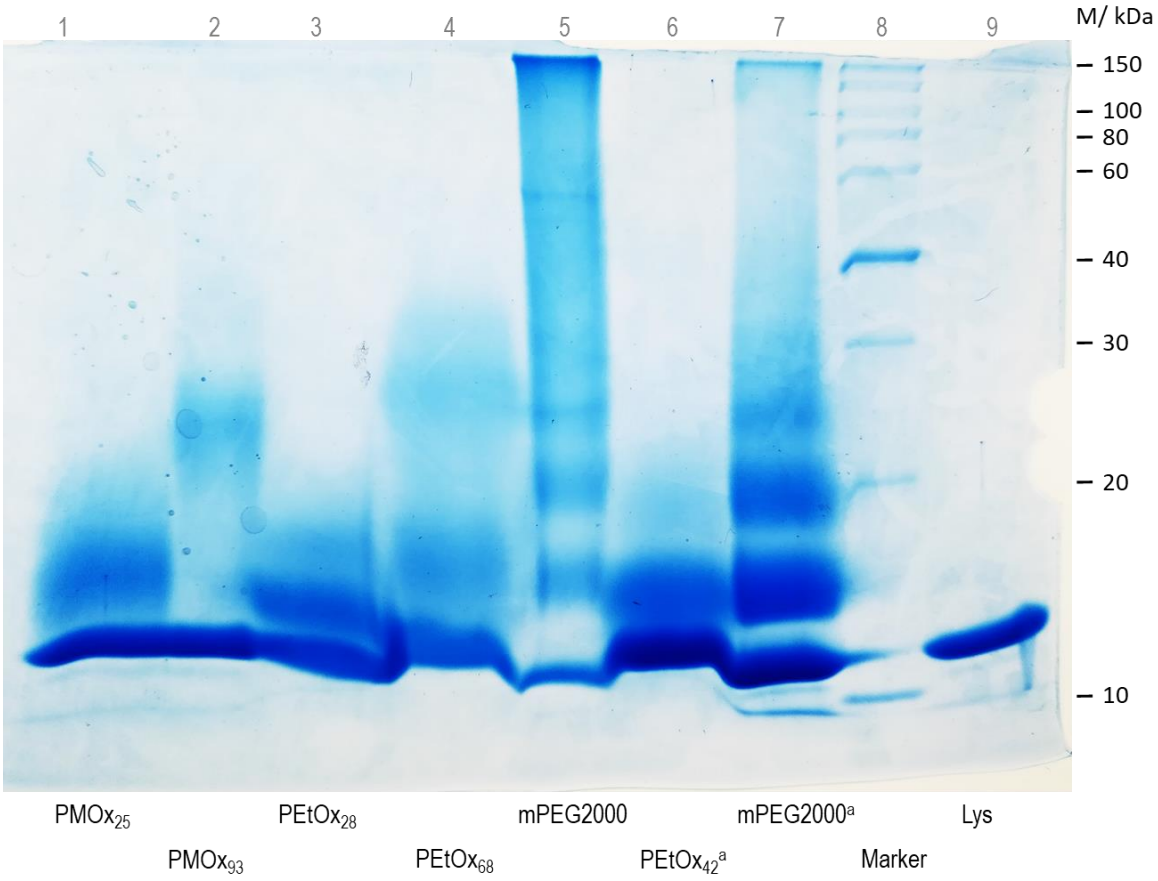

Figure 5.5 SDS-PAGE analysis gel of the conjugation samples conducted at pH 9.8. Lane 1: Lysozyme + $PMOx_{25}$-AA; lane 2: Lysozyme + $PMOx_{93}$-AA; lane 3: Lysozyme + $PEtOx_{28}$-AA; lane 4: Lysozyme + $PEtOx_{68}$-AA; lane 5: Lysozyme + mPEG2000-AA; lane 6: Lysozyme + $PEtOx_{42}$-AA[a]; lane 7: Lysozyme + mPEG2000-AA[a]; lane 8: Protein ladder marker; lane 9: Lysozyme ([a]: doubled conjugate concentration in analysis sample).

In order to investigate the effect of the respective polymer type on the end-group reactivity, the reaction kinetics of the aza-Michael addition reaction between different acrylate-functionalized polymers with comparable chain lengths ($PMOx_{35}$-AA; $PEtOx_{41}$-AA; mPEG2000-AA with 45 PEG units) and the secondary amino group of piperidine as a small model molecule in equimolar ratios were analyzed using ^{1}H NMR spectroscopy. Thereby, the conversion of the acrylate end-group was tracked over a time period of 7 h by carrying out the reactions in deuterated chloroform as solvent to allow immediate NMR measurements after the respective reaction times, yielding the data presented in **Figure 5.6**.

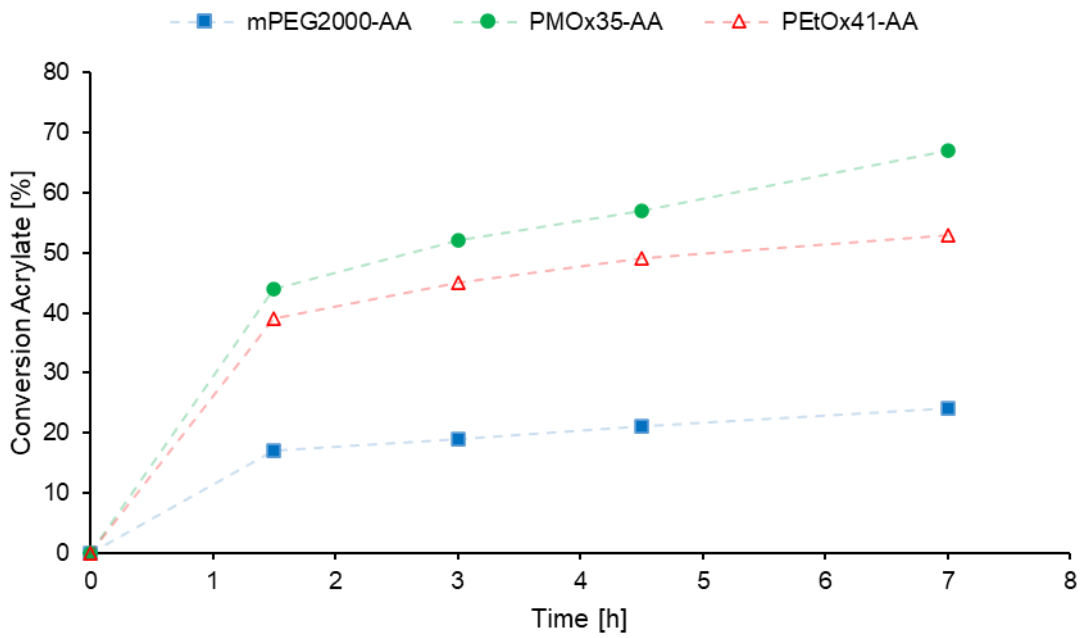

Figure 5.6 Comparison of the time-dependent conversion of polymer acrylate end-groups with piperidine as small molecule reactant (reaction conducted in $CDCl_3$; molar ratio 1:1 polymer:piperidine).

Unexpectedly, the comparison of the collected data for acrylate end-group conversion displayed in **Figure 5.6** obtained through ^{1}H NMR measurements reveals a significantly faster conversion of both POx-based acrylate end-groups, with initially high end-group conversions of 39% for $PEtOx_{41}$-AA up to 44% for $PMOx_{35}$-AA after 1.5 h reaction time. After a reaction time of 7 h, final end-group conversions of 53% for $PEtOx_{41}$-AA and 67% for $PMOx_{35}$-AA were determined. Contrary to that, the acrylate end-group conversion of $mPEG_{45}$-AA was considerably slower in the investigated time period, with an initial conversion of only 17% after 1.5 h, resulting in 24% end-group conversion after 7 h reaction time.

Therefore, based on the discussed findings on the acrylate-conversion in the model addition reaction with piperidine, the determined higher protein-conjugation potential could not be explained based on a generally higher end-group reactivity rate of the PEG acrylate. Additionally, the stability of the acrylate end-groups of the respective polymers under basic conditions was investigated by solving the polymer in carbonate buffer (0.1 M) at pH 10.2 for 6 h at 20 °C and analyzing the reduction of the acrylate group signals with ^{1}H NMR spectroscopy. This study revealed the decrease of acrylate end-groups through basic ester cleavage of 22% for $PMeOx_{25}$-AA, 9% for $PEtOx_{28}$-AA, and 11% for mPEG2000-AA, which still does not give an explanation for the difference in conjugation efficiency of the investigated polymers.

Thus, it was presumed that the interaction between the protein and the respective type of polymer causes the variety in conjugation efficiency, leading to the respective polymer-protein configurations depicted in **Figure 5.7**. PEG is widely known for its strong protein repellent effect[254-256] because of its low refractive index compared with other synthetic water-soluble polymers, leading to particularly low van der Waals interactions with proteins.[257] Since the attracting effect of the low van der Waals interactions between the PEG-chain and the protein is significantly smaller than their steric repulsion, the accessibility of the functional polymer end-groups is increased, resulting in a higher protein modification rate for the PEG-based acrylates. Furthermore, already bound PEG chains should therefore not be able to aggregate on the protein surface, enabling the addition of further end-group functionalized polymers to the protein surface.

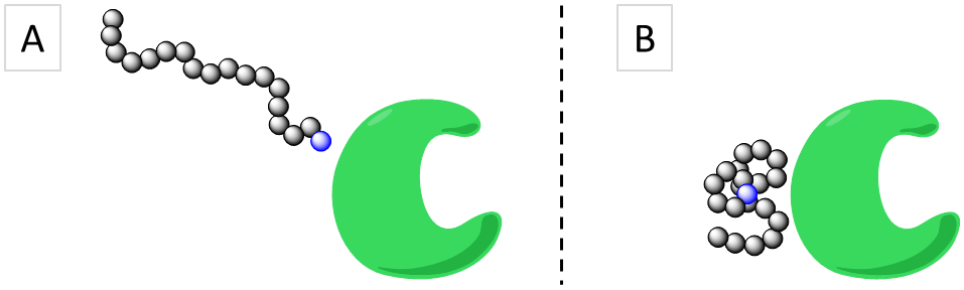

Figure 5.7 Schematic depiction of the presumed interaction-based configuration of the protein surface and the respective telechelic polymers PEG (A) or POx (B) (the functional end-groups are illustrated in blue color).

Although water-soluble POx-based polymers are typically regarded as showing only minor interactions with proteins[161], HIJAZI *et al.* reported a successful approach of non-competitive enzyme inhibition ascribed to the collapse of $PMOx_{31}$ chains on the enzyme (horseradish peroxidase) surface after non-covalent binding using iminodiacetate end-groups.[258] An entropy-driven release of polymer- and enzyme-bound water molecules is assumed to cause the aggregation of the polymer chains on the enzyme surface, yielding a dissociation constant of 0.25 mM determined by isothermal titration calorimetry (ITC). A similar effect could explain the fact that the Michael addition reactions between POx and lysozyme only yielded single-modified proteins in most cases according to SDS-PAGE gels. Bound POx chains presumably aggregate on the lysozyme surface, potentially blocking additional amino groups and thus limiting the addition of further polymer chains. In addition to that, unbound POx chains are assumed to be organized as polymer coils in solution and on the protein surface, limiting the accessibility of the polymer end-groups to the functional groups on the protein surface.

5.4 Conclusions

This study aimed to give a deeper insight into the potential of the aza-Michael addition reaction as a promising tool for the modification of proteins with different polymers. For this, telechelic water-soluble PMOx and PEtOx with varying chain lengths equipped with functional acrylate end-groups were synthesized and compared with two synthesized PEG-acrylates as the gold-standard for the conjugation of proteins. For the addition reaction, lysozyme was chosen as a model protein and the reaction was conducted at pH 8.0 and pH 9.8 to investigate the effect of the pH value on conjugation efficiency. SDS-PAGE characterization of the samples revealed mostly single-modified lysozyme in case of the POx-based conjugation agents and up to fully modified lysozyme using mPEG5000-AA for the protein conjugation. Since this difference in modification efficiency was expected to be caused by varying reaction kinetics of the acrylate end-group depending on the respective polymer chain, a comparative reaction kinetics study of the aza-Michael addition between the end-groups of mPEG2000-AA, $PMOx_{35}$-AA, $PEtOx_{41}$-AA and the cyclic amine piperidine as a small-molecule model substrate was conducted. Unexpectedly, the PEG-acrylate showed the lowest reaction rate during the investigated reaction period of 7 h with an acrylate-group conversion of only 24% compared to 53% for $PEtOx_{41}$-AA and 67% conversion for $PMOx_{35}$-AA.

While the cause for the lower modification efficiency using end-group functionalized POx as conjugating polymers could not be identified this way, interactions between the respective POx chains and the protein surface are assumed to limit the ligation of further polymer chains to the protein, as reported by HIJAZI *et al.* for a PMOx-based enzyme inhibitor.[258] Although the Michael addition is mostly used for the selective formation of bioconjugates utilizing proteinogenic thiol groups of cysteine residues[259], the aza-Michael addition represents a promising strategy for applications that require the modification with numerous polymer chains, such as organosoluble enzymes for the efficient transformation of organic substrates.[146] Current limitations of POx-based protein modification agents are expected to be overcome through targeted adjustment of polymer compositions or optimization of reaction parameters.

5.5 Experimental Section / Methods

Instruments

The ^{1}H NMR spectra were recorded on a Bruker Avance III HD NanoBay Fourier-transformation spectrometer operating at 400 MHz and 25 °C or Agilent AV500/AV400 spectrometers operating at 500/400 MHz and 25 °C. For the measurements, 30 to 40 mg of the polymeric samples were solved in deuterated chloroform ($CDCl_3$) and the obtained

chemical shifts are given in ppm relative to the signal caused by residual non-deuterated solvent.

The molecular weight (M_n, M_w) and the dispersity ($Đ$) of the polymers were obtained by size exclusion chromatography (SEC). The SEC was performed on a Viscotek GPCMax with a refractive index detector at 55 °C and saline *N*,*N*-dimethylformamide (DMF with 20 mmol LiBr) as eluent at 0.7 mL/min flow rate. For each measurement, 4.5 mg of the respective polymer were solved in 1.5 mL eluent, filtered with a syringe filter (0.2 µm pore size; PTFE) and allowed to equilibrate in the solvent for 16 h. Sample separation was conducted using TSKgel® GMH_{HR}-M mixed bed columns (7.8 mm inner diameter; 30 cm length; 5 µm particle size) and polystyrene standards (Viscotek) with narrow dispersities were used for column calibration.

Materials

All solvents were distilled under reduced pressure before usage. For the polymerizations, dry acetonitrile (Fisher Scientific) was purified using a MB SPS Compact (M. Braun GmbH) solvent purification system and stored under argon atmosphere at −20 °C with molecular sieves (3 Å). 2-Methyl-2-oxazoline (MOx, Acros Organics) and 2-ethyl-2-oxazoline (EtOx, Acros Organics) were purified by distillation over CaH_2 (Acros Organics) under argon atmosphere and stored at −20 °C before usage. Methyl tosylate, acrylic acid and triethylamine were distilled under reduced pressure and stored under argon atmosphere at −20 °C. Both monomethoxy polyethylene glycols (mPEG2000 and mPEG5000; Sigma Aldrich) were freshly dried in a vacuum heating oven at 40 °C for at least 20 h prior to usage. Lysozyme was purchased from AppliChem (≥ 20000 U/mg; hen egg white) and used as received. All other chemicals were used as received unless stated otherwise.

Synthesis of acrylate-functionalized mPEG

These syntheses were based on a protocol by LUTOLF *et al.*[247] The respective dried monomethoxy polyethylene glycol (2.0 g mPEG2000 or 5.0 g mPEG5000, 1.0 mmol, 1.0 eq.) was solved in 25.0 mL dichloromethane and cooled to 0 °C under argon atmosphere. 374.3 µL triethylamine (273.2 mg, 2.7 mmol, 2.7 eq.) were added to the polymer solution for deprotonation of the hydroxyl end group followed by dropwise addition of 161.6 µL acryloyl chloride (181.0 mg, 2.0 mmol, 2.0 eq.) and proceeding the reaction over night at room temperature under argon atmosphere. After filtration of the reaction medium and a neutralization step with sodium carbonate, the raw products were filtered again followed by purification through precipitation in cold diethyl ether. Afterwards the raw products were resolved in chloroform, precipitated again in cold diethyl ether, and the respective acrylate-functionalized polymers were dried under high vacuum and yielded white powders with wax-

like consistency (1.79 g, 89.4% yield for mPEG2000-AA; 3.25 g, 65.1% yield for mPEG5000-AA). Since mPEG5000-AA showed residual impurities in the 1H NMR spectrum, an additional dialysis step was performed against water (MWCO = 1000 Da), followed by lyophilization of the product (1.82 g, 36.4% yield).

An exemplary ^{1}H NMR spectrum of the synthesized mPEG2000-AA is shown in **Figure 5.8**.

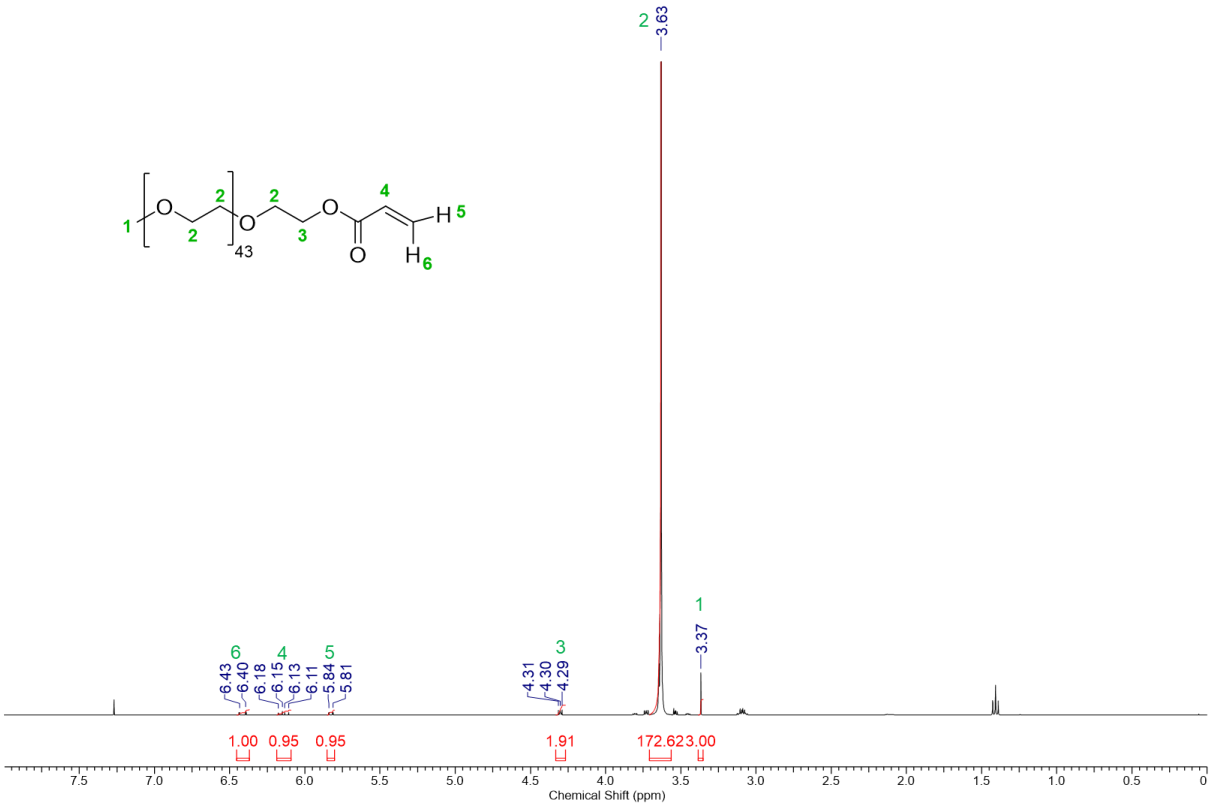

Figure 5.8 ^{1}H NMR spectrum of the acrylate-functionalized mPEG2000-AA in $CDCl_3$.

Synthesis of poly(2-alkyl-2-oxazoline)s with acrylate end groups

The acrylate-functionalized POx were synthesized analogously with varying equivalents of the respective 2-oxazoline monomers according to **Table 5.2**. In general, the respective monomer 2-methyl-2-oxazoline or 2-ethyl-2-oxazoline were added to dry acetonitrile (4 mL solvent per 1 mL monomer) in a Schott flask under argon atmosphere. Afterwards, 177.0 µL methyl tosylate (0.22 g, 1.17 mmol, 1.0 eq.) as initiator were added and the polymerization flask was closed and heated to 110 °C for 3 h under stirring. Afterwards, the living polymerization was terminated by adding 0.82 mL triethylamine (0.59 g, 5.87 mmol, 5 eq.) and 0.40 mL acrylic acid (0.42 g, 5.87 mmol, 5.0 eq.), followed by further heating at 40 °C for 72 h under gently stirring. The solvent was then mainly removed under reduced pressure and the crude product was

subsequently precipitated in ice-cold diethyl ether followed by centrifugation at 5000 rpm for 5 to 10 min. This procedure was repeated two times (redissolved in chloroform) and the respective polymer was dried under vacuum and further purified by dialysis against water for 5 h using benzoylated cellulose membranes (MWCO = 1000 Da). After removal of water through lyophilization, the polymers were obtained as colorless or slightly yellow solids.
Exemplary ^{1}H NMR spectra of synthesized PMOx-AA and PEtOx-AA showing the signal interpretation are provided in **Figure 5.9** and **5.10**, respectively.

Table 5.2 Overview of the reaction mixture compositions for the polymerizations of acrylate functionalized poly(2-oxazoline)s.

Polymer	eq. (monomer)[a] [mmol]	V (monomer) [mL]	V (solvent) [mL]	V (acrylic acid) [mL]	V (TEA) [mL]
$PMOx_{25}$-AA	20.0	1.32	6.6	0.27	0.54
$PMOx_{35}$-AA	25.0	2.50	10.0	0.40	0.82
$PMOx_{47}$-AA	50.0	5.00	20.0	0.40	0.82
$PMOx_{93}$-AA	60.0	1.98	9.9	0.13	0.27
$PEtOx_{24}$-AA	21.5	2.55	10.0	0.40	0.82
$PEtOx_{28}$-AA	20.0	1.59	6.6	0.27	0.54
$PEtOx_{41}$-AA	43.0	5.10	20.0	0.40	0.82
$PEtOx_{42}$-AA	30.0	2.38	9.9	0.27	0.54
$PEtOx_{68}$-AA	50.0	1.98	9.9	0.13	0.27

[a]: eq. with reference to the initiator methyl tosylate.

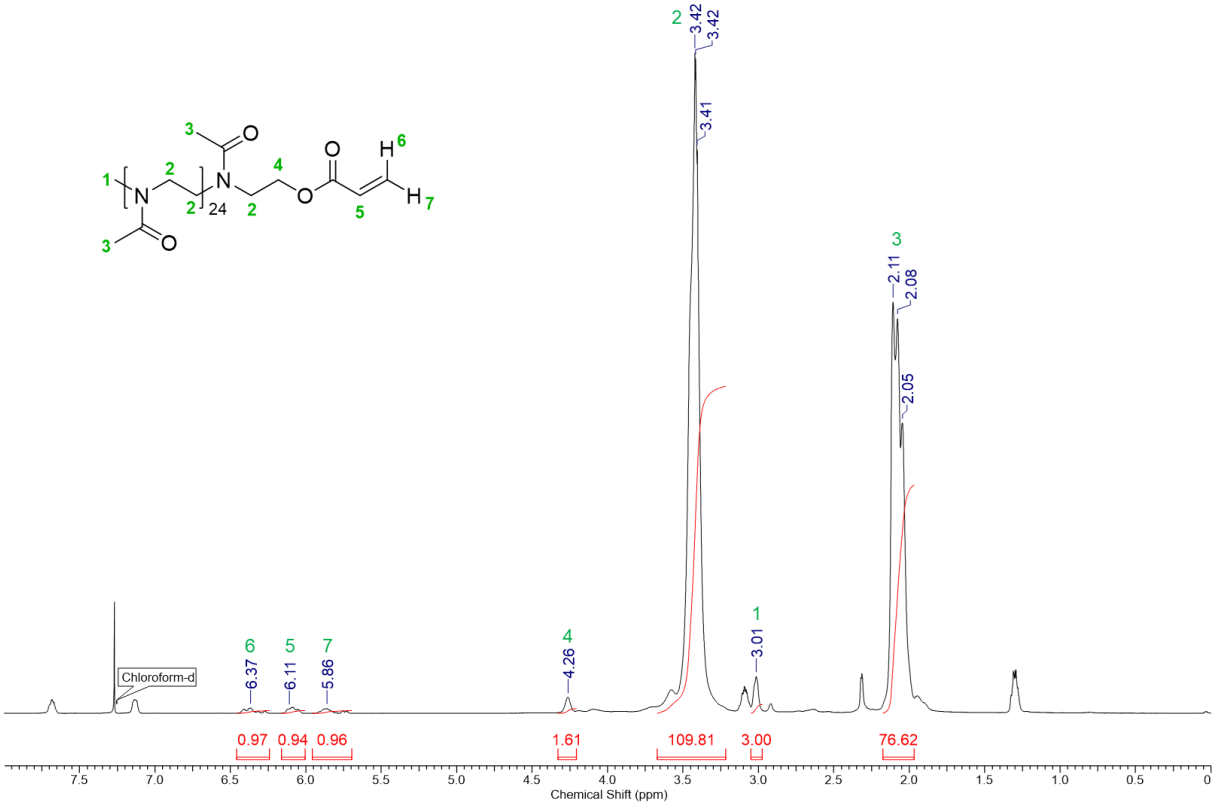

Figure 5.9 ^{1}H NMR spectrum of the acrylic acid terminated $PMOx_{25}$-AA in $CDCl_3$.

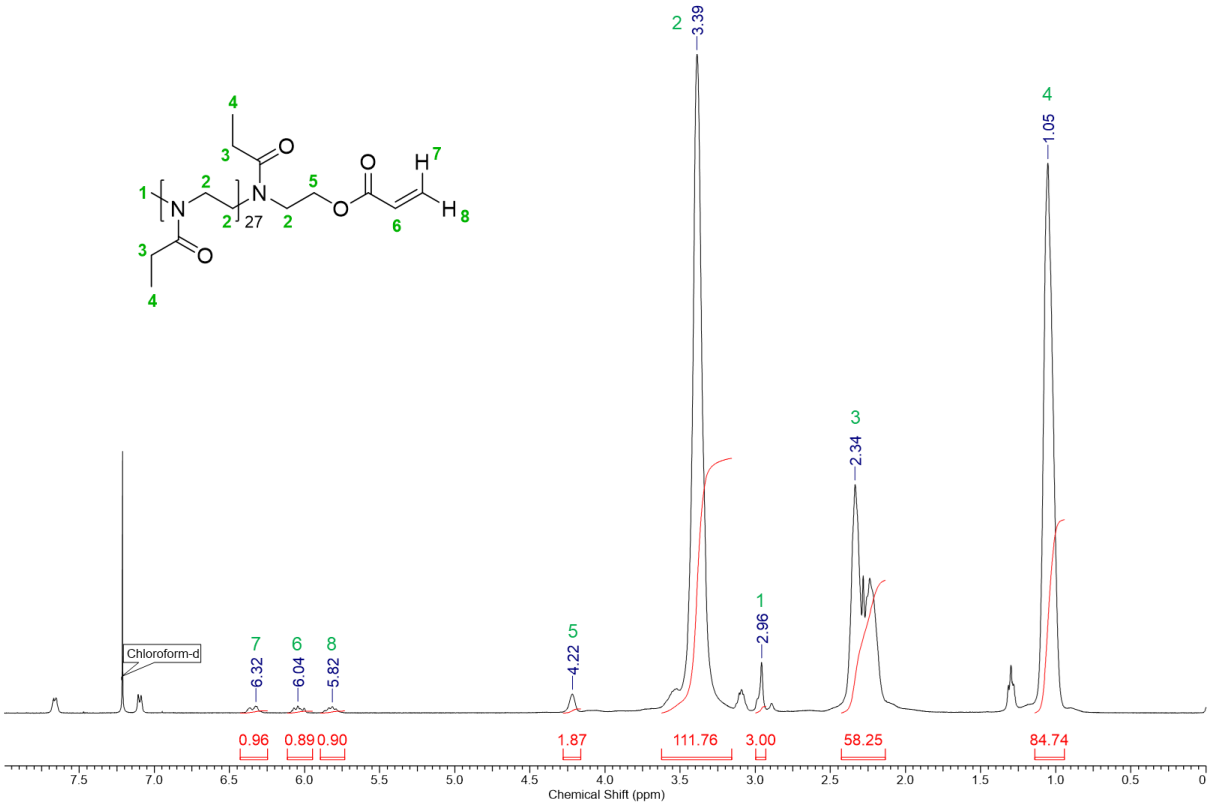

Figure 5.10 ^{1}H NMR spectrum of the acrylic acid terminated $PEtOx_{28}$-AA in $CDCl_3$.

Preparation of polymer-lysozyme conjugates with acrylate-functionalized polymers

Firstly, a stock solution of the model protein lysozyme was prepared in water with a mass concentration of 100 mg/mL. A respective previously synthesized acrylate-functionalized polymer (19.58 µmol, 20 eq. regarding the 7 primary amino groups of the lysozyme) was then dissolved in 980.0 µL of a 0.01 M carbonate buffer (pH 8.0 or pH 9.8, depending on the experiment). Afterwards, 20.0 µL (139.9 nmol, 1.0 eq.) of the aqueous lysozyme solution were added to the polymer solution, followed by gentle stirring at 4 °C for 18 h.

Sodium dodecyl sulfate-polyacrylamide gel electrophoresis (SDS-PAGE)

All SDS-PAGE analyses were conducted according to the method developed by LAEMMLI[253] in the gel electrophoresis chamber Minigel-Twin (Biometra) and all discontinuous gels were analogously prepared using the compositions for stacking gel and separating gel given in **Table 5.3**. The respective mixtures for the gels were freshly prepared and immediately poured into a glass mold (1 mm gel thickness) starting with the separating gel. The prepared gels were stored at 4 °C until further usage.

Table 5.3 Compositions of the prepared solutions for the stacking and separating gels.

Component	Stacking gel (4%)	Separating gel (14%)
Stacking gel buffer (pH 6.8)	0.75 mL	-
Separating gel buffer (pH 8.8)	-	3.00 mL
Water	1.80 mL	4.80 mL
Acrylamide/*N,N'*-Methylenebisacrylamide (29:1 mol. ratio) (aq. solution, 40 wt%)	0.45 mL	4.20 mL
Ammonium persulfate solution (40 wt% in water)	15.00 µL	30.00 µL
N,N,N',N'-Tetramethylethylenediamine	6.00 µL	15.00 µL

For each SDS-PAGE, 10.0 µL of the conjugate sample solution (directly after synthesis), 10.0 µL of the sample buffer (see **Table 5.4**) and 2.0 µL of a 1 M dithiothreitol solution were mixed using a vortex mixer and incubated at 96 °C for 10 min in a thermoshaker. Afterwards, the sample mixtures were cooled to 4 °C and 10.0 µL of the respective solution were pipetted into a well in the gel. In addition to the samples, a molecular-weight size marker (Roti®-Mark 10-150 PLUS; Carl Roth) was loaded onto each gel. Upon application of a voltage of 60 V, the

samples were concentrated in the stacking gel until narrow bands of bromphenol blue from the sample buffer were visible. Then, the voltage was increased to 170 V and the samples were separated in the separating gel until the bromphenol blue band reached the bottom edge of the gel. The gels were afterwards stained by shaking the gels in a Coomassie brilliant blue R250 staining solution (see **Table 5.4**) for multiple hours and excessive staining solution was removed by gently shaking the gels in water over night.

Table 5.4 Compositions of buffers and solutions used for the SDS-PAGE.

Stacking gel buffer (pH 6.8)	
TRIS-base	15.14 g
SDS	1.00 g
Water	250.0 mL
Separating gel buffer (pH 8.8)	
TRIS-base	45.43 g
SDS	1.00 g
Water	250.0 mL
Electrophoresis buffer solution	
TRIS-base	30.20 g
Glycin	144.20 g
SDS	10.00 g
Water	1000.0 mL
Staining solution	
Coomassie brilliant blue R250	29.00 mg
Ethanol	40.0 mL
Acetic acid (conc.)	10.0 mL
Water	50.0 mL

Kinetic study of the aza-Michael addition reaction with piperidine

For the investigation of the reaction kinetics of the aza-Michael addition between the acrylate functionalized polymers and the secondary amine group of piperidine as small model molecule, 150.0 mg of the respective polymer (1.0 eq; 0.075 mmol mPEG2000-AA; 0.049 mmol $PMOx_{35}$-AA; 0.037 mmol $PEtOx_{24}$-AA) were dissolved in 3.0 mL of deuterated chloroform. The reaction was then started by the addition of 1.0 eq. piperidine (7.4 µL piperidine to mPEG2000-AA; 4.9 µL piperidine to $PMOx_{35}$-AA; 3.6 µL piperidine to $PEtOx_{24}$-AA) to the solution followed by stirring of the reaction mixture at room temperature. For each ^{1}H NMR measurement, 0.6 mL

of the reaction mixture were withdrawn shortly before the chosen time period, filled into a NMR tube and analyzed immediately.

6 Conclusions and Outlook

This work was focused on the synthesis and potential application of various well-defined, end-group functionalized poly(2-oxazoline)s (POx) with different chain lengths, solubilities and number of reactive end-groups. The obtained findings demonstrate the versatility of tailor-made POx with regard to their functionalization possibilities and applicability in amphiphilic conetworks or biocatalysis.

In the first part of this study, two novel families of amphiphilic polymer conetworks (APCNs) were synthesized *via* copolymerization of the hydrophobic poly(2-(1-ethylpentyl)-2-oxazoline) (PEPOx) as the macromeric cross-linker and with one of the hydrophilic monomers 2-hydroxyethyl acrylate (HEA) or *N*,*N*-dimethylacrylamide (DMA) with varying polymer compositions, respectively. The obtained APCNs were respectively swollen in the solvents water, toluene, and *n*-heptane, and characterized using gravimetrical swelling experiments and small-angle X-ray scattering (SAXS). While the gravimetrical swelling experiments showed similar swelling behavior of the two APCN families PHEA-*l*-PEPOx and PDMA-*l*-PEPOx, with higher PEPOx contents leading to increased swelling ratios in the hydrophobic solvents for both APCN families, SAXS analysis revealed significant differences in the nanostructural behavior of the conetworks upon solvent uptake as depicted in **Figure 6.1**.

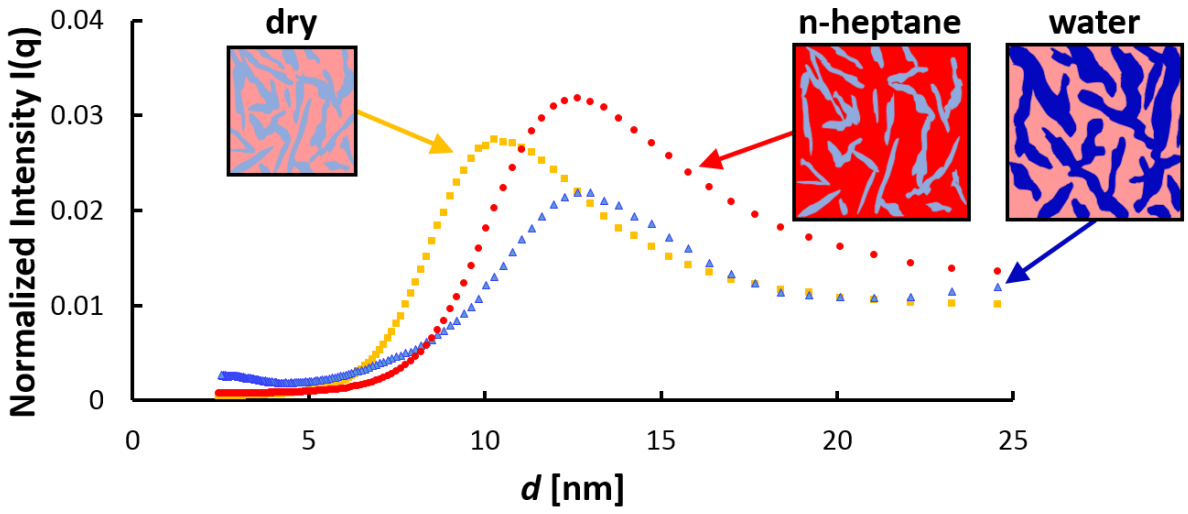

Figure 6.1 Schematic depiction of the nanophasic behavior of PHEA-*l*-PEPOx conetworks upon solvent uptake.[121]

The solvent-induced change of the volume ratios of the nanophases in the PDMA-*l*-PEPOx APCNs caused alterations in the determined nanostructures, especially when swollen in

toluene, as it induced the loss of distinct peaks in the respective SAXS traces for all conetwork compositions. Contrary to this, the HEA-based APCNs with PEPOx contents of 50 to 90 wt% showed no significant changes in their nanophases upon swelling in the chosen phase-selective solvents, representing the first reported APCN family with ideal nanostructural swelling characteristics. Thereby, it was assumed that the formation of hydrogen bonds both inside the PHEA phase and between the PHEA and PEPOx phase stabilizes the nanostructure of the dry APCNs, retaining this structure even in the swollen state. Beyond that, this study successfully demonstrated the potential of SAXS analysis for the characterization of nanophasic materials and their structural alterations caused by solvent uptake.

The second chapter of this work presented an investigation of the nanostructural characteristics of segmented polymer networks composed of the purely hydrophilic polymeric components polyethylene glycol (PEG) and either poly(2-methyl-2-oxazoline) (PMOx) or poly(2-ethyl-2-oxazoline) (PEtOx). Since all chosen polymers exhibit similar structure and polarity, the potential formation of nanophases in these novel materials were examined. For this, respective polymers with bifunctional acrylate end-groups were copolymerized under variation of polymer compositions and characterized by SAXS analysis in the dried and swollen state. While these measurements of synthesized PEG-PEtOx-SPNs indicated no intrinsic nanophase separation, presumably owing to the partial miscibility of the two polymers as confirmed by differential scanning calorimetry (DSC), distinct nanophase separation was observed for analogously prepared PEG-PMOx-SPNs. This nanostructure was detectable in the dry state and even retained upon swelling in toluene as a selective solvent for the PEG phase, leading to approximately similarly increased long-periods d^*. Furthermore, the reduction of the degree of cross-linking of equally composed PEG-PMOx-SPNs led to the absence of SAXS-detectable nanophases in case of a network composition of 50:50 wt% in dried or water swollen network samples. Interestingly, it was possible to induce a distinguished nanophase separation through the uptake of the PEG-selective solvent toluene. It was found by DSC, X-ray diffraction, and atomic force microscopy (AFM), that this observation is caused by PEG crystals formed across the nanophases and thus limiting the formation of ordered morphologies, which can also be overcome by melting these crystals resulting in nanophasic separation as well. This way, a novel SPN family was created, which offers the opportunity to control their nanostructural behavior depending on their composition and *via* the influence of a selective solvent or elevated temperature as illustrated in **Figure 6.2**. Additionally, a possible application for these materials is demonstrated in the form of an easily prepared stabilizing matrix for the immobilization of the enzyme horseradish peroxidase (HRP), which was then employed as a biocatalyst in the organic solvent toluene with retained enzymatic activity.

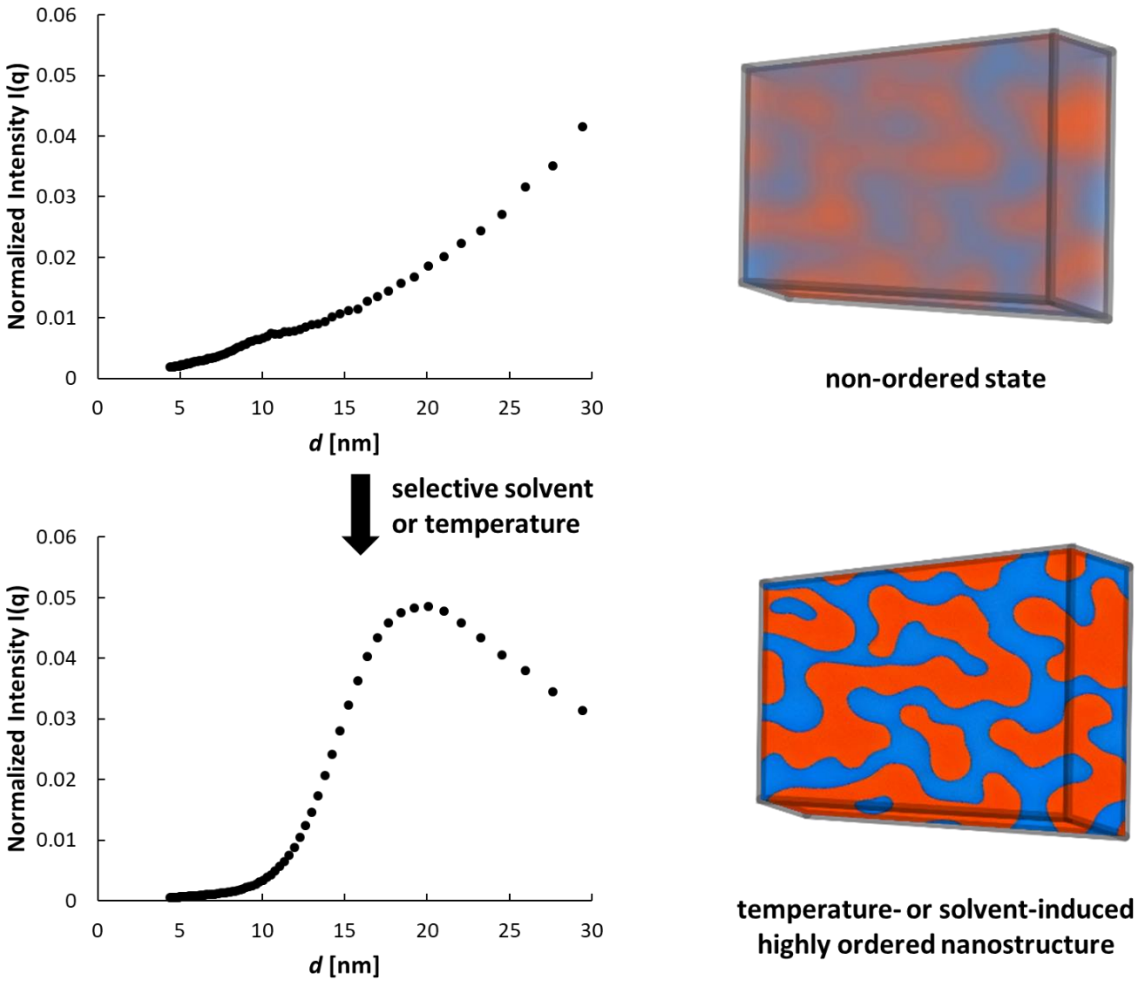

Figure 6.2 Illustration of the influence of a selective solvent or elevated temperature on the nanoscale morphology of the investigated LC-PEG-PMOx-SPNs (50:50 wt%) determined by SAXS analysis.

In the final part of this work, numerous POx-based polymers (PMOx and PEtOx) with varied molar masses and reactive acrylate end-groups were successfully synthesized, characterized and applied as conjugation agents for the modification of proteins, here lysozyme as a model protein. This was conducted in order to evaluate the potential of both, the applicability of water-soluble POx for the modification of proteins as an alternative to the typically chosen PEG, and the aza-Michael addition reaction as a promising tool for the formation of polymer-protein-conjugates. For this, conjugation reactions were performed at two different pH values (pH 8.0 and 9.8) and under variation of chain length and type of acrylate functionalized polymer. Subsequent characterization of the prepared polymer-lysozyme conjugates revealed only low conjugation efficiency for the POx-based polymers, while both PEG-acrylates showed higher coupling efficiency up to fully modified lysozyme. Based on this finding, kinetic studies determining the end-group reactivity of the respective acrylate functionalized polymers and

piperidine as model substrate were conducted and analyzed *via* ^{1}H NMR spectroscopy, demonstrating significantly higher acrylate conversions for both POx-based polymers. Therefore, it was assumed that interactions between bound POx and the protein surface cause the lower conjugation efficiency, as it was reported by HIJAZI *et al*.[258]

In this thesis, several applications of well-defined poly(2-oxazoline)s with functional end-groups in different polymer conetworks with unique properties are demonstrated. This class of polymers represents an exceptionally versatile toolbox in the field of segmented polymer networks and nanostructured materials in general. Future work in this field could focus more on the variation of polymer chain lengths, type of monomer, or even utilize copolymers for the synthesis of segmented polymer networks and study the effect of the respective parameter on the nanostructural behavior of the materials in the dry and swollen state or under additional external stimuli. For this, the polymeric components could be chosen based on the availability of orthogonal solubility or further specifications to develop additional conetworks with ideal swelling behavior of other interesting characteristics. Furthermore, the properties inducing the ideal swelling behavior in the PHEA-*l*-PEPOx conetworks should be further explored by utilizing additional hydrophilic, hydrogen bond forming monomers.

For the application of POx-based conjugation agents in Michael-type addition reactions, further investigations of the interactions between the polymers and the protein surface are expected to provide deeper insights into this promising approach. Based on these results, the polymer compositions, such as (block-)copolymers, and chain lengths could be varied for a better conjugation efficiency to achieve the goal of organosoluble and stabilized enzymes for biocatalytic applications. Furthermore, the optimization of the conjugation reaction parameters and the isolation of unmodified proteins after the conjugation step, e.g. *via* fast protein liquid chromatography (FPLC)[260], are expected to improve the modification and characterization possibilities. As a tool for a more detailed analysis of the conjugation products and binding sites, further investigations using Edman degradation with subsequent mass spectrometry characterization of the individual amino acids could be conducted.[244]

7 References

1 C. K. Varnava, C. S. Patrickios, *Polymer* **2021**, *215*, 123322. doi: 10.1016/j.polymer.2020.123322

2 J. E. Mark, *Physical Properties of Polymers Handbook*, 2 ed., Springer New York, New York, **2007**.

3 J. T. Seitz, *Journal of Applied Polymer Science* **1993**, *49*, 1331-1351. doi: 10.1002/app.1993.070490802

4 R. Hoogenboom, *Angew Chem Int Ed Engl* **2009**, *48*, 7978-7994. doi: 10.1002/anie.200901607

5 T. Lorson, M. M. Lubtow, E. Wegener, M. S. Haider, S. Borova, D. Nahm, R. Jordan, M. Sokolski-Papkov, A. V. Kabanov, R. Luxenhofer, *Biomaterials* **2018**, *178*, 204-280. doi: 10.1016/j.biomaterials.2018.05.022

6 T. X. Viegas, M. D. Bentley, J. M. Harris, Z. Fang, K. Yoon, B. Dizman, R. Weimer, A. Mero, G. Pasut, F. M. Veronese, *Bioconjug Chem* **2011**, *22*, 976-986. doi: 10.1021/bc200049d

7 A. Mero, G. Pasut, L. Dalla Via, M. W. Fijten, U. S. Schubert, R. Hoogenboom, F. M. Veronese, *J Control Release* **2008**, *125*, 87-95. doi: 10.1016/j.jconrel.2007.10.010

8 R. W. Moreadith, T. X. Viegas, M. D. Bentley, J. M. Harris, Z. Fang, K. Yoon, B. Dizman, R. Weimer, B. P. Rae, X. Li, C. Rader, D. Standaert, W. Olanow, *European Polymer Journal* **2017**, *88*, 524-552. doi: 10.1016/j.eurpolymj.2016.09.052

9 E. Vlassi, A. Papagiannopoulos, S. Pispas, *European Polymer Journal* **2017**, *88*, 516-523. doi: 10.1016/j.eurpolymj.2016.10.034

10 V. R. de la Rosa, *J Mater Sci Mater Med* **2014**, *25*, 1211-1225. doi: 10.1007/s10856-013-5034-y

11 M. Schmidt, L. K. Bast, F. Lanfer, L. Richter, E. Hennes, R. Seymen, C. Krumm, J. C. Tiller, *Bioconjug Chem* **2017**, *28*, 2440-2451. doi: 10.1021/acs.bioconjchem.7b00424

12 M. Schmidt, S. Harmuth, E. R. Barth, E. Wurm, R. Fobbe, A. Sickmann, C. Krumm, J. C. Tiller, *Bioconjug Chem* **2015**, *26*, 1950-1962. doi: 10.1021/acs.bioconjchem.5b00393

13 A. Romanovska, M. Schmidt, V. Brandt, J. Tophoven, J. C. Tiller, *J Control Release* **2024**, *368*, 15-23. doi: 10.1016/j.jconrel.2024.02.013

14 A.-L. Kampmann, T. Grabe, C. Jaworski, R. Weberskirch, *RSC Advances* **2016**, *6*, 99752-99763. doi: 10.1039/c6ra22896h

15 T. Kotre, O. Nuyken, R. Weberskirch, *Macromolecular Rapid Communications* **2002**, *23*, 871-876. doi: 10.1002/1521-3927(20021001)23:15<871::aid-marc871>3.0.co;2-g

16 C. Weber, R. Hoogenboom, U. S. Schubert, *Progress in Polymer Science* **2012**, *37*, 686-714. doi: 10.1016/j.progpolymsci.2011.10.002

17 R. Hoogenboom, H. Schlaad, *Polymer Chemistry* **2017**, *8*, 24-40. doi: 10.1039/c6py01320a

18 D. Segiet, R. Jerusalem, F. Katzenberg, J. C. Tiller, *Journal of Polymer Science* **2020**, *58*, 747-755. doi: 10.1002/pol.20190267

19 D. Segiet, T. Raidt, H. Özdem, S. Weckes, J. C. Tiller, F. Katzenberg, *Journal of Polymer Science Part B: Polymer Physics* **2019**, *57*, 1053-1061. doi: 10.1002/polb.24859

20 L. Benski, I. Viran, F. Katzenberg, J. C. Tiller, *Macromolecular Chemistry and Physics* **2020**, *222*. doi: 10.1002/macp.202000292

21 Y. Chujo, K. Sada, K. Matsumoto, T. Saegusa, *Macromolecules* **2002**, *23*, 1234-1237. doi: 10.1021/ma00207a002

22 T. R. Dargaville, J. R. Park, R. Hoogenboom, *Macromol Biosci* **2018**, *18*, e1800070. doi: 10.1002/mabi.201800070

23 L. Yang, F. Wang, P. Ren, T. Zhang, Q. Zhang, *Macromolecular Research* **2023**, *31*, 413-426. doi: 10.1007/s13233-023-00116-x

24 M. Szwarc, *Nature* **1956**, *178*, 1168-1169. doi: 10.1038/1781168a0

25 M. Glassner, M. Vergaelen, R. Hoogenboom, *Polymer International* **2017**, *67*, 32-45. doi: 10.1002/pi.5457

26 T. Kagiya, S. Narisawa, T. Maeda, K. Fukui, *Journal of Polymer Science Part B: Polymer Letters* **2003**, *4*, 441-445. doi: 10.1002/pol.1966.110040701

27 W. Seeliger, E. Aufderhaar, W. Diepers, R. Feinauer, R. Nehring, W. Thier, H. Hellmann, *Angew Chem Int Ed Engl* **1966**, *5*, 875-888. doi: 10.1002/anie.196608751

28 D. A. Tomalia, D. P. Sheetz, *Journal of Polymer Science Part A-1: Polymer Chemistry* **2003**, *4*, 2253-2265. doi: 10.1002/pol.1966.150040919

29 T. G. Bassiri, A. Levy, M. Litt, *Journal of Polymer Science Part B: Polymer Letters* **2003**, *5*, 871-879. doi: 10.1002/pol.1967.110050927

30 T. Saegusa, H. Ikeda, H. Fujii, *Polymer Journal* **1972**, *3*, 35-39. doi: 10.1295/polymj.3.35

31 S. Kobayashi, T. Igarashi, Y. Moriuchi, T. Saegusa, *Macromolecules* **1986**, *19*, 535-541. doi: 10.1021/ma00157a006

32 B. Guillerm, S. Monge, V. Lapinte, J. J. Robin, *Macromol Rapid Commun* **2012**, *33*, 1600-1612. doi: 10.1002/marc.201200266

33 K. Aoi, *Progress in Polymer Science* **1996**, *21*, 151-208. doi: 10.1016/0079-6700(95)00020-8

34 M. Szwarc, M. Levy, R. Milkovich, *Journal of the American Chemical Society* **2002**, *78*, 2656-2657. doi: 10.1021/ja01592a101

35 F. Wiesbrock, R. Hoogenboom, C. H. Abeln, U. S. Schubert, *Macromolecular Rapid Communications* **2004**, *25*, 1895-1899. doi: 10.1002/marc.200400369

36 H. Schlaad, C. Diehl, A. Gress, M. Meyer, A. L. Demirel, Y. Nur, A. Bertin, *Macromol Rapid Commun* **2010**, *31*, 511-525. doi: 10.1002/marc.200900683

37 J. M. Kranenburg, C. A. Tweedie, R. Hoogenboom, F. Wiesbrock, H. M. L. Thijs, C. E. Hendriks, K. J. Van Vliet, U. S. Schubert, *Journal of Materials Chemistry* **2007**, *17*, 2713. doi: 10.1039/b701945a

38 M. Schmidt, T. Raidt, S. Ring, S. Gielke, C. Gramse, S. Wilhelm, F. Katzenberg, C. Krumm, J. C. Tiller, *European Polymer Journal* **2017**, *88*, 562-574. doi: 10.1016/j.eurpolymj.2016.09.046

39 K. Kempe, R. Hoogenboom, S. Hoeppener, C. A. Fustin, J. F. Gohy, U. S. Schubert, *Chem Commun (Camb)* **2010**, *46*, 6455-6457. doi: 10.1039/c001629b

40 A. Lusina, T. Nazim, M. Ceglowski, *Polymers (Basel)* **2022**, *14*. doi: 10.3390/polym14194176

41 M. W. M. Fijten, C. Haensch, B. M. van Lankvelt, R. Hoogenboom, U. S. Schubert, *Macromolecular Chemistry and Physics* **2008**, *209*, 1887-1895. doi: 10.1002/macp.200800226

42 C. Giardi, V. Lapinte, F. Nielloud, J. M. Devoisselle, J. J. Robin, *Journal of Polymer Science Part A: Polymer Chemistry* **2010**, *48*, 4027-4035. doi: 10.1002/pola.24188

43 B. Brissault, C. Guis, H. Cheradame, *European Polymer Journal* **2002**, *38*, 219-228. doi: 10.1016/s0014-3057(01)00157-4

44 R. Hoogenboom, M. W. M. Fijten, U. S. Schubert, *Journal of Polymer Science Part A: Polymer Chemistry* **2004**, *42*, 1830-1840. doi: 10.1002/pola.20024

45 M. Glassner, D. R. D'hooge, J. Young Park, P. H. M. Van Steenberge, B. D. Monnery, M.-F. Reyniers, R. Hoogenboom, *European Polymer Journal* **2015**, *65*, 298-304. doi: 10.1016/j.eurpolymj.2015.01.019

46 T. Saegusa, S. Kobayashi, A. Yamada, *Die Makromolekulare Chemie* **1976**, *177*, 2271-2283. doi: 10.1002/macp.1976.021770805

47 M. W. M. Fijten, R. Hoogenboom, U. S. Schubert, *Journal of Polymer Science Part A: Polymer Chemistry* **2008**, *46*, 4804-4816. doi: 10.1002/pola.22814

48 M. Reif, R. Jordan, *Macromolecular Chemistry and Physics* **2011**, *212*, 1815-1824. doi: 10.1002/macp.201100276

49 P. O. Dubois, Coulembier; Raquez, Jean-Marie, *Handbook of Ring-Opening Polymerization*, 1. ed., Wiley-VCH, Weinheim, **2009**.

50 R. Luxenhofer, Y. Han, A. Schulz, J. Tong, Z. He, A. V. Kabanov, R. Jordan, *Macromol Rapid Commun* **2012**, *33*, 1613-1631. doi: 10.1002/marc.201200354

51 Y. Chujo, E. Ihara, H. Ihara, T. Saegusa, *Macromolecules* **1989**, *22*, 2040-2043. doi: 10.1021/ma00195a003

52 S. Kobayashi, H. Uyama, Y. Narita, J. Ishiyama, *Macromolecules* **1992**, *25*, 3232-3236. doi: 10.1021/ma00038a031

53 B. Guillerm, V. Darcos, V. Lapinte, S. Monge, J. Coudane, J. J. Robin, *Chem Commun (Camb)* **2012**, *48*, 2879-2881. doi: 10.1039/c2cc30191a

54 S. Kobayashi, H. Uyama, T. Mori, Y. Narita, *Chemistry Letters* **1991**, *20*, 1771-1774. doi: 10.1246/cl.1991.1771

55 K. Lava, B. Verbraeken, R. Hoogenboom, *European Polymer Journal* **2015**, *65*, 98-111. doi: 10.1016/j.eurpolymj.2015.01.014

56 L. Y. Qiu, L. Yan, L. Zhang, Y. M. Jin, Q. H. Zhao, *Int J Pharm* **2013**, *456*, 315-324. doi: 10.1016/j.ijpharm.2013.08.071

57 Y. Gao, Y. Li, Y. Li, L. Yuan, Y. Zhou, J. Li, L. Zhao, C. Zhang, X. Li, Y. Liu, *Nanoscale* **2015**, *7*, 597-612. doi: 10.1039/c4nr05738d

58 J. Li, Y. Zhou, C. Li, D. Wang, Y. Gao, C. Zhang, L. Zhao, Y. Li, Y. Liu, X. Li, *Bioconjug Chem* **2015**, *26*, 110-119. doi: 10.1021/bc5004718

59 T. Saegusa, H. Ikeda, *Macromolecules* **1973**, *6*, 808-811. doi: 10.1021/ma60036a004

60 F. Wiesbrock, R. Hoogenboom, M. A. M. Leenen, M. A. R. Meier, U. S. Schubert, *Macromolecules* **2005**, *38*, 5025-5034. doi: 10.1021/ma0474170

61 G. Volet, V. Chanthavong, V. Wintgens, C. Amiel, *Macromolecules* **2005**, *38*, 5190-5197. doi: 10.1021/ma050407u

62 R. Jordan, K. Martin, H. J. Räder, K. K. Unger, *Macromolecules* **2001**, *34*, 8858-8865. doi: 10.1021/ma011573e

63 C. J. Waschinski, V. Herdes, F. Schueler, J. C. Tiller, *Macromol Biosci* **2005**, *5*, 149-156. doi: 10.1002/mabi.200400169

64 R. Weberskirch, J. Preuschen, H. W. Spiess, O. Nuyken, *Macromolecular Chemistry and Physics* **2000**, *201*, 995-1007. doi: 10.1002/1521-3935(20000601)201:10<995::aid-macp995>3.0.co;2-t

65 C. Giardi, V. Lapinte, C. Charnay, J. J. Robin, *Reactive and Functional Polymers* **2009**, *69*, 643-649. doi: 10.1016/j.reactfunctpolym.2009.04.008

66 S. Kobayashi, H. Uyama, *Macromolecules* **1991**, *24*, 5473-5475. doi: 10.1021/ma00019a041

67 S. Kobayashi, M. Kaku, S. j. Sawada, T. Saegusa, *Polymer Bulletin* **1985**, *13*, 447-451. doi: 10.1007/bf01033343

68 T. Bartz, M. Klapper, K. Müllen, *Macromolecular Chemistry and Physics* **1994**, *195*, 1097-1109. doi: 10.1002/macp.1994.021950323

69 K. Kempe, R. Hoogenboom, M. Jaeger, U. S. Schubert, *Macromolecules* **2011**, *44*, 6424-6432. doi: 10.1021/ma201385k

70 M. Einzmann, W. H. Binder, *Journal of Polymer Science Part A: Polymer Chemistry* **2001**, *39*, 2821-2831. doi: 10.1002/pola.1262

71 J. S. Hrkach, K. Matyjaszewski, *Macromolecules* **1992**, *25*, 2070-2075. doi: 10.1021/ma00034a002

72 P. Guinot, L. Bryant, T. Y. Chow, T. Saegusa, *Macromolecular Chemistry and Physics* **1996**, *197*, 1-17. doi: 10.1002/macp.1996.021970101

73 D. Pizzi, J. Humphries, J. P. Morrow, N. L. Fletcher, C. A. Bell, K. J. Thurecht, K. Kempe, *European Polymer Journal* **2019**, *121*, 109258. doi: 10.1016/j.eurpolymj.2019.109258

74 A. Podevyn, K. Arys, V. R. de la Rosa, M. Glassner, R. Hoogenboom, *European Polymer Journal* **2019**, *120*, 109273. doi: 10.1016/j.eurpolymj.2019.109273

75 B. Verbraeken, B. D. Monnery, K. Lava, R. Hoogenboom, **2018**, 1-59. doi: 10.1002/0471440264.pst626.pub2

76 L. Benski, J. C. Tiller, *European Polymer Journal* **2019**, *120*, 109233. doi: 10.1016/j.eurpolymj.2019.109233

77 O. Nuyken, G. Maier, A. Groß, H. Fischer, *Macromolecular Chemistry and Physics* **1996**, *197*, 83-95. doi: 10.1002/macp.1996.021970106

78 C. Krumm, S. Konieczny, G. J. Dropalla, M. Milbradt, J. C. Tiller, *Macromolecules* **2013**, *46*, 3234-3245. doi: 10.1021/ma4004665

79 Z. He, A. Schulz, X. Wan, J. Seitz, H. Bludau, D. Y. Alakhova, D. B. Darr, C. M. Perou, R. Jordan, I. Ojima, A. V. Kabanov, R. Luxenhofer, *J Control Release* **2015**, *208*, 67-75. doi: 10.1016/j.jconrel.2015.02.024

80 S. Kobayashi, E. Masuda, S. Shoda, Y. Shimano, *Macromolecules* **1989**, *22*, 2878-2884. doi: 10.1021/ma00197a002

81 J.-S. Park, K. Kataoka, *Macromolecules* **2006**, *39*, 6622-6630. doi: 10.1021/ma0605548

82 Y. Tsukahara, K. Adachi, in *Encyclopedia of Polymeric Nanomaterials*, 1 ed. (Eds.: S. Kobayashi, K. Müllen), Springer Berlin, Heidelberg, **2015**. doi: 10.1007/978-3-642-29648-2

83 C. A. Uraneck, H. L. Hsieh, O. G. Buck, *Journal of Polymer Science* **1960**, *46*, 535-539. doi: 10.1002/pol.1960.1204614825

84 W. Lequieu, P. Van De Velde, F. E. Du Prez, P. Adriaensens, L. Storme, J. Gelan, *Polymer* **2004**, *45*, 7943-7951. doi: 10.1016/j.polymer.2004.09.024

85 F. E. Du Prez, E. J. Goethals, R. Schué, H. Qariouh, F. Schué, *Polymer International* **1998**, *46*, 117-125. doi: 10.1002/(sici)1097-0126(199806)46:2<117::aid-pi974>3.0.co;2-i

86 C. Fodor, T. Stumphauser, R. Thomann, Y. Thomann, B. Iván, *Polymer Chemistry* **2016**, *7*, 5375-5385. doi: 10.1039/c6py00848h

87 E. J. Kepola, E. Loizou, C. S. Patrickios, E. Leontidis, C. Voutouri, T. Stylianopoulos, R. Schweins, M. Gradzielski, C. Krumm, J. C. Tiller, M. Kushnir, C. Wesdemiotis, *ACS Macro Lett* **2015**, *4*, 1163-1168. doi: 10.1021/acsmacrolett.5b00608

88 N. Fribiczer, K. Hagmann, C. Bunk, F. Böhme, R. von Klitzing, S. Seiffert, *Macromolecular Chemistry and Physics* **2023**, *225*. doi: 10.1002/macp.202300389

89 P. C. Nicolson, J. Vogt, *Biomaterials* **2001**, *22*, 3273-3283. doi: 10.1016/s0142-9612(01)00165-x

90 J. P. Kennedy, G. Fenyvesi, S. Na, B. Keszler, K. S. Rosenthal, **2002**, *833*, 290-299. doi: 10.1021/bk-2002-0833.ch019

91 J. C. Tiller, C. Sprich, L. Hartmann, *J Control Release* **2005**, *103*, 355-367. doi: 10.1016/j.jconrel.2004.12.002

92 J. C. Tiller, L. Hartmann, J. Scherble, *Surface Coatings International Part B: Coatings Transactions* **2005**, *88*, 49-53. doi: 10.1007/bf02699707

93 M. Hanko, N. Bruns, S. Rentmeister, J. C. Tiller, J. Heinze, *Anal Chem* **2006**, *78*, 6376-6383. doi: 10.1021/ac060634+

94 M. Hanko, N. Bruns, J. C. Tiller, J. Heinze, *Anal Bioanal Chem* **2006**, *386*, 1273-1283. doi: 10.1007/s00216-006-0680-2

95 Y. Sun, J. Collett, N. J. Fullwood, S. Mac Neil, S. Rimmer, *Biomaterials* **2007**, *28*, 661-670. doi: 10.1016/j.biomaterials.2006.09.024

96 J. Tobis, Y. Thomann, J. C. Tiller, *Polymer* **2010**, *51*, 35-45. doi: 10.1016/j.polymer.2009.10.055

97 J. Tobis, L. Boch, Y. Thomann, J. C. Tiller, *Journal of Membrane Science* **2011**, *372*, 219-227. doi: 10.1016/j.memsci.2011.02.004

98 N. Bruns, W. Bannwarth, J. C. Tiller, *Biotechnol Bioeng* **2008**, *101*, 19-26. doi: 10.1002/bit.21868

99 N. Bruns, M. Hanko, S. Dech, R. Ladisch, J. Tobis, J. C. Tiller, *Macromol Symp* **2010**, *291-292*, 293-301. doi: 10.1002/masy.201050534

100 D. E. Apostolides, G. Michael, C. S. Patrickios, B. Notredame, Y. Zhang, J. F. Gohy, S. Prevost, M. Gradzielski, F. A. Jung, C. M. Papadakis, *ACS Appl Mater Interfaces* **2024**, *16*, 23813-23825. doi: 10.1021/acsami.3c19189

101 S. Ulrich, L. F. Boesel, N. Bruns, in *Amphiphilic Polymer Co-networks: Synthesis, Properties, Modelling and Applications* (Ed.: C. S. Patrickios), Royal Society of Chemistry, Cambridge, **2020**, pp. 331-363. doi: 10.1039/9781788015769-00331

102 M. Rikkou-Kalourkoti, C. S. Patrickios, *Macromolecules* **2012**, *45*, 7890-7899. doi: 10.1021/ma3012416

103 M. Rikkou-Kalourkoti, E. Loizou, L. Porcar, K. Matyjaszewski, C. S. Patrickios, *Polymer Chemistry* **2012**, *3*, 105-116. doi: 10.1039/c1py00349f

104 Y. Shi, H. Schmalz, S. Agarwal, *Polymer Chemistry* **2015**, *6*, 6409-6415. doi: 10.1039/c5py00962f

105 K. R. McLeod, G. N. Tew, in *Amphiphilic Polymer Co-networks: Synthesis, Properties, Modelling and Applications* (Ed.: C. S. Patrickios), Royal Society of Chemistry, Cambridge, **2020**, pp. 129-155. doi: 10.1039/9781788015769-00129

106 C. S. Patrickios, *Amphiphilic Polymer Co-networks: Synthesis, Properties, Modelling and Applications*, The Royal Society of Chemistry, Cambridge, **2020**.

107 G. Erdodi, J. P. Kennedy, *Progress in Polymer Science* **2006**, *31*, 1-18. doi: 10.1016/j.progpolymsci.2005.11.001

108 N. Bruns, J. C. Tiller, *Nano Lett* **2005**, *5*, 45-48. doi: 10.1021/nl048413b

109 J. Scherble, B. Iván, R. Mülhaupt, *Macromolecular Chemistry and Physics* **2002**, *203*, 1866-1871. doi: 10.1002/1521-3935(200208)203:12<1866::aid-macp1866>3.0.co;2-g

110 M. Doura, Y. Naka, H. Aota, A. Matsumoto, *Macromolecules* **2003**, *36*, 8477-8482. doi: 10.1021/ma0302715

111 C. S. Patrickios, T. K. Georgiou, *Current Opinion in Colloid & Interface Science* **2003**, *8*, 76-85. doi: 10.1016/s1359-0294(03)00005-0

112 M. Delerba, J. R. Ebdon, S. Rimmer, *Macromolecular Rapid Communications* **2003**, *18*, 723-728. doi: 10.1002/marc.1997.030180814

113 C. S. Gudipati, J. A. Finlay, J. A. Callow, M. E. Callow, K. L. Wooley, *Langmuir* **2005**, *21*, 3044-3053. doi: 10.1021/la048015o

114 L. Mespouille, J. L. Hedrick, P. Dubois, *Soft Matter* **2009**, *5*, 4878. doi: 10.1039/b910041p

115 I. Barakat, P. Dubois, R. Jérôme, P. Teyssié, E. Goethals, *Journal of Polymer Science Part A: Polymer Chemistry* **1994**, *32*, 2099-2110. doi: 10.1002/pola.1994.080321112

116 I. Barakat, P. Dubois, C. Grandfils, R. Jerome, *Journal of Polymer Science Part A: Polymer Chemistry* **1999**, *37*, 2401-2411. doi: 10.1002/(sici)1099-0518(19990715)37:14<2401::aid-pola14>3.0.co;2-9

117 C. S. Huang, S. Yakunin, J. Avaro, X. Kang, M. I. Bodnarchuk, M. Liebi, X. Sun, R. M. Rossi, M. V. Kovalenko, L. F. Boesel, *Advanced Energy Materials* **2022**, *12*. doi: 10.1002/aenm.202200441

118 L. Zhang, C. Zhang, X. Peng, C. He, *RSC Advances* **2016**, *6*, 17228-17238. doi: 10.1039/C5RA25007B

119 C. Lin, I. Gitsov, *Macromolecules* **2010**, *43*, 3256-3267. doi: 10.1021/ma9026564

120 C. Fodor, G. Kali, R. Thomann, Y. Thomann, B. Iván, R. Mülhaupt, *RSC Advances* **2017**, *7*, 6827-6834. doi: 10.1039/c6ra25356c

121 S. A. Wilhelm, M. Maricanov, V. Brandt, F. Katzenberg, J. C. Tiller, *Polymer* **2022**, *242*, 124582. doi: 10.1016/j.polymer.2022.124582

122 B. R. Clarke, G. N. Tew, *Macromolecules* **2022**, *55*, 5131-5139. doi: 10.1021/acs.macromol.2c00449

123 P. A. Benitez-Duif, M. Breisch, D. Kurka, K. Edel, S. Gökcay, D. Stangier, W. Tillmann, M. Hijazi, J. C. Tiller, *Advanced Functional Materials* **2022**, *32*, 2204837. doi: 10.1002/adfm.202204837

124 C. Bunk, N. Fribiczer, L. Lucas, M. Geisler, V. Brigitte, S. Seiffert, K. Saalwächter, M. Lang, F. Böhme, *Polymer* **2024**, *304*, 127149. doi: 10.1016/j.polymer.2024.127149

125 L. Löser, C. Bunk, R. Scholz, M. Lang, F. Böhme, K. Saalwächter, *Macromolecules* **2024**, *57*, 940-954. doi: 10.1021/acs.macromol.3c02139

126 D. G. Tsalikis, M. Ciobanu, C. S. Patrickios, Y. Higuchi, *Macromolecules* **2023**, *56*, 9299-9311. doi: 10.1021/acs.macromol.3c01392

127 C. Mugemana, P. Grysan, R. Dieden, D. Ruch, N. Bruns, P. Dubois, *Macromolecular Chemistry and Physics* **2020**, *221*, 1900432. doi: 10.1002/macp.201900432

128 J. M. Hutchison, B. K. Mayer, M. Vega, W. E. Chacha, J. L. Zilles, *Water Res X* **2021**, *12*, 100112. doi: 10.1016/j.wroa.2021.100112

129 U. Hanefeld, F. Hollmann, C. E. Paul, *Chem Soc Rev* **2022**, *51*, 594-627. doi: 10.1039/d1cs00100k

130 S. P. France, R. D. Lewis, C. A. Martinez, *JACS Au* **2023**, *3*, 715-735. doi: 10.1021/jacsau.2c00712

131 M. M. Muller, *Biochemistry* **2018**, *57*, 177-185. doi: 10.1021/acs.biochem.7b00861

132 A. Abuchowski, T. van Es, N. C. Palczuk, F. F. Davis, *J. Biol. Chem.* **1977**, *252*, 3578-3581. doi: n.a.

133 A. Abuchowski, J. R. McCoy, N. C. Palczuk, T. van Es, F. F. Davis, *J. Biol. Chem.* **1977**, *252*, 3582-3586. doi: n.a.

134 P. Milla, F. Dosio, L. Cattel, *Curr Drug Metab* **2012**, *13*, 105-119. doi: 10.2174/138920012798356934

135 C. Ginn, H. Khalili, R. Lever, S. Brocchini, *Future Med Chem* **2014**, *6*, 1829-1846. doi: 10.4155/fmc.14.125

136 S. Herman, G. Hooftman, E. Schacht, *Journal of Bioactive and Compatible Polymers* **1995**, *10*, 145-187. doi: 10.1177/088391159501000205

137 G. Pasut, F. M. Veronese, in *Polymer Therapeutics I. Advances in Polymer Science, Vol. 192* (Eds.: R. Satchi-Fainaro, R. Duncan), Springer, Heidelberg, **2005**, pp. 95-134. doi: 10.1007/12_022

138 F. F. Davis, *Adv Drug Deliv Rev* **2002**, *54*, 457-458. doi: 10.1016/s0169-409x(02)00021-2

139 J. Zhou, S. Hu, J. Ding, J. Xu, J. Shi, N. Dong, *Biomed Eng Online* **2013**, *12*, 87. doi: 10.1186/1475-925X-12-87

140 J. M. Harris, N. E. Martin, M. Modi, *Clin Pharmacokinet* **2001**, *40*, 539-551. doi: 10.2165/00003088-200140070-00005

141 G. DeSantis, J. B. Jones, *Curr Opin Biotechnol* **1999**, *10*, 324-330. doi: 10.1016/S0958-1669(99)80059-7

142 Y. Inada, K. Takahashi, T. Yoshimoto, A. Ajima, A. Matsushima, Y. Saito, *Trends in Biotechnology* **1986**, *4*, 190-194. doi: 10.1016/0167-7799(86)90244-1

143 M. W. Baillargeon, P. E. Sonnet, *Journal of the American Oil Chemists' Society* **1988**, *65*, 1812-1815. doi: 10.1007/bf02542388

144 K. Takahashi, H. Nishimura, T. Yoshimoto, Y. Saito, Y. Inada, *Biochem Biophys Res Commun* **1984**, *121*, 261-265. doi: 10.1016/0006-291x(84)90716-2

145 H. Lee, K. Takahashi, Y. Kodera, K. Ohwada, T. Tsuzuki, A. Matsushima, Y. Inada, *Biotechnology Letters* **1988**, *10*, 403-407. doi: 10.1007/bf01087438

146 M. A. Gauthier, H.-A. Klok, *Polymer Chemistry* **2010**, *1*, 1352. doi: 10.1039/c0py90001j

147 C. Pina, D. Clark, H. Blanch, *Biotechnology Techniques* **1989**, *3*, 333-338. doi: 10.1007/bf01875632

148 F. Zhang, M. R. Liu, H. T. Wan, *Biol Pharm Bull* **2014**, *37*, 335-339. doi: 10.1248/bpb.b13-00661

149 B. M. Chen, T. L. Cheng, S. R. Roffler, *ACS Nano* **2021**, *15*, 14022-14048. doi: 10.1021/acsnano.1c05922

150 R. P. Garay, R. El-Gewely, J. K. Armstrong, G. Garratty, P. Richette, *Expert Opin Drug Deliv* **2012**, *9*, 1319-1323. doi: 10.1517/17425247.2012.720969

151 K. Knop, R. Hoogenboom, D. Fischer, U. S. Schubert, *Angew Chem Int Ed Engl* **2010**, *49*, 6288-6308. doi: 10.1002/anie.200902672

152 X. Yao, C. Qi, C. Sun, F. Huo, X. Jiang, *Nano Today* **2023**, *48*, 101738. doi: 10.1016/j.nantod.2022.101738

153 S. Shi, C. Yao, J. Cen, L. Li, G. Liu, J. Hu, S. Liu, *Angew Chem Int Ed Engl* **2020**, *59*, 18172-18178. doi: 10.1002/anie.202006687

154 P. Zhang, F. Sun, S. Liu, S. Jiang, *Journal of Controlled Release* **2016**, *244*, 184-193. doi: 10.1016/j.jconrel.2016.06.040

155 M. Miyamoto, K. Naka, M. Shiozaki, Y. Chujo, T. Saegusa, *Macromolecules* **1990**, *23*, 3201-3205. doi: 10.1021/ma00215a001

156 K. Naka, Y. Chujo, M. Miyamoto, T. Saegusa, *Journal of Macromolecular Science, Part A* **1997**, *34*, 123-132. doi: 10.1080/10601329708014940

157 K. Naka, Y. Chujo, M. Miyamoto, T. Saegusa, *Journal of Macromolecular Science, Part A* **1997**, *34*, 35-48. doi: 10.1080/10601329708014932

158 J. Tong, R. Luxenhofer, X. Yi, R. Jordan, A. V. Kabanov, *Mol Pharm* **2010**, *7*, 984-992. doi: 10.1021/mp100102p

159 J. Tong, X. Yi, R. Luxenhofer, W. A. Banks, R. Jordan, M. C. Zimmerman, A. V. Kabanov, *Mol Pharm* **2013**, *10*, 360-377. doi: 10.1021/mp300496x

160 M. Glassner, S. Maji, V. R. de la Rosa, N. Vanparijs, K. Ryskulova, B. G. De Geest, R. Hoogenboom, *Polymer Chemistry* **2015**, *6*, 8354-8359. doi: 10.1039/c5py01280e

161 O. Sedlacek, V. R. de la Rosa, R. Hoogenboom, *European Polymer Journal* **2019**, *120*, 109246. doi: 10.1016/j.eurpolymj.2019.109246

162 S. Konieczny, C. P. Fik, N. J. Averesch, J. C. Tiller, *J Biotechnol* **2012**, *159*, 195-203. doi: 10.1016/j.jbiotec.2012.01.016

163 S. Konieczny, C. Krumm, D. Doert, K. Neufeld, J. C. Tiller, *Journal of Biotechnology* **2014**, *181*, 55-63. doi: 10.1016/j.jbiotec.2014.03.035

164 M. Leurs, Doctoral thesis, TU Dortmund **2019**.

165 M. Hijazi, P. Spiekermann, C. Krumm, J. C. Tiller, *Biotechnol Bioeng* **2019**, *116*, 272-282. doi: 10.1002/bit.26877

166 G. Gil Alvaradejo, M. Glassner, R. Hoogenboom, G. Delaittre, *RSC Adv* **2018**, *8*, 9471-9479. doi: 10.1039/c8ra00948a

167 J. F. Nawroth, J. R. McDaniel, A. Chilkoti, R. Jordan, R. Luxenhofer, *Macromol Biosci* **2016**, *16*, 322-333. doi: 10.1002/mabi.201500376

168 L. Benski, I. Viran, F. Katzenberg, J. C. Tiller, *Macromolecular Chemistry and Physics* **2020**, *222*, 2000292. doi: 10.1002/macp.202000292

169 C. S. Patrickios, K. Matyjaszewski, *Polymer International* **2020**, *70*, 10-13. doi: DOI 10.1002/pi.6138

170 G. Savin, N. Bruns, Y. Thomann, J. C. Tiller, *Macromolecules* **2005**, *38*, 7536-7539. doi: 10.1021/ma0509715

171 S. Dech, T. Cramer, R. Ladisch, N. Bruns, J. C. Tiller, *Biomacromolecules* **2011**, *12*, 1594-1601. doi: 10.1021/bm1015877

172 C. Fodor, G. Kali, B. I. Iván, *Macromolecules* **2011**, *44*, 4496-4502. doi: 10.1021/ma200700m

173 G. Kali, S. Vavra, K. László, B. Iván, *Macromolecules* **2013**, *46*, 5337-5344. doi: 10.1021/ma400535r

174 L. Shi, P. Xie, Z. Li, Y. Wu, J. Deng, *Macromolecular Chemistry and Physics* **2013**, *214*, 1375-1383. doi: 10.1002/macp.201200729

175 M. Achilleos, T. Krasia-Christoforou, C. S. Patrickios, *Macromolecules* **2007**, *40*, 5575-5581. doi: 10.1021/ma070614p

176 M. D. Rikkou, M. Kolokasi, K. Matyjaszewski, C. S. Patrickios, *Journal of Polymer Science Part A: Polymer Chemistry* **2010**, *48*, 1878-1886. doi: 10.1002/pola.23951

177 E. J. Kepola, E. Loizou, C. S. Patrickios, E. Leontidis, C. Voutouri, T. Stylianopoulos, R. Schweins, M. Gradzielski, C. Krumm, J. C. Tiller, M. Kushnir, C. Wesdemiotis, *ACS Macro Letters* **2015**, *4*, 1163-1168. doi: 10.1021/acsmacrolett.5b00608

178 X. Zhang, K. Kyriakos, M. Rikkou-Kalourkoti, E. N. Kitiri, C. S. Patrickios, C. M. Papadakis, *Colloid and Polymer Science* **2016**, *294*, 1027-1036. doi: 10.1007/s00396-016-3856-0

179 S. Meskath, G. Urban, J. Heinze, *Sensors and Actuators B: Chemical* **2011**, *151*, 327-332. doi: 10.1016/j.snb.2010.07.028

180 S. Meskath, G. Urban, J. Heinze, *Sensors and Actuators B: Chemical* **2013**, *186*, 367-373. doi: 10.1016/j.snb.2013.06.007

181 S. Ulrich, A. Osypova, G. Panzarasa, R. M. Rossi, N. Bruns, L. F. Boesel, *Macromol Rapid Commun* **2019**, *40*, e1900360. doi: 10.1002/marc.201900360

182 S. Dech, V. Wruk, C. P. Fik, J. C. Tiller, *Polymer* **2012**, *53*, 701-707. doi: 10.1016/j.polymer.2011.12.027

183 I. Schoenfeld, S. Dech, B. Ryabenky, B. Daniel, B. Glowacki, R. Ladisch, J. C. Tiller, *Biotechnol Bioeng* **2013**, *110*, 2333-2342. doi: 10.1002/bit.24906

184 I. Sittko, K. Kremser, M. Roth, S. Kuehne, S. Stuhr, J. C. Tiller, *Polymer* **2015**, *64*, 122-129. doi: 10.1016/j.polymer.2015.03.038

185 C. Lin, I. Gitsov, *Macromolecules* **2010**, *43*, 10017-10030. doi: 10.1021/ma102044n

186 C.-W. Wang, C. Liu, X.-W. Zhu, Z.-Y. Yang, H.-F. Sun, D.-L. Kong, J. Yang, *Journal of Polymer Science Part A: Polymer Chemistry* **2016**, *54*, 407-417. doi: 10.1002/pola.27790

187 B. Nutan, A. K. S. Chandel, D. V. Bhalani, S. K. Jewrajka, *Polymer* **2017**, *111*, 265-274. doi: 10.1016/j.polymer.2017.01.057

188 Y. Zare, A. Dabbaghi, S. Rahmani, *Polymers for Advanced Technologies* **2019**, *30*, 2790-2801. doi: 10.1002/pat.4711

189 K. Schöller, S. Küpfer, L. Baumann, P. M. Hoyer, D. de Courten, R. M. Rossi, A. Vetushka, M. Wolf, N. Bruns, L. J. Scherer, *Advanced Functional Materials* **2014**, *24*, 5194-5201. doi: 10.1002/adfm.201400671

190 C.-S. Huang, K. Jakubowski, S. Ulrich, S. Yakunin, M. Clerc, C. Toncelli, R. M. Rossi, M. V. Kovalenko, L. F. Boesel, *Nano Energy* **2020**, *76*, 105039. doi: 10.1016/j.nanoen.2020.105039

191 B. Ivan, M. Haraszti, G. Erdodi, J. Scherble, R. Thomann, R. Mülhaupt, *Macromol Symp* **2005**, *227*, 265-273. doi: 10.1002/masy.200550926

192 N. Bruns, J. C. Tiller, *Macromolecules* **2006**, *39*, 4386-4394. doi: 10.1021/ma052592h

193 C. Zhou, L. Deng, F. Yao, L. Xu, J. Zhou, G. D. Fu, *Industrial & Engineering Chemistry Research* **2014**, *53*, 19239-19248. doi: 10.1021/ie503649t

194 A. Domján, G. Erdödi, M. Wilhelm, M. Neidhöfer, K. Landfester, B. Iván, H. W. Spiess, *Macromolecules* **2003**, *36*, 9107-9114. doi: 10.1021/ma034891h

195 A. Domján, P. Mezey, J. Varga, *Macromolecules* **2012**, *45*, 1037-1040. doi: 10.1021/ma202388f

196 C. N. Tironi, R. Graf, I. Lieberwirth, M. Klapper, K. Müllen, *ACS Macro Letters* **2015**, *4*, 1302-1306. doi: 10.1021/acsmacrolett.5b00714

197 C. N. Walker, K. C. Bryson, R. C. Hayward, G. N. Tew, *ACS Nano* **2014**, *8*, 12376-12385. doi: 10.1021/nn505026a

198 G. Kali, T. K. Georgiou, B. Ivan, C. S. Patrickios, E. Loizou, Y. Thomann, J. C. Tiller, *Langmuir* **2007**, *23*, 10746-10755. doi: 10.1021/la7012478

199 M. Vamvakaki, C. S. Patrickios, P. Lindner, M. Gradzielski, *Langmuir* **2007**, *23*, 10433-10437. doi: 10.1021/la700933p

200 D. Kafouris, M. Gradzielski, C. S. Patrickios, *Macromolecules* **2009**, *42*, 2972-2980. doi: 10.1021/ma802859d

201 M. D. Rikkou, E. Loizou, C. S. Patrickios, L. Porcar, *European Polymer Journal* **2010**, *46*, 441-449. doi: 10.1016/j.eurpolymj.2009.10.024

202 T. Hiroi, S. Kondo, T. Sakai, E. P. Gilbert, Y.-S. Han, T.-H. Kim, M. Shibayama, *Macromolecules* **2016**, *49*, 4940-4947. doi: 10.1021/acs.macromol.6b00842

203 D. E. Apostolides, C. S. Patrickios, T. Sakai, M. Guerre, G. Lopez, B. Améduri, V. Ladmiral, M. Simon, M. Gradzielski, D. Clemens, C. Krumm, J. C. Tiller, B. Ernould, J.-F. Gohy, *Macromolecules* **2018**, *51*, 2476-2488. doi: 10.1021/acs.macromol.7b02475

204 E. N. Kitiri, C. K. Varnava, C. S. Patrickios, C. Voutouri, T. Stylianopoulos, M. Gradzielski, I. Hoffmann, *Journal of Polymer Science Part A: Polymer Chemistry* **2018**, *56*, 2161-2174. doi: 10.1002/pola.29176

205 B. A. Iván, K.; Mortensen, K.; Johannsen, I.; Kops, J., *Macromolecules* **2001**, *34*, 1579-1585. doi: 10.1021/ma000062+

206 P. D. Mezey, A.; Ivàn, B.; Thomann, R.; Mülhaupt, R., *Life Sciences, Medicine and Bio Materials, Technical Proceedings of the 2008 NSTI Nanotechnology Conference and Trade Show* **2008**, *2*, 715 - 718. doi: n.a.

207 G. Guzman, T. Nugay, J. P. Kennedy, M. Cakmak, *Langmuir* **2016**, *32*, 3445-3451. doi: 10.1021/acs.langmuir.6b00587

208 T. Stumphauser, G. Kasza, A. Domjan, A. Wacha, Z. Varga, Y. Thomann, R. Thomann, B. Pasztoi, T. M. Trotschler, B. Kerscher, R. Mulhaupt, B. Ivan, *Polymers (Basel)* **2020**, *12*. doi: 10.3390/polym12102292

209 S. Ulrich, A. Sadeghpour, R. M. Rossi, N. Bruns, L. F. Boesel, *Macromolecules* **2018**, *51*, 5267-5277. doi: 10.1021/acs.macromol.8b00841

210 K. Kempe, A. Baumgaertel, R. Hoogenboom, U. S. Schubert, *Journal of Polymer Science Part A: Polymer Chemistry* **2010**, *48*, 5100-5108. doi: 10.1002/pola.24308

211 M. M. Pradas, J. L. G. Ribelles, A. S. Aroca, G. G. Ferrer, J. S. Anton, P. Pissis, *Polymer* **2001**, *42*, 4667-4674. doi: 10.1016/s0032-3861(00)00742-4

212 E. R. Jones, O. O. Mykhaylyk, M. Semsarilar, M. Boerakker, P. Wyman, S. P. Armes, *Macromolecules* **2016**, *49*, 172-181. doi: 10.1021/acs.macromol.5b02385

213 J. Scherble, R. Thomann, Béla, R. Mülhaupt, *Journal of Polymer Science Part B: Polymer Physics* **2001**, *39*, 1429-1436. doi: 10.1002/polb.1114

214 B. Iván, J. P. Kennedy, P. W. Mackey, **1991**, *469*, 203-212. doi: 10.1021/bk-1991-0469.ch019

215 S. Dech, T. Cramer, R. Ladisch, N. Bruns, J. C. Tiller, *Biomacromolecules* **2011**, *12*, 1594-1601. doi: 10.1021/bm1015877

216 N. Bruns, W. Bannwarth, J. C. Tiller, *Biotechnology and Bioengineering* **2008**, *101*, 19-26. doi: 10.1002/bit.21868

217 D. Christova, R. Velichkova, W. Loos, E. J. Goethals, F. D. Prez, *Polymer* **2003**, *44*, 2255-2261. doi: 10.1016/s0032-3861(03)00139-3

218 J. C. Tiller, C. Sprich, L. Hartmann, *Journal of Controlled Release* **2005**, *103*, 355-367. doi: 10.1016/j.jconrel.2004.12.002

219 N. A. Yanul, Y. E. Kirsh, S. Verbrugghe, E. J. Goethals, F. E. Du Prez, *Macromolecular Chemistry and Physics* **2001**, *202*, 1700-1709. doi: 10.1002/1521-3935(20010601)202:9<1700::aid-macp1700>3.0.co;2-f

220 P. Adriaensens, L. Storme, R. Carleer, J. Gelan, F. E. Du Prez, *Macromolecules* **2002**, *35*, 3965-3970. doi: 10.1021/ma0117763

221 K. Yamamoto, E. Ito, S. Fukaya, H. Takagi, *Macromolecules* **2009**, *42*, 9561-9567. doi: 10.1021/ma9009774

222 T. Kyu, J. P. Kennedy, G. C. Richard, *Macromolecules* **2002**, *26*, 572-574. doi: 10.1021/ma00056a003

223 S. T. R. Velasquez, D. Jang, P. Jenkins, P. Liu, L. Yang, L. T. J. Korley, N. Bruns, *Advanced Functional Materials* **2022**, *32*. doi: 10.1002/adfm.202207317

224 W. Lequieu, F. E. Du Prez, *Polymer* **2004**, *45*, 749-757. doi: 10.1016/j.polymer.2003.12.012

225 H. W. Kammer, J. Kressler, C. Kummerloewe, **1993**, *106*, 31-85. doi: 10.1007/BFb0025861

226 R.-D. Maier, R. Thomann, J. Kressler, R. Mülhaupt, B. Rudolf, *Journal of Polymer Science Part B: Polymer Physics* **1997**, *35*, 1135-1144. doi: 10.1002/(sici)1099-0488(199705)35:7<1135::aid-polb12>3.0.co;2-a

227 D. Pfefferkorn, S. O. Kyerematen, K. Busse, H.-W. Kammer, T. Thurn-Albrecht, J. Kressler, *Macromolecules* **2011**, *44*, 2953-2963. doi: 10.1021/ma102867d

228 D. Christova, R. Velichkova, E. J. Goethals, F. E. Du Prez, *Polymer* **2002**, *43*, 4585-4590. doi: 10.1016/s0032-3861(02)00313-0

229 M. Bauer, C. Lautenschlaeger, K. Kempe, L. Tauhardt, U. S. Schubert, D. Fischer, *Macromol Biosci* **2012**, *12*, 986-998. doi: 10.1002/mabi.201200017

230 X. Li, M. Basko, S. F. Du Prez, I. F. Vankelecom, *J Phys Chem B* **2008**, *112*, 16539-16545. doi: 10.1021/jp805117z

231 K. Cosaert, E. Eeckhout, E. Goethals, F. D. Prez, P. Guégan, H. Cheradame, *Polymer International* **2002**, *51*, 1231-1237. doi: 10.1002/pi.896

232 I. Krakovský, J. Pleštil, J. Baldrian, M. Wübbenhorst, *Polymer* **2002**, *43*, 4989-4996. doi: 10.1016/s0032-3861(02)00287-2

233 Q. Guo, R. Thomann, W. Gronski, R. Staneva, R. Ivanova, B. Stühn, *Macromolecules* **2003**, *36*, 3635-3645. doi: 10.1021/ma0340154

234 C. De Rosa, R. Di Girolamo, A. Malafronte, M. Scoti, G. Talarico, F. Auriemma, O. Ruiz de Ballesteros, *Polymer* **2020**, *196*, 122423. doi: 10.1016/j.polymer.2020.122423

235 M. Hijazi, C. Krumm, S. Cinar, L. Arns, W. Alachraf, W. Hiller, W. Schrader, R. Winter, J. C. Tiller, *Chemistry - A European Journal* **2018**, *24*, 4523-4527. doi: 10.1002/chem.201800168

236 M. Hijazi, P. Spiekermann, C. Krumm, J. C. Tiller, *Biotechnology and Bioengineering* **2019**, *116*, 272-282. doi: 10.1002/bit.26877

237 L. Neukirch, Practical Course Report, TU Dortmund, **2020**.

238 T. Luhmann, M. Schmidt, M. N. Leiske, V. Spieler, T. C. Majdanski, M. Grube, M. Hartlieb, I. Nischang, S. Schubert, U. S. Schubert, L. Meinel, *ACS Biomater Sci Eng* **2017**, *3*, 304-312. doi: 10.1021/acsbiomaterials.6b00578

239 T. A. Wright, R. C. Page, D. Konkolewicz, *Polym Chem* **2019**, *10*, 434-454. doi: 10.1039/C8PY01399C

240 O. Sedlacek, B. D. Monnery, S. K. Filippov, R. Hoogenboom, M. Hruby, *Macromol Rapid Commun* **2012**, *33*, 1648-1662. doi: 10.1002/marc.201200453

241 V. Kumar, D. S. Kalonia, *AAPS PharmSciTech* **2006**, *7*, 62. doi: 10.1208/pt070362

242 M. D. McSweeney, Z. C. Versfeld, D. M. Carpenter, S. K. Lai, *Clin Transl Sci* **2018**, *11*, 162-165. doi: 10.1111/cts.12537

243 P. Farkas, J. Korcova, J. Kronek, S. Bystricky, *Eur J Med Chem* **2010**, *45*, 795-799. doi: 10.1016/j.ejmech.2009.11.002

244 C. Sornay, V. Vaur, A. Wagner, G. Chaubet, *R Soc Open Sci* **2022**, *9*, 211563. doi: 10.1098/rsos.211563

245 A. Matsushima, M. Okada, Y. Inada, *FEBS Lett* **1984**, *178*, 275-277. doi: 10.1016/0014-5793(84)80615-8

246 A. Yu. Rulev, *European Journal of Organic Chemistry* **2023**, *26*. doi: 10.1002/ejoc.202300451

247 M. P. Lutolf, N. Tirelli, S. Cerritelli, L. Cavalli, J. A. Hubbell, *Bioconjug Chem* **2001**, *12*, 1051-1056. doi: 10.1021/bc015519e

248 R. Canfield, *The Journal of Biological Chemistry* **1963**, *238*, 2698-2707. doi: n.a.

249 B. C. Ranu, S. Banerjee, *Tetrahedron Letters* **2007**, *48*, 141-143. doi: 10.1016/j.tetlet.2006.10.142

250 S. Bräse, J. Bülle, A. Hüttermann, *Organische und bioorganische Chemie: Das Basiswissen für Master– und Diplomprüfungen*, 2 ed., Wiley-VCH Verlag GmbH, **2008**.

251 L. Konermann, *eLS, (Ed.).* **2012**. doi: 10.1002/9780470015902.a0003004.pub2

252 M. Roth, Master's thesis, TU Dortmund **2014**.

253 U. K. Laemmli, *Nature* **1970**, *227*, 680-685. doi: 10.1038/227680a0

254 C. Bernhard, S. J. Roeters, J. Franz, T. Weidner, M. Bonn, G. Gonella, *Phys Chem Chem Phys* **2017**, *19*, 28182-28188. doi: 10.1039/c7cp05445a

255 J. Blummel, N. Perschmann, D. Aydin, J. Drinjakovic, T. Surrey, M. Lopez-Garcia, H. Kessler, J. P. Spatz, *Biomaterials* **2007**, *28*, 4739-4747. doi: 10.1016/j.biomaterials.2007.07.038

256 K. Hoger, T. Becherer, W. Qiang, R. Haag, W. Friess, S. Kuchler, *Eur J Pharm Biopharm* **2013**, *85*, 756-764. doi: 10.1016/j.ejpb.2013.04.005

257 S. I. Jeon, J. D. Andrade, *Journal of Colloid and Interface Science* **1991**, *142*, 159-166. doi: 10.1016/0021-9797(91)90044-9

258 M. Hijazi, C. Krumm, S. Cinar, L. Arns, W. Alachraf, W. Hiller, W. Schrader, R. Winter, J. C. Tiller, *Chemistry* **2018**, *24*, 4523-4527. doi: 10.1002/chem.201800168

259 M. Ahangarpour, I. Kavianinia, M. A. Brimble, *Org Biomol Chem* **2023**, *21*, 3057-3072. doi: 10.1039/d2ob02262a

260 D. Sheehan, S. O'Sullivan, *Methods Mol Biol* **2004**, *244*, 253-258. doi: 10.1385/1-59259-655-x:253

8 List of Abbreviations

Abbreviation	Definition
1M2P	1-Methoxy-2-propanol
AA	Acrylic Acid
AFM	Atomic force microscopy
APCN	Amphiphilic polymer conetwork
BSA	Bovine serum albumin
$CDCl_3$	Deuterated Chloroform
CROP	Cationic ring-opening polymerization
CT	A-Chymotrypsin
DA	Diacrylate
DBB	1,4-Dibromo-2-butene
DMA	Dynamic mechanical analysis
DMA	*N*,*N*-Dimethylacrylamide
DMAP-MAA	*N*-[3-(Dimethylamino)-propyl]-methacrylamide
DMPDA	*N*,*N*-dimethyl-*p*-phenylene diamine
DF	Degree of functionalization
DP	Degree of polymerization
DSC	Differential scanning calorimetry
EPOx	(2-(1-Ethylpentyl)-2-oxazoline)
eq.	Molar equivalents
EtOx	2-Ethyl-2-oxazoline
FRET	Fluorescence resonance energy transfer
HC	Highly cross-linked
HEA	2-Hydroxyethyl acrylate
^{1}H NMR	Proton nuclear magnetic resonance spectroscopy
HRP	Horseradish peroxidase
IDA	2,2'-Imino diacetic acid
ITC	Isothermal titration calorimetry
LC	Lowly cross-linked
LCST	Lower critical solution temperature
Lys	Lysozyme
MOx	2-Methyl-2-oxazoline
mPEG	Monomethoxy poly(ethylene glycol)
MW	Molecular weight

MWCO	Molecular weight cut-off
NMR	Nuclear magnetic resonance
PADA	Pyromellitic acid dianhydride
PCL	Poly(*ε*-caprolactone)
PDMA	Poly(*N*,*N*-dimethylacrylamide)
PDMS	Poly(dimethyl siloxane)
PEG	Poly(ethylene glycol)
PEhAc	Poly(2-ethylhexyl acrylate)
PEPOx	Poly(2-(1-ethylpentyl)-2-oxazoline)
PEtOx	Poly(2-ethyl-2-oxazoline)
PHEA	Poly(2-hydroxyethyl acrylate)
PMMA	Poly(methyl methacrylate)
PMOx or PMeOx	Poly(2-methyl-2-oxazoline)
POx	Poly(2-oxazoline)
PPFPA	Poly(*N*-pyridin-4-yl)acrylamide)
PTFE	Poly(tetrafluoroethylene)
RT	Room temperature
SAXS	Small-angle X-ray scattering
SANS	Small-angle neutron scattering
SDS-PAGE	Sodium dodecyl sulfate-polyacrylamide gel electrophoresis
SEC	Size exclusion chromatography
SEM	Scanning electron microscopy
SPN	Segmented polymer network
TEA	Triethylamine
TEM	Transmission electron microscopy
THF	Tetrahydrofurane
TRIS	Tris(hydroxymethyl)aminomethane
TTEGDA	Tetra(ethylene glycol) diacrylate
UV-VIS	Ultraviolet-visible
Wt%	Weight percent
XRD	X-ray diffraction